

**NEUROTROPHIC FACTOR GRADIENT
GENERATION FOR 2D AND 3D *IN VITRO* AND *IN
VIVO* NEURONAL AND SCHWANN CELL
GUIDANCE**

By

Kellin Daniel Krick

A dissertation submitted to Johns Hopkins University in conformity with the
requirements for the degree of Doctor of Philosophy

Baltimore, Maryland

March 2016

©2016 Kellin Daniel Krick

All Rights Reserved

Abstract

Delivery of neurotrophic factor gradients offers exciting potential for improving the regenerative outcomes in peripheral nerve injuries by enhancing the complete regeneration of nerves across large injury gaps. However, a major limitation to current gradient generation platforms has been the inability to develop gradient generation methodologies that exhibit control of gradient characteristics suitable for *in vitro* gradient screening while also being scalable to length scales relevant for *in vivo* nerve regeneration paradigms. Few studies have reported the influence of NF gradients on Schwann cell migration. We developed two gradient generation platforms capable of highly controlled, centimeter-scale gradient generation, which are capable of gradient delivery in both *in vitro* and *in vivo* gradient guidance paradigms. Furthermore, we developed a novel combinatorial cell migration platform, which combines topographical and biochemical guidance to investigate the effect of surface topography and gradient characteristics on the guidance of human Schwann cells. Using a live-cell imaging and analysis platform, we elucidated extensive details of the influence of these cues on the migration kinetics of Schwann cells, examining the roles of aligned fiber diameter and NF gradient characteristics in directing Schwann cell migration. Finally, we created a nerve guide that combines topographical and biochemical gradient guidance and demonstrated the utility of NF gradient delivery in enhancing regeneration in acute, short gap and long-term, large gap *in vivo* peripheral nerve injury models. The advances in gradient generation and delivery presented in this thesis offer new platforms for characterizing gradient guidance of a variety of neuronal and glial cell types and for enhancing nerve regeneration through *in vivo* NF gradient delivery.

Advisor: Hai-Quan Mao, Ph.D.

Thesis Committee: Ahmet Höke (co-advisor), M.D., Ph.D.; Feilim Mac Gabhann, Ph.D.;

Warren Grayson, Ph.D.

Acknowledgements

There have been so many people who have helped me and guided me throughout my time at Hopkins. They have inspired me to move forward with my passions, both academic and in life, and without them I would not be where I am today.

I first want to thank my incredible Ph. D. advisor, Dr. Hai-Quan Mao, for being a constant advocate and mentor to me throughout my graduate studies. He was a major factor in my initial decision to pursue my Ph. D. at Hopkins, and I am incredibly thankful that I did. From the start, he has been encouraging and supportive, granting me freedom to pursue new avenues of research while providing the guidance necessary to keep me moving forward. I have thoroughly enjoyed our many discussions and the numerous times when I was able to walk into his office just to chat. Witnessing his approach to scientific inquiry and his consistent mentorship has been an inspiration to me, and I am forever grateful that he gave me the opportunity to work with him these past years.

I would like to thank my thesis committee members, Dr. Ahmet Höke, Dr. Feilim Mac Gabhann, and Dr. Warren Grayson, for all of their advice, input, and mentorship throughout my time at Hopkins. I especially would like to thank Dr. Höke, with whom I have worked closely throughout my time at Hopkins and who has provided an incredible amount of insight into my research. I would also like to thank Dr. Ruifa Mi for the unbelievable amount of work he did to help me with my *in vivo* peripheral nerve regeneration projects. I would like to acknowledge collaborators Dr. Yu-Ja Huang, who was instrumental in all of my *in vitro* live-cell imaging studies, Dr. Peter Searson for his consistent input, and Dr. Ali Khademhosseini for developing an incredible gradient generation technique which was instrumental to my thesis. To my other collaborators, Dr.

Feilim Mac Gabhann, Lindsay Wendell-Clegg, Dr. Donald Zach, Dr. Val Sluch, Dr. Thomas Brushart, Dr. Karim Sarhane, Dr. Zuhaib Ibrahim, and Dr. Gerald Brandacher, I have been so inspired by the work all of you do and have been incredibly thankful to have had the pleasure to work with you.

I have an incredible group of colleagues I have worked with in the Mao Lab, who have made my time at Hopkins incredibly rewarding. I want to first acknowledge the nerve regeneration team: Dr. Russ Martin, Markus Tammia, Jose Roman, Brian Ginn, Digs Ardoña, Dr. Jisuk Choi, Dr. Huanhuan Liu, and Dr. Xiaowei Li. I have thoroughly enjoyed our countless discussions, your constant support, your hard work, your brilliance, and most of all your friendship. I would like to thank the undergraduates who have worked with me throughout the years and who gave me the unbelievable opportunity to mentor them: Letitia Chim, Andrew Han, Ashish Aman, Kalina Martinova, John DiCapua, Clay Andrews, Cameron Nemeth, Diane Hwang, and Lauren Lee. I wish you all the best in your future endeavors. I would also like to thank the rest of my fellow Mao lab members: Dr. Xuesong Jiang, Dr. Yong Ren, Charles Hu, Jason Lee, Dr. Shuming Zhang, and Dr. John-Michael Williford. All of you have contributed to making the Mao lab a great place to call my “home”.

To my friends and family, I cannot possibly express how much you have enriched my life and my time at Hopkins. You helped make me who I am today, and for that I am humbled and grateful. To my parents, you have made all of this possible with your unwavering and unending support and love, and I am blessed to be your son. Lastly, I owe tremendous gratitude to my future wife, Tracy, whose unconditional love and support, kindness, graciousness, and patience has allowed me to pursue my dreams.

Table of Contents

Abstract.....	ii
Acknowledgements	iv
Table of Contents	vi
List of Figures and Tables.....	ix

Chapter 1: Tissue engineering and peripheral nerve regeneration: utilizing engineering principles to enhance nerve regeneration

1.1 Introduction.....	1
1.1.1 Tissue engineering	1
1.1.2 Peripheral nerve regeneration	3
1.1.3 Biochemical cues in nerve tissue development and applications in nerve regeneration.....	4
1.1.4 Anisotropy and overcoming the “candy store” effect.....	8
1.2 Hypothesis and Specific Aims of the Thesis	12
1.3 Figures.....	16
1.4 References	17

Chapter 2: Gradient Generation Platforms for *In Vitro* and *In Vivo* Neurotrophic Factor Delivery

2.1 Introduction.....	26
2.2 Materials and Methods.....	28
2.2.1 Methacrylated gelatin synthesis.....	28

2.2.2 Fabrication of microfluidic devices	28
2.2.3 Convection and diffusion-based microfluidics gradient platform	29
2.2.4 Controlled release of growth factor gradients.....	30
2.2.5 Diffusion-based gradient generation platform.....	30
2.2.6 Hydrogel loading using diffusion-based gradient generation technique	31
2.2.7 Data analysis	32
2.3 Results and Discussion.....	32
2.3.1 Microfluidics gradient characterization.....	32
2.3.2 Release of gradients from methacrylated gelatin hydrogel.....	34
2.3.3 Diffusion-based gradient generation platform characterization	36
2.3.4 Use of diffusion-based gradient generation method for establishment of gradients in hydrogel films.....	38
2.4 Conclusions.....	40
2.5 Figures.....	42
2.6 References	55

Chapter 3: Effect of Neurotrophic Factor Gradient Profile on Schwann Cell Migration in Culture

3.1 Introduction.....	60
3.2 Methods.....	63
3.2.1 Aligned nanofiber electrospinning setup	63
3.2.2 Aligned fiber coverslip preparation for fiber diameter screening.....	63

3.2.3 Live-cell tracking of human Schwann cells on aligned nanofibers	64
3.2.4 Combinatorial biochemical gradient and topographical guidance cell tracking platform.....	64
3.2.5 Cell tracking and analysis programming	65
3.3 Results and Discussion.....	66
3.3.1 Effect of aligned nanofiber diameter on Schwann cell migration	66
3.3.2 Influence of NF type on Schwann cell migration	68
3.3.3 Effects of GDNF gradient characteristics on chemotaxis.....	69
3.5 Conclusions.....	74
3.6 Figures and Tables.....	76
3.7 References	86

**Chapter 4: Effect of GDNF Gradient Delivery on Peripheral Nerve Regeneration in
Rat and Canine Models**

4.1 Introduction.....	89
4.2 Methods.....	92
4.2.1 Electrospinning and preparation of S-Shaped nerve guide.....	92
4.2.2 Gradient hydrogels for nerve guidance conduits	93
4.2.3 Sciatic nerve transection and repair in rats	93
4.2.4 Electrophysiology assessments in rat model.....	94
4.2.5 Harvesting of regenerated nerves in rat model	94
4.2.6 Canine model protocol overview	94
4.2.7 Preparation of NGCs for canine model.....	95
4.2.8 Canine peroneal nerve injury surgery preparation.....	95

4.2.9 Canine peroneal nerve injury surgical procedure	96
4.2.10 Electrophysiology assessments in canine model	97
4.2.11 Harvesting of regenerated nerves in canine model	97
4.2.12 Histomorphometric analysis	98
4.2.13 Statistical analysis	98
4.3 Results and Discussion.....	98
4.3.1 Nerve Guidance Conduit Design	98
4.3.1 Non-critical injury gap model for study of acute nerve regeneration	99
4.3.2 Large gap injury, long-term nerve regeneration model	101
4.4 Conclusions.....	105
4.5 Figures.....	107
4.6 References	122
Chapter 5: Conclusions and future directions for NF gradient-guided nerve regeneration	
5.1 Conclusions.....	125
5.2 Future Directions	126
5.3 References	129
Biographical Sketch	131
Curriculum Vitae	132

List of Figures and Tables

- Figure 1.1:** Signaling cue presentation and cell-incorporation approaches to enhance nerve regeneration. NGC functionality can be enhanced by incorporating (a) topographical and adhesion signaling, (b) neurotrophic factor (NF) gradients, (c) Schwann cells over-expressing NFs, and (d) adult stem cells such as mesenchymal stem cells (MSCs) and bone marrow-derived stromal cells (BMSCs). Figure reproduced by permission from Elsevier Publishers Ltd: Current Opinion in Biotechnology, Copyright 2011.16
- Figure 2.1:** Schematics of the convection-based gradient generation method. (a) Microfluidics channel with tailorable channel dimensions, channel height of 100 μm . (b) Channel is pre-filled with photocrosslinkable methacrylated gelatin (MG), large volume of MG is pipetted onto outlet, and small volume of NF pipetted onto inlet. (c) Surface tension drives convection-based flow of NF droplet into channel and establishes gradient. (d) After UV crosslinking, gradient is encapsulated in hydrogel.42
- Figure 2.2:** Generation of multi-centimeter scale gradients of FITC-lysozyme using convection-based gradient generation method with controllable gradient concentration and steepness.43
- Figure 2.3:** Gradient length can be tailored by modifying channel dimensions. (a) Gradient of FITC-lysozyme in 8 mm long channel. (b) Parallel channel configuration developed for increased scalability of gradient generation method.44
- Figure 2.4:** Gradient release from GDNF gradient-loaded hydrogel film ($N = 3$). Films were produced in triplicate and were sectioned into six pieces and release was measured

using GDNF ELISA and compared to standards per ELISA instructions. Bar graph denotes mean \pm Standard Error.....	45
Figure 2.5: Cumulative release of GDNF from methacrylated gelatin with different levels of methacrylated heparin loading (N=3). Release was measured using GDNF ELISA and compared to standards per ELISA instructions. Error bars denote standard error.....	46
Figure 2.6: Diffusion-based gradient generation platform consisting of a microfluidics channel (10 mm length by 4 mm width by 100 μ m height) with a 3 mm diameter “source” well and 3 mm diameter “sink” well. Channel is filled with media or PBS, and “source” and “sink” wells are filled with media/PBS or NF. Diffusion gradient establishes in channel due to differences in concentration between the “source” and “sink” wells.....	47
Figure 2.7: Time-progression of diffusion-based gradients. (a) COMSOL modeling of diffusion-based gradient generation platform showing time-course of gradient generation. (b) Experimental generation of FITC-lysozyme gradient in diffusion-based gradient channels. Gradient was measured using a Typhoon Gel Reader and compared against channel standards.....	48
Figure 2.8: Human Schwann cell viability in diffusion-based gradient channel in 0-10 ng/mL NRG1 gradient. (a) Schwann cells were well-adhered 4 hours after beginning gradient generation. (b) Schwann cells remained viable for at least 18 hours after beginning gradient generation.....	49
Figure 2.9: Modification of diffusion-based gradient generation platform for functionalization of hydrogel films. Hydrogel films (1 cm \times 4 cm \times 500 μ m) are	

polymerized in PDMS frames. Gradient channels are placed over the films and gradients are generated in the channel, transferring to the underlying hydrogel film. 50

Figure 2.10: FITC-Lysozyme gradient in fibrin hydrogel fiber sheet generated using diffusion-based gradient generation method. High concentration (100 $\mu\text{g}/\text{mL}$) of FITC-Lysozyme located on the right end of the channel. Visualized using 2.5 \times objective on Nikon Inverted Fluorescence Microscope.51

Figure 2.11: FITC-Lysozyme gradient generated in collagen hydrogel using diffusion-based gradient method. (a) Gradient in channel above hydrogel. (b) Gradient in collagen hydrogel after channel has been removed. Gradient was measured using a Typhoon Gel Reader and compared against hydrogel and channel standards.....52

Figure 2.12: Directed motor neuron (red) migration in spinal cord organotypic culture on collagen hydrogel loaded with 0–1 ng/mL GDNF gradient using modified diffusion-based gradient method.53

Figure 2.13: Dorsal root ganglion explants cultured on Matrigel, showing neuron survival and growth after 3 days in 0-10 ng/mL NGF gradient culture in modified diffusion gradient channels. Visualized using Nikon Inverted Microscope with 10 \times objective. Scale bar is 200 μm54

Table 3.1: Maximum GDNF concentration in different gradient regions based on loading concentration of GDNF in hydrogel.76

Figure 3.1: Schematic of electrospinning setup used to generate aligned nanofiber substrates. A voltage is applied to an extruded polymer solution, which is deposited onto an electrically-grounded spinning metal wheel, resulting in the formation of aligned, thin-fiber sheets.77

Figure 3.2: Human Schwann cells visualized on aligned nanofibers with fluorescence microscope. Cells are stained with Hoechst stain to increase contrast against underlying fiber substrate.....	78
Figure 3.3: Average migration rate of human Schwann cells on aligned fiber sheets with different fiber diameters (N > 1500 cells). (a) Migration speed distribution of cells in different regions of fiber sheets. (b) Weighted average migration speed of cells. Error bars signify standard error.	79
Figure 3.4: Population distribution of human Schwann cell migration speed on aligned fiber sheets with different fiber diameters (N > 1500 cells).	80
Figure 3.5: Schematic for production of combinatorial migration chambers incorporating aligned fiber topographical guidance and hydrogel-based NF gradient delivery for live-cell imaging and analysis.	81
Figure 3.6: Human Schwann cell migration bias in response to gradients of GDNF, NGF, and NRG-1 (N>1000 cells).....	82
Figure 3.7: Directional guidance of human Schwann cell migration to GDNF gradients (N>1000 cells). (a) Directional bias heat map of Schwann cells in 1 $\mu\text{g}/\text{mL}/\text{cm}$ GDNF gradient. Dots represent position of cells in gradient. Red dots represent cells exhibiting positive directional bias. Blue dots represent cells exhibiting negative directional bias. (b) Directional bias heat map of Schwann cells in 10 $\mu\text{g}/\text{mL}/\text{cm}$ GDNF gradient. (c) Directional bias heat map of Schwann cells in 20 $\mu\text{g}/\text{mL}/\text{cm}$ GDNF gradient. (d) Percent of negative, neutral, or positive migrating cells in different regions of 1 $\mu\text{g}/\text{mL}/\text{cm}$ GDNF gradient. (e) Percent of negative, neutral, or positive migrating cells	

in different regions of 10 $\mu\text{g/mL/cm}$ GDNF gradient. (f) Percent of negative, neutral, or positive migrating cells in different regions of 20 $\mu\text{g/mL/cm}$ GDNF gradient.....83

Figure 3.8: Population distribution of directional guidance of human Schwann cell migration to GDNF gradients ($N > 1000$ cells). (a) Directional bias distribution of Schwann cells in 1 $\mu\text{g/mL/cm}$ GDNF gradient in different hour ranges. (b) Directional bias distribution of Schwann cells in 10 $\mu\text{g/mL/cm}$ GDNF gradient in different hour ranges. (c) Directional bias distribution of Schwann cells in 20 $\mu\text{g/mL/cm}$ GDNF gradient in different hour ranges. (d) Percent of negative, neutral, or positive migrating cells in total cell population of cells in different gradient conditions.84

Figure 3.9: Migration rate of human Schwann cells in GDNF gradients ($N > 1000$ cells). (a) Migration rate heat map of Schwann cells in 1 $\mu\text{g/mL/cm}$ GDNF gradient. Dots represent position of cells in gradient. Red dots represent cells migrating at average rate of 20 $\mu\text{m/h}$. Blue dots represent non-migratory cells. (b) Migration rate heat map of Schwann cells in 10 $\mu\text{g/mL/cm}$ GDNF gradient. (c) Migration rate heat map of Schwann cells in 20 $\mu\text{g/mL/cm}$ GDNF gradient. (d) Average migration rate of total cell populations in different gradient conditions. Error bars represent Standard Error.85

Table 4.1: Generations of conduit designs incorporating aligned fiber topographical guidance and NF delivery. The 3rd generation of conduit was selected for use in our animal models.107

Figure 4.1: Fabrication of S-shaped conduit containing aligned fiber topography and hydrogel-based NF gradient delivery. (a) Gradient-containing hydrogels placed between aligned fiber sheets and rolled into S-shaped conduit. (b) Aligned fibers with

average diameter of 1.2 μm . Scale bar = 10 μm . (c) Scanning electron micrograph of S-shaped conduit. Scale bar is 100 μm	108
Figure 4.2: Histomorphometric analysis of the small gap, acute regeneration rat sciatic nerve injury model (N > 5). (a) Representative images of nerve cross sections obtained using 63x objective. Scale bars are 10 μm . (b) Average nerve area of different NGC groups. Error bars represent Standard Deviation. Differences considered statistically significant for $P < 0.05$	109
Figure 4.3: Average axon count of different NGC groups in small gap, acute regeneration rat sciatic nerve injury model (N > 5). Error bars represent Standard Deviation. Differences considered statistically significant for $P < 0.05$	110
Figure 4.4: Electrophysiological measurement of different NGC groups in small gap, acute regeneration rat sciatic nerve injury model (N > 5).	111
Figure 4.5: Histological cross-sections of nerves of different NGC groups in large gap, long-term regeneration canine peroneal nerve injury model. (a) Mid-graft of autograft control. (b) 3-mm distal to autograft control. (c) Mid-graft of no-GDNF S-shaped NGC. (d) 3-mm distal to no-GDNF S-shaped NGC. (e) Mid-graft of uniform GDNF S-shaped NGC. (f) 3-mm distal to uniform GDNF S-shaped NGC. (g) Mid-graft of gradient GDNF S-shaped NGC. (h) 3-mm distal to gradient GDNF S-shaped NGC. Images obtained with 2.5 \times objective. Scale bars are 300 μm	112
Figure 4.6: Histology of nerve regions showing that PCL fibers remain 7 months after implantation. Fibers (white dots, red arrows) are surrounded by fibrotic tissue, whereas nerve tissue is localized in regions where fibers are not present (tissue border noted by red line). Images obtained with 63x objective. Scale bars are 10 μm	113

Figure 4.7: Average nerve area of different NGC groups in large gap, long-term regeneration canine peroneal nerve injury model (N > 5). Error bars represent Standard Error. Differences considered statistically significant for $P < 0.05$114

Figure 4.8: Representative histological cross-sections of nerves of different NGC groups in large gap, long-term regeneration canine peroneal nerve injury model. (a) Mid-graft No-GDNF S-shaped NGC. (b) Mid-graft uniform GDNF S-shaped NGC. (b) Mid-graft gradient GDNF S-shaped NGC. Images obtained with 63x objective. Scale bars are 10 μm115

Figure 4.9: Average nerve density of different NGC groups in large gap, long-term regeneration canine peroneal nerve injury model (N > 5). Error bars represent Standard Error.116

Figure 4.10: Average total axon count of different NGC groups in large gap, long-term regeneration canine peroneal nerve injury model (N > 5). Error bars represent Standard Error.117

Figure 4.11: Average onset latency of different NGC groups in large gap, long-term regeneration canine peroneal nerve injury model, measured with CNAP (N = 10). Error bars represent Standard Deviation. Differences considered statistically significant for $P < 0.05$118

Figure 4.12: Average peak latency of different NGC groups in large gap, long-term regeneration canine peroneal nerve injury model, measured with CNAP (N = 10). Error bars represent Standard Deviation. Differences considered statistically significant for $P < 0.05$119

Figure 4.13: Average signal amplitude of different NGC groups in large gap, long-term regeneration canine peroneal nerve injury model, measured with CNAP (N = 10). Error bars represent Standard Deviation. Differences considered statistically significant for $P < 0.05$120

Figure 4.14: Average peak area of different NGC groups in large gap, long-term regeneration canine peroneal nerve injury model, measured with CNAP (N = 10). Error bars represent Standard Deviation. Differences considered statistically significant for $P < 0.05$121

Chapter 1 : Tissue engineering and peripheral nerve regeneration: utilizing engineering principles to enhance nerve regeneration

1.1 Introduction

1.1.1 Tissue Engineering

There is a story in Greek mythology about a Titan named Prometheus, who betrayed the Greek god Zeus. As punishment, Prometheus was chained to the top of a mountain where, every day, an eagle would consume his liver. However, due to Prometheus' immortality, he would survive and the liver would regenerate every night, and thus his punishment would continue day after day. For thousands of years, mankind has envisioned the ability for humans to regenerate our organs and tissues and heal wounds beyond the capacity for the human body to normally regenerate.

The practice of tissue engineering, utilizing knowledge of the structure and function of mammalian tissues to design biological substitutes for the repair of irreparably damaged organs and tissues, first arose in the mid-20th century [1]. However, it was not until 1988 that the field of "tissue engineering" was clearly defined, formally establishing an exciting field of academic pursuit and ushering in an era of increased research and development in the tissue engineering and regenerative medicine (TERM) fields. Since the first publication in the journal *Tissue Engineering* in 1995 [1], the field has rapidly expanded in breadth, encompassing research in the repair and replacement of all nearly all organs and tissues. From January 2012 to September 2013 alone, there were 8000 publications in the TERM fields [2], an incredible demonstration of the amount of effort that researchers are putting

into this rapidly advancing field. Elite research universities around the world have established academic centers with the expressed purpose of conducting TERM research, including the Translational Tissue Engineering Center at Johns Hopkins University, demonstrating the importance of TERM research in the future of modern medicine.

With the continued advancement in development of biologically-active materials and scaffolds and obtaining patient-specific cells which circumvent issues with tissue rejection typically seen in allogeneic organ transplants, the tools for modifying or creating tissues has increased exponentially since the TERM fields were first established [2, 3]. However, regulatory hurdles and safety concerns continue to hinder the clinical application of more recent technologies [3]. As researchers continue their efforts to improve our understanding of human biology, physiological development, and how human bodies respond and adapt to injury, the safety and efficacy of the latest TERM technologies will continue to improve. Considerable effort has been placed on the production of materials which mimic the form and function of mammalian tissues, recreating or redesigning the extracellular milieu of tissue-specific cells to control the migration and phenotypic function of these cells into organized, 3-dimensional engineered tissues for drug testing or tissue replacement as alternatives to organ transplantation. Engineered tissue scaffolds can be designed to mimic the biochemical and structural composition of their native tissues, and technologies for building these tissue scaffolds into complex, 3-D, hierarchical structures continues to advance. Through advancing our understanding of how native tissues are formed during development and the relationship between tissue structure and function, the TERM fields are constantly edging closer to being able to safely and effectively recreate or enhance the regeneration of damaged tissues and improve the lives of countless patients

suffering from disease and trauma for which current clinical practice has limited regenerative potential.

1.1.2 Peripheral nerve regeneration

Peripheral nerve injuries are a major cause of loss of limb function in patients worldwide, with nerve injuries occurring in 2.8% of traumatic injuries [4]. In the United States alone, approximately 360,000 people suffer from various forms of upper body paralysis on an annual basis [5]. The preferred surgical treatment is end-to-end anastomosis, but for injuries which produce a large gap in a nerve, the clinical gold standard is to use an autologous nerve graft. However, autologous nerve grafts have several major drawbacks limiting their use and efficacy, including donor site morbidity, motor/sensory nerve mismatch, neuroma formation, size restrictions, and limitation in functional regeneration [6]. Alternative FDA-approved products are available for applications in which large gap injuries occur, but the lack of directional guidance in these products limits their regenerative capacity, especially as gap size increases [7]. Newer approaches to nerve regeneration aiming to overcome the limitations of current clinically-available nerve regeneration methods utilize strategies ranging from biomaterials engineering to cell-based therapies, incorporating endogenous or exogenous sources of cells, extracellular scaffolds, or biochemical cues to enhance the regeneration of injured nerves [8]. Our lab is currently investigating methods for enhancing nerve regeneration through the design of nerve guidance conduits (NGCs) containing topographical and biochemical guidance, and delivery of genetically-modified glial or stem cells to the site of nerve injury (**Figure 1.1**). By using a combinatorial NGC incorporating nanofiber-based topographical guidance and biochemical gradients of neurotrophic factors to promote growth across the entirety of a

large nerve gap, we intend to improve nerve regeneration beyond levels achievable by current clinical standards.

1.1.3 Biochemical cues in nerve tissue development and applications in nerve regeneration

The human body provides tissue engineers a near limitless toolbox of biochemical cues consisting of growth factors, adhesive ligands, extracellular matrix proteins and peptides which guide human development, maintain the form and function of the body, and which are naturally produced after injury to promote regeneration. Many of the neurotrophic factors (NFs) which are effective in promoting regeneration in the adult mammals have primary roles in the development of the mammalian nervous system, providing selective differentiation of sympathetic, parasympathetic, cholinergic, adrenergic, dopaminergic, motor, and sensory neurons [9]. Cordes summarized many of the genes and proteins involved in the development of mouse cranial nerves and sensory ganglia and categorized the genes and proteins based on function within the developing nervous system and emphasized the specificity of their activity for specific nerve populations [9]. Many of these genes and proteins have significant roles in the development of both the central and peripheral nervous systems and have been investigated to enhance regeneration of injuries in the central and peripheral nervous systems.

A subpopulation of proteins, collectively known neurotrophic factors, are of particular interest in nerve regeneration due to their characteristic activity promoting neuron survival, growth, and in some cases neuronal chemotaxis. Of the neurotrophin family of neurotrophic factors, nerve growth factor (NGF) is the most studied and is known to act specifically on small primary sensory and sympathetic neurons [10]. The effects of

NGF were first discovered by Elmer Bueker, who demonstrated that fragments of mouse sarcoma grafted in the body of three-day chick embryos promoted sensory nerve fibers to infiltrate the tumor from dorsal root ganglia adjacent to the tumor [11]. In normal nerves, NGF is expressed at similar levels in motor and sensory neurons, but following injury NGF expression is substantially upregulated in denervated sensory roots compared to levels expressed in denervated motor roots [12]. Herrup demonstrated that administration of NGF to chick dorsal ganglia promote upregulation of NGF receptors [13], indicating a potential feedback loop following an injury where NGF upregulation results in increased expression of NGF receptor and changes in sensitivity towards the growth factor. Whereas NGF has substantial effects on growth and survival of embryonic sensory neurons, the effect decreases in adult large sensory neurons [14] but is necessary for collateral sprouting of nociceptive and sympathetic axons into denervated skin [14, 15]. NGF has been shown to promote chemotaxis of sympathetic [16], dorsal root ganglion neurons [17-20], and PC12 neurons [21, 22], and increases Schwann cell migration from nerve explants [23]. Additionally, NGF has been utilized to enhance regeneration of peripheral nerve injuries via controlled release in nerve guidance conduits [24-30], osmotic pump [31, 32], or lentiviral-based overexpression [33, 34]. However, due to the specificity of NGF towards sensory and sympathetic neurons, the potential for use as a suitable growth factor for enhancing regeneration of mixed nerve populations (i.e. motor and sensory), commonly found in peripheral nerve injuries, is limited due to the limited trophic activity of NGF towards motor neurons.

Brain-derived neurotrophic factor (BDNF) and neurotrophin-3 (NT-3) are members of the neurotrophin family which possess greater motor neuron trophic potential. BDNF is

expressed in uninjured motor and sensory neurons, but is primarily upregulated in sensory neurons following injury [12] and in Schwann cells in the distal stump of an injury [35]. The result by Höke *et. al.* showing greater upregulation in injured sensory neurons compared to injured motor neurons [12] is interesting considering the general role of BDNF and dose-dependent response on motor neuron survival and growth [35], but its upregulation in the distal stump of motor neuron-containing injuries is indicative of its influence on motor neuron survival and regeneration. NT-3 is expressed in adult skeletal muscle and exhibits a trophic role on motoneurons *in vitro* [36] and type 2b fast muscle fiber associated neurons [37], but has also been shown to enhance the survival of proprioceptive and mechano-receptive sensory neurons [38, 39]. Expression of NT-3 is generally higher in sensory roots compared to motor roots but have minimal difference in expression after injury [12].

Neuregulins (NRGs) are derived from alternative splicings of the NRG1 gene and consist of 14 separate protein variations [40]. NRGs elicit substantial influence of Schwann cell activity directed by cell-cell interactions with axons, which express both soluble and membrane-bound variants [40]. One of the most widely studied neuregulins is the glial growth factor (GGF), which is a soluble, paracrine signaling isoform of NRG expressed by sensory, motor and sympathetic neurons [41, 42]. GGF has pronounced effects on Schwann cells, as demonstrated by Mahanthappa *et. al.* who showed delivery of soluble GGF2 increased Schwann cell migration from sciatic nerve cryosections [43]. GGF expression is upregulated in damaged sensory neurons and coincides with a coordinated upregulation of its receptor in Schwann cells, indicating coordination in NRG regulation in Schwann cells and axons following nerve injury [44, 45]. While NRG largely effects Schwann cell

activity, NRGs are expressed by axons and Schwann cells and act via autocrine or paracrine mechanisms [40, 45].

Glial-derived neurotrophic factor (GDNF) is an increasingly studied neurotrophic factor of the TGF α -1 superfamily, and has trophic effects on sensory, motor and autonomic neurons [46-52]. Overexpression of GDNF in the central nervous system promotes dramatic survival of motor neurons after axotomy [53]. Additionally, GDNF has been shown to be a potent chemotactic agent and binding ligand for Schwann cell precursors [54], providing strong trophic activity to both neurons and glial cells in the central and peripheral nervous system. GDNF is upregulated in both motor and sensory neurons following nerve injury [12] which subsequently upregulates the GDNF receptor [55], indicating its important role in neurotrophic support in both motor and sensory neuron populations. Comparison of the recovery of sciatic nerve injury following release of GDNF or NGF by synthetic nerve guidance conduit revealed significantly higher regeneration of both motor and sensory neurons using sustained GDNF delivery compared with NGF delivery [30], indicating greater regenerative potential of GDNF compared to widely-studied NGF. Furthermore, GDNF plays an important role in myelination by inducing Schwann cell proliferation and axon myelination, and is even capable of promoting myelination of axons which are normally unmyelinated [56]. The significant trophic effect of GDNF and its ability to mediate axon-glial interactions made GDNF the primary neurotrophic factor of interest for the studies involved in this thesis, investigating novel methodologies for delivering GDNF which will maximize its influence in enhancing peripheral nerve regeneration.

1.1.4 Anisotropy and overcoming the “candy store” effect

Although delivery of GDNF has been shown to improve the nerve regeneration potential of nerve guidance conduits by improving motor and sensory neuron survival and outgrowth, delivery of locally elevated levels of GDNF causes an axon trapping effect known as the “candy store” effect [57]. Axons are attracted to locations of high GDNF concentration, and maintenance of persistent levels of GDNF causes trapping of regenerating axons at the site of overexpression, preventing axons from migrating distally to their muscle and sensory targets [33, 58]. Several studies have demonstrated a neurotropic effect of GDNF, in which axons preferentially migrate towards regions of maximum GDNF expression and concentration [59, 60]. Similar effects have been elicited by lentiviral overexpression of BDNF [61] and NT-3 [62]. While the chemotropic effect of NFs can be utilized to guide nerve outgrowth, careful consideration must be made in designing a NF delivery method which is capable of harnessing the chemotropic capability of neurons without hindering their progression towards their reinnervation targets. One method of circumventing the axonal trapping effect is by expressing GDNF in the target muscle rather than at the injury site, a method which has been shown to enhance functional regeneration in a mouse crush injury model [63]. While promising, the positive effects of target-derived expression may be limited to injuries which are located close to the target site. For injuries in which the neurons must traverse large distances to reach the target muscle or sensory input, the likelihood for NFs expressed at the target site to diffuse to and reach the regenerating neurons may be severely limited. For injuries which are located large distances from innervation targets, localized delivery of NFs remains to be the most

effective method for promoting nerve regeneration through a nerve injury and into the distal nerve.

Recently, a promising method for delivering localized GDNF in a temporally-controlled manner was developed by Marquardt *et. al.*. By transfecting Schwann cells with a tetracycline-inducible GDNF lentivirus and injecting the transfected Schwann cells into the distal nerve of a 3 cm sciatic nerve defect bridged by fibrin-modified acellular nerve grafts, they were able to modify the duration of GDNF overexpression based on the duration of doxycycline administration and control release of GDNF using an affinity-based release system. They found that 6 weeks of overexpression produced the greatest regenerative outcome compared to 4 or 8 week overexpression, exhibiting the greatest axonal regrowth in the midgraft and distal nerve and promoting the greatest mass recovery of target muscle. The study provided excellent insight into the importance developing a platform which provides temporal control of GDNF delivery to enhance regeneration across an injury gap while preventing the excessive localized GDNF overexpression that results in decreased functional recovery due to the “candy store” effect. However, tetracycline-inducible GDNF expression provides limited control over precise GDNF concentration levels, resulting in potentially sub-optimal GDNF expression levels and difficulty in controlling the spatial distribution of GDNF across the injury site. Additionally, the requirement for lentivirus-transfected, exogenous Schwann cells limits the potential for this method to be developed as an off-the-shelf product and reduces its potential clinical use.

Controlled-release methods which deliver NFs by administration of NF-loaded microspheres [60, 64-66], polymeric films [30], lipid microtubules [26], nanofibers [67],

and crosslinked [27] or affinity-based hydrogels [68] can overcome the limitations of lentivirus-based NF overexpression by providing improved spatial and temporal control of NF delivery. With these methods, nerve guidance conduits can be designed to specific lengths and conduit diameter depending on the location and size of the injury and loaded with a variety of NFs at specified concentrations. The ability to manufacture nerve guidance conduits containing these controlled release platforms improves their potential for development of off-the-shelf products for clinical applications compared to transfection-based platforms.

Effective nerve regeneration requires not only the promotion of the axonal outgrowth, but also directional guidance of the regenerating axons towards the target site. Methods of guiding axons within the NGC have thus been employed to promote directional regrowth. A study by Parrinello *et al.* revealed that Ephrin signaling between fibroblasts and dedifferentiated and migrating Schwann cell progenitors is important in forming cords of Schwann cells, akin to the Bands of Büngner *in vivo*, which then serve as regenerating tracks guiding axonal regrowth [69]. This process can be recreated *in vitro* by generating Ephrin-B2 bands on growth matrix that organize Schwann cells into a band-like structure. Such directional guidance promoted axonal growth along the Schwann cell bands [69]. This strategy can certainly be adopted in NGC design to enhance the ability of Schwann cells to organize into Bands of Büngner, therefore enhancing directional axon regrowth. Gradients of NFs and adhesive molecules have also been employed in NGCs due to their ability to promote directional axonal growth and their enhancement of nerve regeneration and function compared to isotropic concentrations of similar molecules [26]. Dodla *et al.* incorporated gradients of nerve growth factor (NGF) and laminin into a NGC and

compared the results of various combinations of NGCs containing isotropic concentrations of the two signaling molecules or combinations of isotropic and anisotropic concentrations. They found that functional recovery was significantly higher in the NGCs containing gradients of both laminin and NGF when compared to those containing isotropic concentrations of the two molecules [26]. Although the author did not include data for axon length, number, and myelination for the isotropic NGCs, the significant difference in functional recovery between isotropic and anisotropic NGCs demonstrates that gradients of NFs and adhesive molecules provide greater ability to promote axon regrowth across the lesion than their isotropic counterparts. Moreover, the gradient approach is capable of providing directional cues along the entire length of the lesion, both promoting growth from the proximal stump to the distal stump and allowing axons to grow into the distal stump and target tissue. The latter is of particular importance to avoid axonal entrapment within the NGC caused by the “candy store” effect.

The simple incorporation of a gradient does not necessarily ensure maximal regenerative capacity. Mortimer *et al.* created a model to predict the response of neurites to varying concentrations and gradients of NGFs. Their model predicted that both the gradient steepness and concentration range determine the regenerative capability of a NF gradient, a prediction confirmed by culturing DRG explants on collagen sheets printed with different NGF gradient concentration ranges and steepnesses [19]. Not only does this paper demonstrate the importance of multiple variables of a NF gradient, but it also provides a means to better predict the optimal conditions with which to develop and apply a NF gradient to a NGC. In addition, variation in nerve response to gradients depends upon the location of the injury [70], and the type of nerve can determine which NFs may provide

the greatest regeneration effect [12, 71]. This characteristic of NFs enables high specificity in nerve regeneration by selecting NF cocktails tailored for a particular nerve type. This approach may be advantageous to regenerate the desired nerve type and function and avoid formation of undesired nerve connections. Therefore, NF gradients provide an effective approach to improve the speed and directionality of nerve regrowth, which can synergize well with other nerve regeneration approaches.

1.2 Hypothesis and Specific Aims of the Thesis

Current gradient generation platforms are limited by the length of gradients which can be produced, lack of scalability, and poor control of gradient characteristics. Many gradient methods are specialized for the study of cell migration in gradients of short length scales (<1 mm), or limited to long-range (>1 cm) length scales due to limited control of gradient production and can only be used in large gap nerve injury models. The significant discrepancies in the scale at which current gradient can be produced results in the inability to develop *in vitro* gradient guidance platforms for screening NF gradients and gradient conditions for their efficacy in guiding neuronal and Schwann cell outgrowth which can be easily translated to *in vivo* gradient delivery platforms. To address this knowledge gap, we developed two unique gradient generation techniques, as described in **Chapter 2**. The first technique is a rapid, convection-driven method developed in collaboration with the Khademhosseini lab at MIT which is capable of generating NF gradients of tailorable concentration ranges and millimeter to centimeter length, which encapsulates the gradients in a UV-crosslinkable methacrylated gelatin hydrogel. This method allows for rapid, scalable production of gradients over a large range of length scales and is a suitable platform for use in *in vitro* neuron and Schwann cell migration guidance assays for the

screening of the effects of gradient characteristics on migration behavior. Additionally, the ability to generate gradients of multi-centimeter length scales allows for utilization of this method to generate gradients for implantation in nerve guidance conduits for critical gap nerve injury (>10 cm) regeneration. The second method we developed is a diffusion-based method capable of gradient generation at centimeter scales in cell culture environments and is capable of generating gradients in a variety of hydrogel film materials for *in vitro* and *in vivo* delivery. Our first hypothesis is the rapid convection-based method can be utilized to for *in vitro* migration guidance assays investigating both aligned nanofiber topographical guidance and can be easily translated into our combinatorial NGCs for *in vivo* peripheral nerve regeneration. Our second hypothesis is that the diffusion-based platform will be an ideal model for investigating the mechanisms underlying the response of Schwann cells and neurons in 2D and 3D *in vitro* culture platforms.

After developing and characterizing the two gradient platforms, we found both gradient platforms exhibited excellent control over gradient characteristics and were able to utilize heparin conjugation to control the release of NFs from methacrylated gelatin hydrogels. Hydrogels generated by the convection-based platform were then incorporated into a novel cell migration chamber which cultures cells on aligned nanofibers of controllable diameters and which delivers NF gradients via gradient-loaded methacrylated gelatin hydrogel. In **Chapter 3**, we used these novel gradient/nanofiber chambers and developed a live-cell imaging and analysis program to evaluate the migration of Schwann cells in response to fibers of different diameters, gradients of different NFs, and different gradient steepness and concentration range conditions. Our hypotheses are (1) that there exists an optimal fiber diameter upon which Schwann cell migration rate will be

maximized, (2) that gradients of GDNF, NGF, and NRG1 will elicit different migration behavior, and (3) that Schwann cell migration kinetics will differ depending on gradient concentration and steepness.

While evaluating the migration response of Schwann cells in our combinatorial migration chambers, we found that Schwann cell migration rate was fastest on 1.2 μm diameter aligned fibers, GDNF elicited the strongest chemotactic response of the three NFs tested, and that both gradient steepness and concentration range were important characteristics in guiding Schwann cell directional migration *in vitro*. In **Chapter 4**, we evaluated the effect of GDNF gradient delivery in our combinatorial NGC in two *in vivo* models: (1) a 7-mm gap, rat sciatic nerve model which was used to evaluate the effect of gradient steepness on axonal growth and to select a gradient condition for the second model, (2) a canine peroneal nerve 20-mm gap model to evaluate the efficacy of GDNF gradient delivery in enhancing nerve regeneration across a critical nerve injury gap. We hypothesize that (1) gradient steepness is an important characteristic for enhancing *in vivo* nerve growth and (2) that delivery of GDNF as a gradient will enhance the regeneration of axons across a critical nerve injury gap and improve functional recovery compared to uniform GDNF delivery.

The following specific aims were pursued in this thesis to test the aforementioned hypotheses.

Aim 1 (Chapter 2): Develop platforms for generating/delivering diffusible NF gradients on 2D substrates and encapsulating gradients in 3D hydrogels as a gradient delivery vehicle for in vitro and in vivo cell migration and nerve regeneration.

Two gradient generation techniques were developed: (1) rapid, scalable method for *in vitro* and *in vivo* gradient delivery, and (2) diffusion-based method for generation of

gradients in live-cell, 2D and 3D migration platforms. The rapid, convection-based method was modified to improve scalability and release kinetics were controlled via heparin-conjugation. The diffusion-based platform was modeled using COMSOL and utility as a hydrogel-based gradient-loading method was established.

Aim 2 (Chapter 3): Establish live-cell imaging and cell migration analysis platform for investigating effects of growth factor gradient delivery and topographical guidance on the migration guidance of Schwann cells.

Schwann cell migration on aligned nanofibers and in response to gradients of GDNF, NGF, and NRG1 was tested in novel migration chambers. Live cell imaging and migration analysis was conducted to evaluate influence of nanofiber diameter and gradient characteristics on *in vitro* migration kinetics of Schwann cells.

Aim 3 (Chapter 4): Evaluate efficacy of NF gradient delivery in small and large animal in vivo peripheral nerve injury models.

GDNF gradients were incorporated into aligned nanofiber NGCs and evaluated for efficacy in improving *in vivo* peripheral nerve regeneration. Two gradient steepness conditions were evaluated for efficacy in an *in vivo* non-critical gap model to select most effective gradient for increasing axonal outgrowth. Gradient NGC was then tested in an *in vivo* critical gap defect model and evaluated for efficacy in improving axonal growth across entirety of critical gap and functional recovery.

1.3 Figures

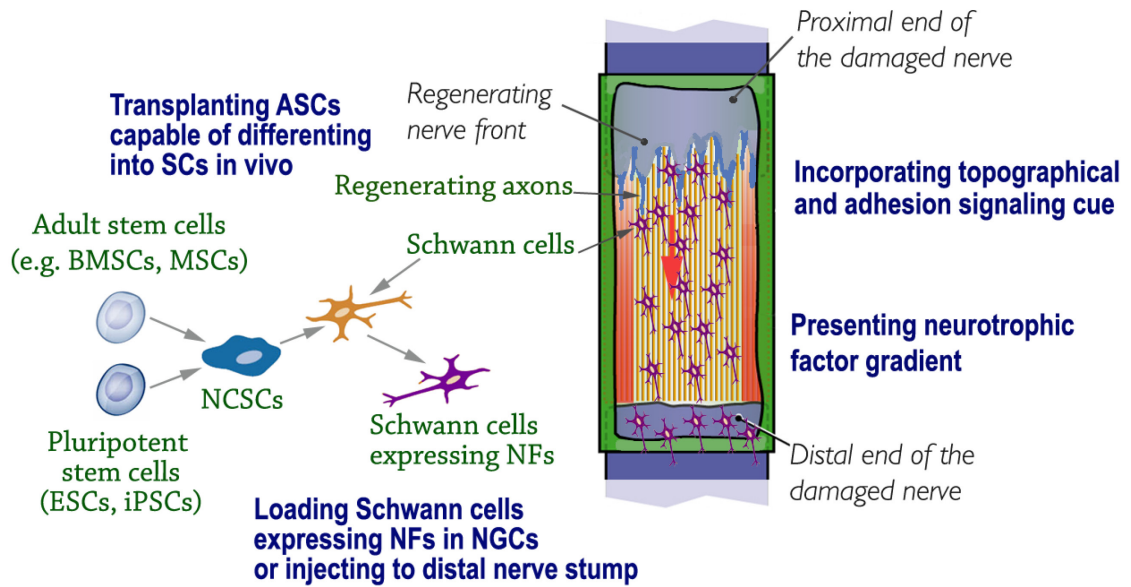


Figure 1.1: Signaling cue presentation and cell-incorporation approaches to enhance nerve regeneration. NGC functionality can be enhanced by incorporating (a) topographical and adhesion signaling, (b) neurotrophic factor (NF) gradients, (c) Schwann cells over-expressing NFs, and (d) adult stem cells such as mesenchymal stem cells (MSCs) and bone marrow-derived stromal cells (BMSCs). Figure reproduced by permission from Elsevier Publishers Ltd: *Current Opinion in Biotechnology*,⁸ copyright 2011.

1.4 References

1. Nerem, R.M. and A. Sambanis, *Tissue engineering: from biology to biological sciences*. Tissue Engineering, 1995. **1**(1): p. 3-13.
2. Harrison, R.H., J.P. St-Pierre, and M.M. Stevens, *Tissue engineering and regenerative medicine: a year in review*. Tissue Engineering: Part B, 2014. **20**(1): p. 1-16.
3. Lin, X., et al., *Tissue engineering and regenerative medicine in applied research: a year in review of 2014*. Tissue Engineering: Part B, 2015. **21**(2): p. 177-86.
4. Noble, J., et al., *Analysis of upper and lower extremity peripheral nerve injuries in a population of patients with multiple injuries*. Journal of Trauma-Injury Infection Critical Care, 1998. **45**(1): p. 116-122.
5. Belkas, J.S., M.S. Shoichet, and R. Midha, *Peripheral nerve regeneration through guidance tubes*. Journal of Neurological Research, 2004. **26**: p. 151-160.
6. Evans, G.R., *Peripheral nerve injury: a review and approach to tissue engineered constructs*. Anatomical Record, 2001. **263**(4): p. 396-404.
7. Kehoe, S., X.F. Zhang, and D. Boyd, *FDA approved guidance conduits and wraps for peripheral nerve injury: a review of materials and efficacy*. Injury, 2012. **43**(5): p. 553-72.
8. Krick, K., et al., *Signaling cue presentation and cell delivery to promote nerve regeneration*. Current Opinion in Biotechnology, 2011. **22**(5): p. 741-6.
9. Cordes, S.P., *Molecular genetics of cranial nerve development in mouse*. Nature Reviews Neuroscience, 2001. **2**: p. 11-23.

10. Levi-Montalcini, R., *The Nerve Growth Factor: Thirty-Five Years Later*. Bioscience Reports, 1987. **7**(9): p. 681-699.
11. Bueker, E.D., *Implantation of tumors in the hind limb field of the embryonic chick and the developmental response of the lumbosacral nervous system*. Anatomical Record, 1948. **102**(3): p. 369-389.
12. Hoke, A., et al., *Schwann cells express motor and sensory phenotypes that regulate axon regeneration*. Journal of Neuroscience, 2006. **26**(38): p. 9646-55.
13. Herrup, K. and E.M. Shooter, *Properties of the beta-nerve growth factor receptor in development*. Journal of Cell Biology, 1975. **67**: p. 118-125.
14. Diamond, J., et al., *Evidence that endogenous beta nerve growth factor is responsible for the collateral sprouting, but not the regeneration, of nociceptive axons in adult rats*. PNAS, 1987. **84**(18): p. 6596-6600.
15. Gloster, A. and J. Diamond, *Sympathetic nerves in adult rats regenerate normally and restore pilomotor function during an anti-NGF treatment that prevents their collateral sprouting*. Journal of Comparative Neurology, 1992. **326**: p. 363-374.
16. Campenot, R.B., *Local control of neurite development by nerve growth factor*. PNAS, 1977. **74**(10): p. 4516-4519.
17. Letourneau, P.C., *Chemotactic response of nerve fiber elongation to nerve growth factor*. Developmental Biology, 1978. **66**: p. 183-196.
18. Gundersen, R.W. and J.N. Barrett, *Neuronal chemotaxis: chick dorsal-root axons turn toward high concentrations of nerve growth factor*. Science, 1979. **206**(4422): p. 1079-1080.

19. Mortimer, D., et al., *A Bayesian Model predicts the response of axons to molecular gradients*. PNAS, 2009. **106**(25): p. 10296-10301.
20. Catig, G.C., S. Figueroa, and M.J. Moore, *Experimental and computational models of neurite extension at a choice point in response to controlled diffusive gradients*. Journal of Neural Engineering, 2015. **12**(4): p. 046012.
21. Cao, X. and M.S. Shoichet, *Defining the concentration gradient of nerve growth factor for guided neurite outgrowth*. Journal of Neuroscience, 2001. **103**(3): p. 831-840.
22. Kapur, T.A. and M.S. Shoichet, *Immobilized concentration gradients of nerve growth factor guide neurite outgrowth*. Journal of Biomedical Materials Research Part A, 2003. **68A**(2): p. 235-243.
23. Anton, E.S., et al., *Nerve growth factor and its low-affinity receptor promote Schwann cell migration*. PNAS, 1994. **91**(7): p. 2795-2799.
24. Rich, K.M., et al., *Nerve Growth Factor Enhances Regeneration through Silicone Chambers*. Experimental Neurology, 1989. **105**: p. 162-170.
25. Xu, X., et al., *Peripheral nerve regeneration with sustained release of poly(phosphoester) microencapsulated nerve growth factor within nerve guide conduits*. Biomaterials, 2003. **24**(13): p. 2405-2412.
26. Dodla, M.C. and R.V. Bellamkonda, *Differences between the effect of anisotropic and isotropic laminin and nerve growth factor presenting scaffolds on nerve regeneration across long peripheral nerve gaps*. Biomaterials, 2008. **29**(1): p. 33-46.

27. Madduri, S., et al., *Effect of controlled co-delivery of synergistic neurotrophic factors on early nerve regeneration in rats*. *Biomaterials*, 2010. **31**(32): p. 8402-9.
28. Wood, M.D., et al., *Heparin-binding-affinity-based delivery systems releasing nerve growth factor enhance sciatic nerve regeneration*. *Journal of Biomaterials Science*, 2010. **21**(6-7): p. 771-87.
29. Tang, S., et al., *The effects of gradients of nerve growth factor immobilized PCL scaffolds on neurite outgrowth in vitro and peripheral nerve regeneration in rats*. *Biomaterials*, 2013. **34**(29): p. 7086-96.
30. Fine, E.G., et al., *GDNF and NGF released by synthetic guidance channels support sciatic nerve regeneration across a long gap*. *European Journal of Neuroscience*, 2002. **15**: p. 589-601.
31. Kemp, S.W., et al., *A novel method for establishing daily in vivo concentration gradients of soluble nerve growth factor (NGF)*. *Journal of Neuroscience Methods*, 2007. **165**(1): p. 83-8.
32. Unezaki, S., et al., *Effects of neurotrophic factors on nerve regeneration monitored by in vivo imaging in thyl-YFP transgenic mice*. *Journal of Neuroscience Methods*, 2009. **178**(2): p. 308-15.
33. Tannemaat, M.R., et al., *Differential effects of lentiviral vector-mediated overexpression of nerve growth factor and glial cell line-derived neurotrophic factor on regenerating sensory and motor axons in the transected peripheral nerve*. *European Journal of Neuroscience*, 2008. **28**(8): p. 1467-79.
34. Hoyng, S.A., et al., *A comparative morphological, electrophysiological and functional analysis of axon regeneration through peripheral nerve autografts*

- genetically modified to overexpress BDNF, CNTF, GDNF, NGF, NT3 or VEGF.*
Experimental Neurology, 2014. **261**: p. 578-93.
35. Boyd, J. and T. Gordon, *Glial cell line-derived neurotrophic factor and brain-derived neurotrophic factor sustain the axonal regeneration of chronically axotomized motoneurons in vivo.* Experimental Neurology, 2003. **183**(2): p. 610-619.
36. Braun, S., et al., *Neurotrophins increase motoneurons' ability to innervate skeletal muscle fibers in rat spinal cord-human muscle cocultures.* Journal of the Neurological Sciences, 1996. **136**: p. 17-23.
37. D., S.G., et al., *Neurotrophin-3-enhanced nerve regeneration selectively improves recovery of muscle fibers expressing myosin heavy chains 2b.* Journal of Cell Biology, 1997. **139**(3): p. 709-715.
38. Ernfors, P., et al., *Expression of mRNAs for neurotrophin receptors in the dorsal root ganglion and spinal cord during development and following peripheral or central axotomy.* Molecular Brain Research, 1993. **17**: p. 217-226.
39. Airaksinen, M.S., et al., *Specific subtypes of cutaneous mechanoreceptors require neurotrophin-3 following peripheral target innervation.* Neuron, 1996. **16**: p. 287-295.
40. Falls, D., *Neuregulins: functions, forms, and signaling strategies.* Experimental Cell Research, 2003. **284**(1): p. 14-30.
41. Marchionni, M.A., et al., *Glial growth factors are alternatively spliced erbB2 ligands expressed in the nervous system.* Nature, 1993. **362**: p. 312-318.

42. Chen, L. and C.-P. Ko, *Extension of synaptic extracellular matrix during nerve terminal sprouting in living frog neuromuscular junctions*. Journal of Neuroscience, 1994. **14**(2): p. 796-808.
43. Mahanthappa, N.K., E.S. Anton, and W.D. Matthew, *Glial growth factor 2, a soluble neuregulin, directly increases Schwann cell motility and indirectly promotes neurite outgrowth*. Journal of Neuroscience, 1996. **16**(15): p. 4673-4683.
44. Li, H., G. Terenghi, and S.M. Hall, *Effects of delayed re-innervation on the expression of c-erbB receptors by chronically denervated rat Schwann cells in vivo*. Glia, 1997. **20**: p. 333-347.
45. Carroll, S.L., et al., *Expression of neuregulins and their putative receptors, ErbB2 and ErbB3, is induced during Wallerian degeneration*. Journal of Neuroscience, 1997. **17**(5): p. 1642-1659.
46. Buj-Bello, A., et al., *GDNF is an age-specific survival factor for sensory and autonomic neurons*. Neuron, 1995. **15**: p. 821-828.
47. Ebendal, T., et al., *Glial cell line-derived neurotrophic factor stimulates fiber formation and survival in cultured neurons from peripheral autonomic ganglia*. Journal of Neuroscience Research, 1995. **40**: p. 276-284.
48. Baloh, R.H., et al., *Artemin, a novel member of the GDNF ligand family, supports peripheral and central neurons and signals through the GFRalpha3-RET receptor complex*. Neuron, 1998. **21**: p. 1291-1302.
49. Henderson, C.E., et al., *GDNF: a potent survival factor for motoneurons present in peripheral nerve and muscle*. Science, 1994. **266**(5187): p. 1062-1064.

50. Hoke, A., et al., *A decline in glial cell-line-derived neurotrophic factor expression is associated with impaired regeneration after long-term Schwann cell denervation*. Experimental Neurology, 2002. **173**(1): p. 77-85.
51. Matheson, C.R., et al., *Long-term survival effects of GDNF on neonatal rat facial motoneurons after axotomy*. NeuroReport, 1997. **8**: p. 1739-1742.
52. Trupp, M., et al., *Complementary and overlapping expression of glial cell line-derived neurotrophic factor (GDNF), c-ret proto-oncogene, and GDNF receptor-alpha indicates multiple mechanisms of trophic actions in the adult rat CNS*. Journal of Neuroscience, 1997. **17**(10): p. 3554-3567.
53. Zhao, Z., et al., *Overexpression of glial cell line-derived neurotrophic factor in the CNS rescues motoneurons from programmed cell death and promotes their long-term survival following axotomy*. Experimental Neurology, 2004. **190**(2): p. 356-72.
54. Cornejo, M., et al., *Effect of NRG1, GDNF, EGF and NGF in the migration of a Schwann cell precursor line*. Neurochemical Research, 2010. **35**(10): p. 1643-51.
55. Hoke, A., C. Cheng, and D. Zochodne, *Expression of glial cell line-derived neurotrophic factor family of growth factors in peripheral nerve injury in rats*. NeuroReport, 2000. **11**(8): p. 1651-1654.
56. Hoke, A., et al., *Glial cell line-derived neurotrophic factor alters axon Schwann cell units and promotes myelination in unmyelinated nerve fibers*. Journal of Neuroscience, 2003. **23**(2): p. 561-567.
57. Blits, B., et al., *Rescue and sprouting of motoneurons following ventral root avulsion and reimplantation combined with intraspinal adeno-associated viral*

- vector-mediated expression of glial cell line-derived neurotrophic factor or brain-derived neurotrophic factor*. *Experimental Neurology*, 2004. **189**(2): p. 303-16.
58. Santosa, K.B., et al., *Nerve allografts supplemented with schwann cells overexpressing glial-cell-line-derived neurotrophic factor*. *Muscle and Nerve*, 2013. **47**(2): p. 213-23.
59. Batchelor, P., *Macrophages and Microglia Produce Local Trophic Gradients That Stimulate Axonal Sprouting Toward but Not beyond the Wound Edge*. *Molecular and Cellular Neuroscience*, 2002. **21**(3): p. 436-453.
60. Lin, Y.C., et al., *Spatially controlled delivery of neurotrophic factors in silk fibroin-based nerve conduits for peripheral nerve repair*. *Annals of Plastic Surgery*, 2011. **67**(2): p. 147-55.
61. Bonner, J.F., et al., *Promoting directional axon growth from neural progenitors grafted into the injured spinal cord*. *Journal of Neuroscience Research*, 2010. **88**(6): p. 1182-92.
62. Taylor, L., et al., *Neurotrophin-3 gradients established by lentiviral gene delivery promote short-distance axonal bridging beyond cellular grafts in the injured spinal cord*. *Journal of Neuroscience*, 2006. **26**(38): p. 9713-21.
63. Magill, C.K., et al., *The differential effects of pathway- versus target-derived glial cell line-derived neurotrophic factor on peripheral nerve regeneration*. *Journal of Neurosurgery*, 2010. **113**(1): p. 102-9.
64. Wood, M.D., et al., *Fibrin gels containing GDNF microspheres increase axonal regeneration after delayed peripheral nerve repair*. *Regenerative Medicine*, 2013. **8**(1): p. 27-37.

65. Tajdaran, K., et al., *A glial cell line-derived neurotrophic factor delivery system enhances nerve regeneration across acellular nerve allografts*. *Acta Biomaterialia*, 2016. **29**: p. 62-70.
66. Kokai, L.E., et al., *Sustained growth factor delivery promotes axonal regeneration in long gap peripheral nerve repair*. *Tissue Engineering: Part A*, 2011. **17**(9-10): p. 1263-75.
67. Chew, S.Y., et al., *Aligned Protein-Polymer Composite Fibers Enhance Nerve Regeneration: A Potential Tissue-Engineering Platform*. *Advanced Functional Materials*, 2007. **17**(8): p. 1288-1296.
68. Moore, A.M., et al., *Controlled delivery of glial cell line-derived neurotrophic factor enhances motor nerve regeneration*. *Journal of Hand Surgery*, 2010. **35**(12): p. 2008-17.
69. Parrinello, S., et al., *EphB signaling directs peripheral nerve regeneration through Sox2-dependent Schwann cell sorting*. *Cell*, 2010. **143**(1): p. 145-55.
70. Vetter, I., Z. Pujic, and G.J. Goodhill, *The response of dorsal root ganglion axons to nerve growth factor gradients depends on spinal level*. *Journal of Neurotrauma*, 2010. **27**(8): p. 1379-86.
71. Lindsay, R.M., et al., *Neurotrophic factors: from molecule to man*. *Trends in Neuroscience*, 1994. **17**(5): p. 182-190.

Chapter 2 : Gradient Generation Platforms for *In Vitro* and *In Vivo* Neurotrophic Factor Delivery

2.1 Introduction

The pioneering work of Paul Letourneau provided the first evidence that neurons exhibit a chemotactic response to NF gradients, developing the first platform for studying axonal extension under well-defined NGF gradient conditions [1]. The study was concrete evidence that axonal migration can be directed through control of NF presentation. Since that study, numerous methods have been developed to improve our understanding of neuronal chemotaxis in efforts to utilize NF gradient delivery as a method for enhancing central and peripheral nerve regeneration [2-29]. Microfluidics-based methods offer excellent control of gradient characteristics and provide insight into neuronal guidance in short-range (<1 cm) *in vitro* gradients [7, 17, 18, 20, 29, 30], but suffer from the inability to scale the method to centimeter length scales relevant to *in vivo* nerve applications. Surface-immobilized gradient techniques provide a greater potential range of gradient lengths, but suffer from limited control of gradient concentration and restrict the influence of gradient presentation to only cells in direct contact with the gradient-immobilized surface [3, 4, 7, 24, 30, 31]. Gradients formed by mixing of NFs into electrospun or extruded fibers are capable of establishing long-range (>1 cm) macroscopic gradients for *in vivo* application, but suffer from a lack of localized gradient control limiting their efficacy for investigating *in vitro* neuronal guidance in response to finely-tuned gradient conditions [25, 26, 28]. Printing-based methods offer adequate gradient control and a range of length scales suitable for *in vitro* and *in vivo* gradient applications, but gradients are rapidly diminished after printing and the requirement for specialized printing machines

limits the potential scalability of the platform [10, 19, 22]. The lack of scalable gradient-generation techniques, which provide precision control of gradient characteristics and are capable of generation of stable centimeter-scale gradients has limited the advancement of our understanding of how localized gradient conditions effect macroscopic neuronal outgrowth on multi-centimeter scales. Furthermore, the limitations of current gradient generation platforms result in the specialization of the gradient generation techniques for either *in vitro* or *in vivo*-specific applications, limiting their capability to be utilized both as *in vitro* neuron guidance screening tools while being easily translated into *in vivo* nerve regeneration platforms.

In this chapter, we discuss the development of multiple gradient generation techniques capable of generating gradients with tailorable and well-controlled gradient characteristics, which provide scalable gradient production and are capable of delivery of gradients in both *in vitro* and *in vivo* gradient guidance platforms. First, we developed a rapid, convection-driven gradient generation technique in collaboration with the Ali Khademhosseini lab [32, 33] which provided tailorable, scalable gradient generation immobilized in a crosslinked methacrylated gelatin hydrogel for controlled delivery in *in vitro* and *in vivo* gradient guidance assays. By modifying the channel dimensions and changing the hydrogel composition, we were able to establish a scalable, controllable gradient generation platform with tailorable gradient release kinetics. We then discuss the development of a diffusion-based microfluidics gradient generation method capable of generation of centimeter-scale gradients under cell-friendly conditions for 2D and 3D tissue cultures. With this platform, we demonstrate the ability to generate stable centimeter-length gradients under shear-free conditions for high-throughput live-cell migration assays

in 2D and 3D culture conditions, which can be utilized for generating gradients in hydrogel films for *in vitro* and *in vivo* delivery.

2.2 Materials and Methods

2.2.1 Methacrylated gelatin synthesis

Methacrylated gelatin (MG) was prepared as described by Nichol *et al.* [33]. Type A porcine skin gelatin (Sigma) was dissolved in Dulbecco's phosphate buffered saline (DPBS, Gibco) at 10% (w/v) and heated at 60°C until dissolved. The solution was then reduced to 50°C and 1 mL of methacrylic anhydride was slowly added to the gelatin slurry at 0.5 mL/min while being stirred. The solution was reacted for 1 hour, after which the solution was diluted 5× with DPBS warmed to 40°C to stop the reaction. The mixture was then dialyzed in distilled water in 12 – 14 kDa cutoff dialysis tubing at 4°C for one week, with the dialysis solution being replaced daily. After one week, the MG solution was distributed into 50 mL conical tubes, frozen at -20°C, transferred to -80°C, and lyophilized until dry. The tubes were then stored at -20°C until ready for use.

2.2.2 Fabrication of microfluidic devices

All microfluidic devices were fabricated using standard soft-lithography methods. Photomasks with channel patterns were designed using Microsoft PowerPoint and printed on transparencies at 10,000 dpi resolution (In Tandem Design, Baltimore, MD). Master molds were prepared at 100 µm thickness by patterning a negative photoresist (SU-8 2050) on a silicon wafer. PDMS molds were prepared by curing pre-polymer (Sylgard 184, Kreyden) on the silicon masters. PDMS molds were prepared using a 10:1 ratio of elastomer to curing agent. The PDMS prepolymer solution was poured on the silicon master and baked at 80°C for 2 hours. The PDMS molds were then peeled off the silicon

master, and inlet and outlet of the microchannels were created for each channel using a 1 mm hole punch. Each microfluidic device consisted of a top PDMS channel and a bottom glass or TCPS slide or well.

2.2.3 Convection and diffusion-based microfluidics gradient platform

Gradients immobilized in MG were prepared by modifying the method originally described by Du *et al.* [32]. For gradient characterization, microfluidics channels of 100 μm height, 4 mm width, and 4 cm length were used. MG was dissolved in PBS at 5% (w/v) with 0.5% (w/v) Irgacure 2959 and heated to 37°C. PDMS channels were placed on glass slides and placed in a petri dish containing a damp paper towel soaked in water and warmed to 37°C on a hot plate. The PDMS channel was filled with warmed MG solution. A 200- μL droplet of MG was added to the outlet, and a 10- μL solution of MG containing the molecule of interest was added to the inlet. The petri dish was then covered and the gradients were allowed to generate for before crosslinking the MG using a UV lamp. After crosslinking, the channels were removed from the glass and the crosslinked gradient hydrogels were dried before use in *in vitro* or *in vivo* gradient delivery experiments. To characterize gradient formation, FITC-lysozyme was used as the molecule of interest in the inlet and gradients were visualized using a Typhoon Gel Reader.

Further modifications to the method were later made to increase the gradient generation throughput by reducing the channel size to 8 mm length by 2 mm width by 100 μm height and producing larger numbers of channels parallel to one another. Gradients were established similar to the method described above but using modified volumes of 100 μL solution at the outlet and 2 μL at the inlet. The smaller channels were used for

establishing gradients for *in vitro* migration cultures and were characterized using FITC-lysozyme fluorescent gradients visualized using a Typhoon Gel Reader.

2.2.4 Controlled release of growth factor gradients

Release studies were conducted by producing in 4 cm long MG hydrogels using the method described previously. Briefly, gradients of glial-derived neurotrophic factor (GDNF) were generated by loading 20 mg/mL GDNF in MG solution in the inlet, after which the gradients were immobilized in the MG by crosslinking the hydrogel with UV. Gradients were also prepared using GDNF co-loaded with methacrylated heparin (graciously provided by the Khademhosseini lab, Harvard-MIT) at 1:1 and 10:1 ratios of heparin to GDNF. All gels were dried and cut into 6 equal sized segments, with each segment being placed in separate wells of a 96 well plate, and 50 μ L of PBS was added to each well. The 96 well plate was sealed with parafilm and placed in a 4°C refrigerator. On days 1, 3, 7, and 14, the PBS was collected and replaced. After the release study was finished, a GDNF ELISA (R&D Systems) was used to measure the release of GDNF. GDNF ELISA values were compared to standards as instructed in the ELISA kit and measured in a plate reader.

2.2.5 Diffusion-based gradient generation platform

A novel diffusion-based gradient platform was developed for determining the effect of establishing centimeter-scale gradients in the presence of cells. Channels were microfabricated with the dimensions of 0.1 mm (height) \times 4 mm (width) \times 10 mm (length). PDMS was polymerized at a thickness of 5 mm and wells were bored at each end of the channel using a 3 mm hole punch. To generate gradients, the channels were placed on glass or TCPS and filled with PBS or media. The “inlet” was then sealed with a thin wafer of

PDMS and the “outlet” was filled with PBS or media. The “outlet” was then sealed with a thin PDMS wafer, the “inlet” on the wafer removed, and the “inlet” was filled with PBS or media containing the molecule of interest. The “inlet” was then sealed with a PDMS wafer and the gradient allowed to establish for 4-24 hours depending on the molecular weight of the molecule of interest. Gradients were characterized by establishing a gradient of FITC-lysozyme and imaged using a Typhoon Gel Reader.

2.2.6 Hydrogel loading using diffusion-based gradient generation technique

The diffusion-based platform described in 2.2.5 was modified to be able to encapsulate gradients in a large variety of hydrogel materials. Thin 500 μm PDMS films were polymerized between aluminum plates and cut into frames with outer dimensions of 14 mm (length) \times 8 mm (width) and inner frame dimensions of 10 mm (length) \times 4 mm (width). Hydrogel films of fibrin, collagen, MG, or hyaluronan-PEG were then polymerized in the frames to form 500- μm thick hydrogels films. For gradient characterization studies, collagen films were polymerized in the frames by mixing 8 parts chilled 10 mg/mL collagen type I, 1 part chilled 7.5% (w/v) sodium bicarbonate, and 1 part chilled 10 \times PBS, and pipetting the solution into separate frames before incubating at 37°C for one hour. The diffusion gradient channels were then placed over the hydrogel frame and gradients of FITC-lysozyme were established using the method described in section 2.2.5. As gradients established in the channels, they diffused into the underlying hydrogel, which could then be obtained for delivery of the NF gradient for *in vitro* or *in vivo* applications.

2.2.7 Data analysis

Gradient establishment in both methods was imaged using the Typhoon Gel Reader and fluorescence was analyzed using Image J. Fluorescence was compared against standards. Plots of GDNF release represent mean \pm Standard Error.

2.3 Results and Discussion

2.3.1 Microfluidics gradient characterization

In order to generate centimeter-scale gradients encapsulated in hydrogel films for *in vitro* and *in vivo* delivery, we have adopted a technique developed previously by Khademhosseini *et al.* [32]. This technique allows for the rapid (one hour or shorter) generation of gradients of tailorable concentration ranges and length scales ranging from millimeters to centimeters using a single microfluidics channel which are encapsulated within UV-crosslinked methacrylated gelatin strips (**Figure 2.1**). In brief, the gradient generation platform consists of a single microfluidics channel with a single inlet at outlet at each end of the channel. The channel is filled with a UV-crosslinkable hydrogel precursor solution. A large volume of hydrogel precursor solution is pipetted onto the outlet and a small volume of hydrogel solution containing the molecule of interest is pipetted onto the inlet. The differences in solution volume at the outlet and inlet causes a differences in surface tension which causes the small droplet at the inlet to be driven into the channel via convection-based flow, establishing a gradient. As the gradient generation continues, diffusion and backflow caused by evaporation at the inlet further elongates the gradient, allowing for greater control over the gradient characteristics. Once the gradients have been generated, the channel contents are exposed to UV light to crosslink the hydrogel and encapsulate the gradient in a hydrogel strip. The hydrogel can then be extracted from the

channel and placed in a variety of *in vitro* cell migration platforms or in nerve guide conduits for *in vivo* nerve regeneration. Use of methacrylated gelatin as the selected hydrogel material creates a highly-crosslinked hydrogel which provides prolonged release of NF and which is stable at physiological conditions [33].

Gradient length scales are easily tailored by controlling the channel dimensions and further modified by changing the amount of time the gradients are established or by changing the inlet volume. By controlling the concentration of NF pre-loaded into the channel and NF in the droplet placed at the inlet, linear gradients of controllable concentration ranges and length scales can be established, as seen in **Figure 2.2**. The ability to use this method to generate well-controlled gradients at multi-centimeter scales allows for translation of gradient delivery for *in vitro* migration assays similar to those established using microfluidics-based platforms [7, 17, 18, 20, 29, 30], but with the scalability and ability to transfer the gradients into NGCs for *in vivo* gradient delivery, which is currently only feasible using gradient techniques for which gradient characteristics are less defined [16, 25, 26, 28].

In addition to the multi-centimeter scale configuration originally developed by Khademhosseini *et al.*, we modified the technique to decrease the length scale and increase the gradient generation throughput by fabricating parallel channel arrays (**Figure 2.3**) with which we could simultaneously produce numerous gradient hydrogels on smaller scales for easier incorporation in our *in vitro* cell migration platforms. By increasing the scalability of this method, we can simultaneously establish numerous gradient-loaded hydrogels for gradient delivery for high-throughput *in vitro* NF gradient screening and to ease production of gradient-loaded NGCs. The scalability of this method exhibits a

substantial advantage compared to microfluidics-based methods [7, 17, 18, 20, 29, 30], printing-based methods [10, 19], segmented gradients [16], or gradients generated using gradient mixers [9, 13] or electrospinning and extrusion methods [25, 26, 28], which generally require gradients to be produced one at a time. An additional benefit of this method is that it requires only small volumes of NF solution (<20 μL) to produce centimeter-scale gradients. By developing a low-volume gradient generation method, minimal NF is wasted during the gradient generation process and a significantly greater number of gradients can be produced from one NF stock compared to other gradient generation platforms. Printing-methods require small droplet volumes on the nanoliter scale, but it is unclear as to how many droplets are required to generate a centimeter-scale gradient [10, 19, 22] and the limited scalability and gradient stability reduce the potential applicability of these methods. Gradient chambers [6, 8, 34] and gradient mixers [9, 13] are capable of generating controllable centimeter-scale gradients, but require significantly greater volumes of NF solution (100-1000 μL) to produce equivalent gradient characteristics. The high degree of gradient control at multi-centimeter length scales and ease of scalability make this gradient generation platform very unique in its capability for both short (<1 cm) and long (>1 cm) gradient generation for both *in vitro* and *in vivo* delivery that is difficult to achieve using other methods.

2.3.2 Release of gradients from methacrylated gelatin hydrogel

After loading of gradients into MG hydrogels, we needed to determine if NF gradients loaded into the MG hydrogels were released in a gradient-like fashion. We designed a release study investigating if GDNF was released in gradient hydrogels at rates that were proportional to the loading concentration within the different regions of the

hydrogel (i.e. differences between release rates in the high concentration regions versus the low concentration regions). Briefly, we established GDNF gradients in triplicate in MG hydrogels and cut the hydrogels into six equal-sized segments. Each segment was placed in separate wells of a 96-well plate and immersed in PBS. The PBS solution was collected and replaced on days 1, 3, 7, and 14, and GDNF release into the solutions collected was measured by use of an ELISA. From our release studies, we were able to see that release rates from the hydrogels differed in the 6 regions of the hydrogels, with higher release rates occurring in the highest concentration regions of the hydrogel and decreasing with decreasing GDNF loading (**Figure 2.4**). The greatest percentage of release was on day 1 with gradient release continuing for at least 14 days. After the 14 days, the hydrogels largely remained intact and much of the initial GDNF loaded in the hydrogels remained sequestered within the hydrogels.

Additionally, we tested whether incorporation of methacrylated heparin into the MG hydrogels during the GDNF loading phase altered the release rate of GDNF from the hydrogels. For this release study, methacrylated heparin was mixed with GDNF at 1:1 or 10:1 ratios of heparin to GDNF and allowed to bind for 1 hour before pipetting the heparin/GDNF solutions onto the inlet of their respective gradient channels. Hydrogels were sectioned into six equal sized segments and the release study was conducted as before. Methacrylated heparin was used to conjugate the heparin to the MG hydrogel and act as an additional method to sequester GDNF to the hydrogel through heparin-GDNF binding. We initially hypothesized that the inclusion of heparin in the hydrogel formulation would reduce the release rate of GDNF from the MG hydrogel. Heparin-based controlled release systems have been used to prolong the release of NFs in nerve guides to enhance the

therapeutic efficacy of NF delivery [35-37]. However, from this study, we saw that the inclusion of heparin increased the rate of release from our hydrogels (**Figure 2.5**) compared to MG hydrogels without heparin. The release rate was actually highest for the highest concentration of methacrylated heparin. One possible explanation is that the inclusion of methacrylated heparin decreases the crosslinking density of the MG hydrogel by competitively conjugating to the methacrylate groups on the gelatin. Even though heparin itself is capable of binding to GDNF and slowing release, the data indicate that the potential decrease in crosslinking density offsets any benefits of heparin binding and causes a faster rate of release from the hydrogel. Due to these findings, future studies using MG hydrogels in *in vitro* and *in vivo* gradient delivery experiments did not include the use of methacrylated heparin in the formulations in order to provide more sustained release of NF from the hydrogels.

2.3.3 Diffusion-based gradient generation platform characterization

In addition to making modifications to the microfluidics-based convection-driven gradient method for *in vitro* cell migration studies, we developed a convection-free, tailorable, scalable gradient generation platform capable of creating NF gradients in the presence of cultured cells. Our gradient platform relies primarily on the diffusion of NFs in a microfabricated channel between a “source” and “sink” well (**Figure 2.6**). In this setup, the channel is filled with media, PBS, hydrogel, or cell solution in order to seed cells at the base of the channel prior to gradient establishment. If studying a non-zero baseline concentration of growth factor, the baseline level of growth factor can be loaded at this step, or can be loaded at the next step of the process. After pre-filling the channel, one of the wells is sealed with a removable PDMS stamp. The unsealed “sink” well is filled with

media or PBS containing no growth factor or containing the baseline concentration of the growth factor. After filling the “sink” well, it is sealed with a removable PDMS stamp and the stamp on the “source” well is removed. The “source” well is then filled with the highest desired concentration of growth factor and sealed with a PDMS stamp. Concentration differences between the “source” and “sink” wells result in a diffusion gradient being established between the two wells over the course of 4 – 24 hours depending on the molecular weight of the molecule of interest (**Figure 2.7b**). During this time, a well-controlled linear gradient is established between the two wells, which can be easily modeled using COMSOL (**Figure 2.7a**). As seen in **Figure 2.7**, centimeter-scale gradients can be generated using this method, beyond the size limitations of most microfluidics-based designs [7, 17, 18, 20, 29, 30] while still maintaining excellent control of gradient characteristics for prolonged periods of time (>24 hours).

The use of the seal on the wells prevents gravity-driven flow from occurring in the channel after loading one of the wells, allowing the contents of each individual well to be replaced without disturbing the contents of the central channel or of the opposite well and keeping gradient generation convection-free. Convection-free gradient generation allows for the examination of the influence of gradients on shear-sensitive cell types, which would not be capable in flow-based systems [17, 32]. Neurons are known to be sensitive to shear and exhibit axonal retraction under excessive fluid shear conditions [17], for which convection-based gradient generation methods are not suitable. **Figure 2.8** shows human Schwann cells cultured in gradient-generation channels prior at different time points after gradient generation was begun. Cells were seeded in the channels before beginning the gradient generation process. As can be seen, cells were viable after 4 hours of gradient

generation (**Figure 2.8a**) and remained viable 18 hours after gradient generation began (**Figure 2.8b**). Diffusion-based gradient generation does not rely on convection or flow to generate gradient profiles, and therefore does not exert fluid shear on cells during the gradient generation process and making this method compatible with neurons and Schwann cell cultures. Although gradient generation using this method is slower than for the convection-driven method, the ease of gradient generation using this method allows for fast and simple generation of a high number of simultaneous samples, increasing the scalability of gradient generation and allowing for the simultaneous testing of many gradient conditions. The scalability of this method provides a major advantage over methods for which gradient production must occur sequentially [7, 9, 10, 13, 16-20, 25, 26, 28-30]. Our diffusion-based gradient method, like the convection-driven gradient method, requires only small volumes of NF solution (<20 μL) to produce centimeter-scale gradients, using significantly lower volumes of NF and minimizing NF waste compared to comparable methods [6, 8, 9, 13, 34]. The volumetric efficiency of this method is incredibly important when using expensive NFs or drug compounds.

2.3.4 Use of diffusion-based gradient generation method for establishment of gradients in hydrogel films

In addition to being able to form gradients directly in the channel using our novel diffusion-based gradient generation method, we are able to utilize this method to establish gradients within hydrogel films using a wide variety of hydrogel materials. Hydrogel films are first formed within PDMS frames of tailorable dimensions. First, a thin PDMS sheet is created by polymerizing Sylgard 184 monomer and crosslinker at 10:1 mass ratio between aluminum plates, using double-sided tape to control the spacing of the plates and allowing

for easy control of PDMS sheet thickness. PDMS frames are then cut to the desired dimensions from the sheet. Hydrogels can then be polymerized within the frames to produce thin frames of hydrogels with easily tailorable dimensions, and a wide variety of hydrogel materials can be used, including but not limited to collagen, methacrylated gelatin, fibrin, Matrigel, hyaluronic acid, and PEG-based materials. After the hydrogels are formed, gradient channels are placed over the PDMS frame and gradients are established using the method described in section 2.2.5. While the gradients form in the channel, the molecule of interest diffuses into the underlying hydrogel, simultaneously encapsulating the gradient in the hydrogel (**Figure 2.9**). Comparable gradient generation techniques which create hydrogel-based gradients suffer from the requirement for vastly higher volumes of NF (100-1000 μ L per sample) [6, 8, 9, 13, 16, 34] compared to our diffusion-based gradient method. Furthermore, this method has been adopted for functionalizing various other material platforms developed in our lab, including hydrogel-based electrospun fiber sheets (**Figure 2.10**), further demonstrating the extensive utility of this gradient generation technique.

In collagen hydrogels, the gradient generation in the channel and in the hydrogel was characterized by establishing gradients of FITC-lysozyme and imaging the channel and hydrogel before and after removal of the channel using a Typhoon Gel Reader. After four hours of gradient establishment, it can be seen that the gradients in the channels (**Figure 2.11a**) were transferred to the collagen hydrogel (**Figure 2.11b**), forming a highly linear gradient in the hydrogel film. The hydrogel film can then be dried and transferred for use in *in vitro* or *in vivo* gradient delivery platforms, similar to the hydrogel created using the convection-based gradient generation method. Using this method, we have begun

investigating guidance of motor neurons in an *in vitro* spinal cord organotypic model to demonstrate the influence of GDNF gradients on directional motor neuron outgrowth (**Figure 2.12**). Additionally, this method can be modified to generate gradients in the presence of cells cultured on hydrogel films. Cells can be pre-seeded within or on top of the hydrogel films prior to gradient generation, and live-cell 2D and 3D cell migration studies can be conducted using this gradient generation platform, further increasing the utility of this method. The technique of separately sealing the wells allows for simple replacement of “source” and “sink” well contents and for use in long-term gradient studies. An example is shown in **Figure 2.13** where dorsal root ganglion neurons were cultured on a Matrigel film in a 0-10 ng/mL NGF gradient for three days, with the contents of the “source” and “sink” wells being replenished daily. The DRGs demonstrated robust survival over the course of the 3 days and confirmed the viability of this platform for use in long-term, multi-day gradient migration assays.

2.4 Conclusions

We were able to establish two scalable gradient generation platforms which both demonstrate excellent control of gradient characteristics and are capable of generating centimeter-length gradients. The first method provides rapid, scalable, convection-based generation of multi-centimeter gradients encapsulated within a crosslinked methacrylated gelatin hydrogel for ease of *in vitro* and *in vivo* gradient delivery. By conjugation of methacrylated heparin, the release kinetics of the hydrogel can be tailored depending on the desired rate of release. The second method provides shear-free gradient generation, which demonstrates significant utility, capable of generating highly controlled, stable centimeter-length gradients in the presence of cells, can be used to establish gradients in

2D and 3D culture systems, and which is capable of long-term gradient culture. The combination of these two gradient techniques will provide significant insight into the influence of NF gradient delivery on neuron and Schwann cell guidance using *in vitro* live-cell migration to analyze cell migration kinetics and translating the gradients into our NGCs for *in vivo* nerve regeneration applications.

2.5 Figures

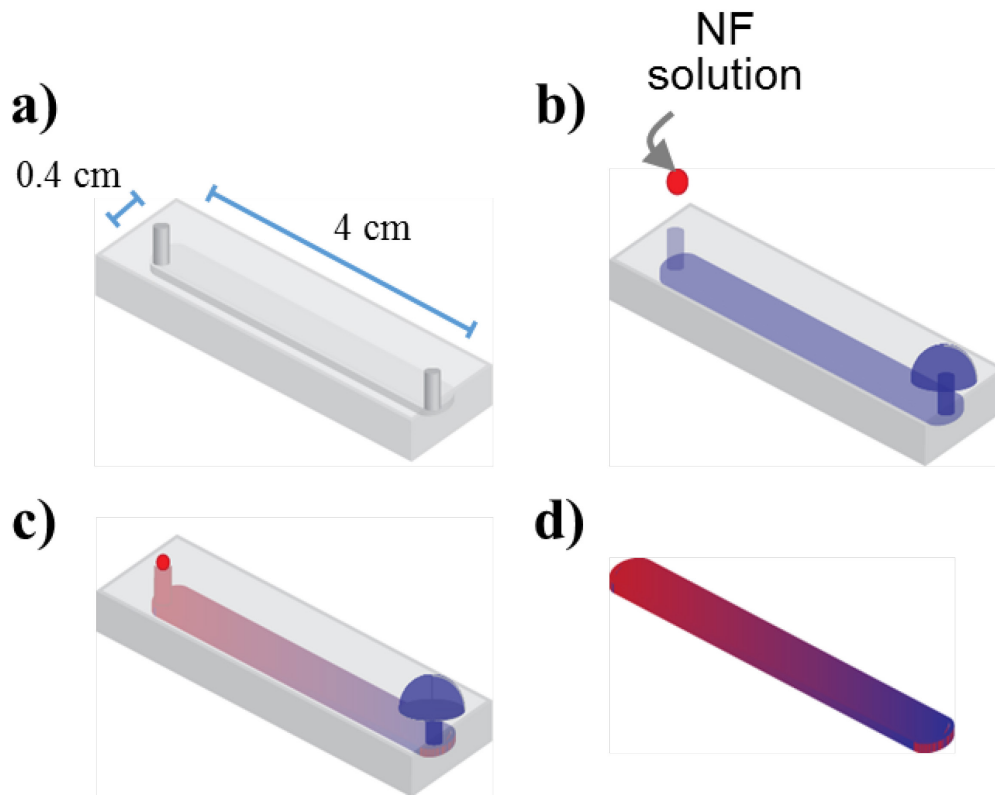


Figure 2.1: Rapid, convection-based gradient generation method. (a) Microfluidics channel with tailorable channel dimensions, channel height of 100 μm . (b) Channel is pre-filled with photocrosslinkable methacrylated gelatin (MG), large volume of MG is pipetted onto outlet, and small volume of NF pipetted onto inlet. (c) Surface tension drives convection-based flow of NF droplet into channel and establishes gradient. (d) After UV crosslinking, gradient is encapsulated in hydrogel.

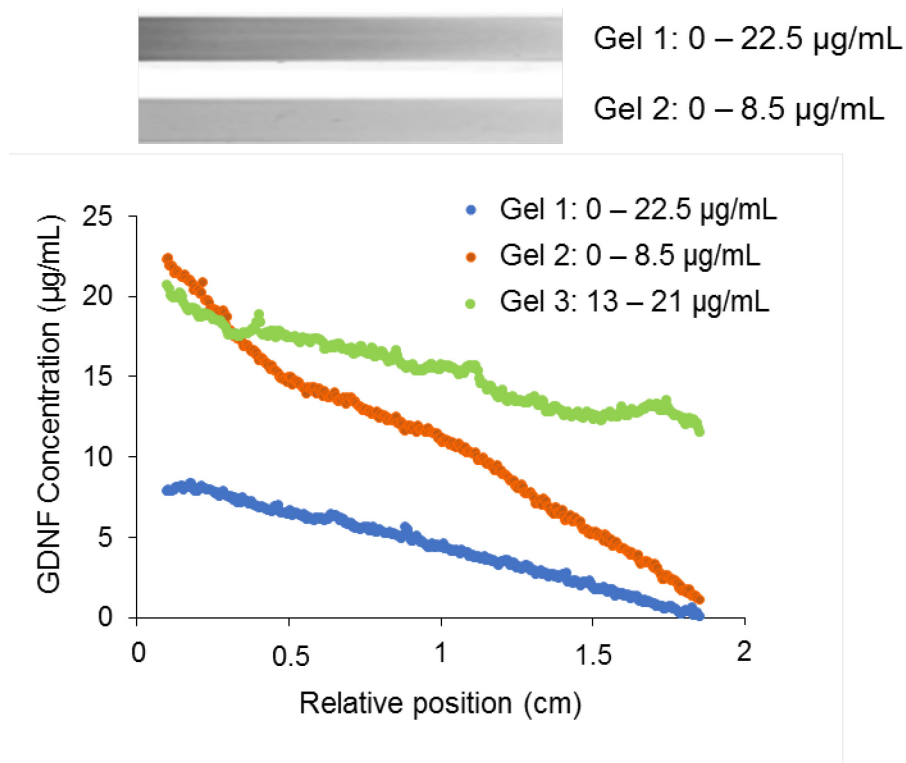


Figure 2.2: Generation of multi-centimeter scale gradients of FITC-lysozyme using convection-based gradient generation method with controllable gradient concentration and steepness.

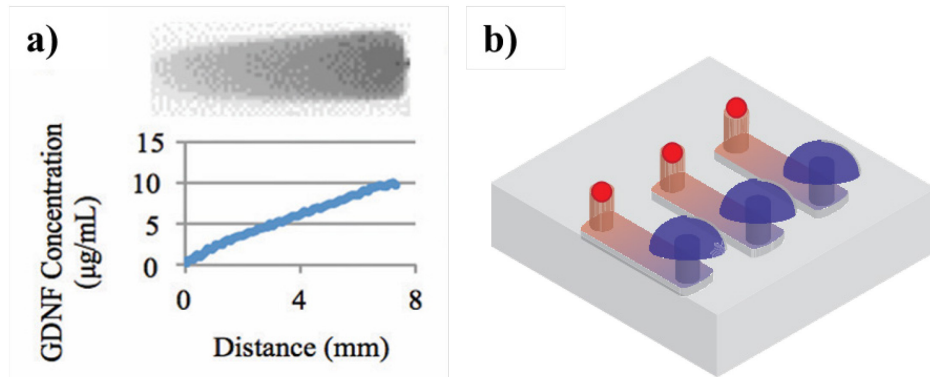


Figure 2.3: Gradient length can be tailored by modifying channel dimensions. (a) Gradient of FITC-lysozyme in 8 mm long channel. (b) Parallel channel configuration developed for increased scalability of gradient generation method.

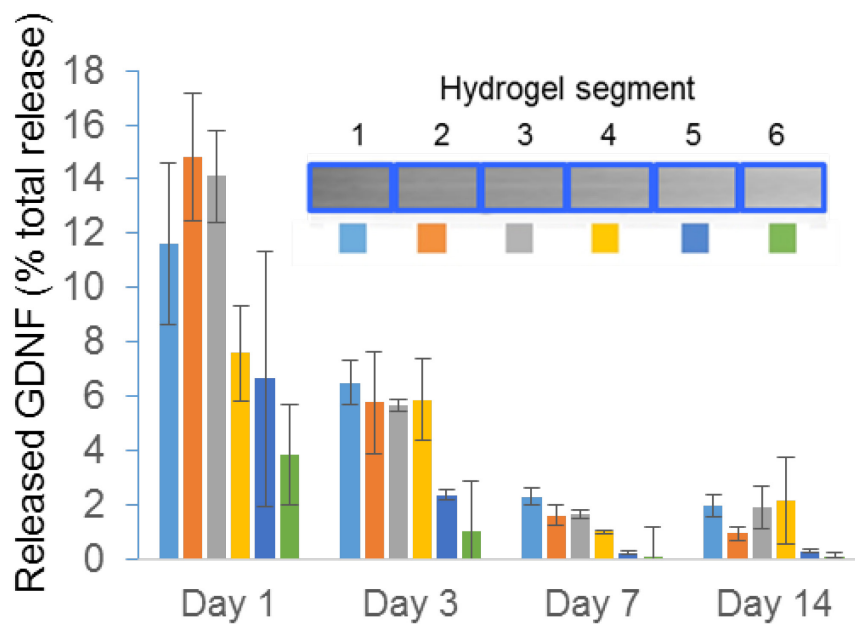


Figure 2.4: Gradient release from GDNF gradient-loaded hydrogel film (N = 3). Films were produced in triplicate and were sectioned into six pieces and release was measured using GDNF ELISA and compared to standards per ELISA instructions. Bar graph denotes mean \pm Standard Error.

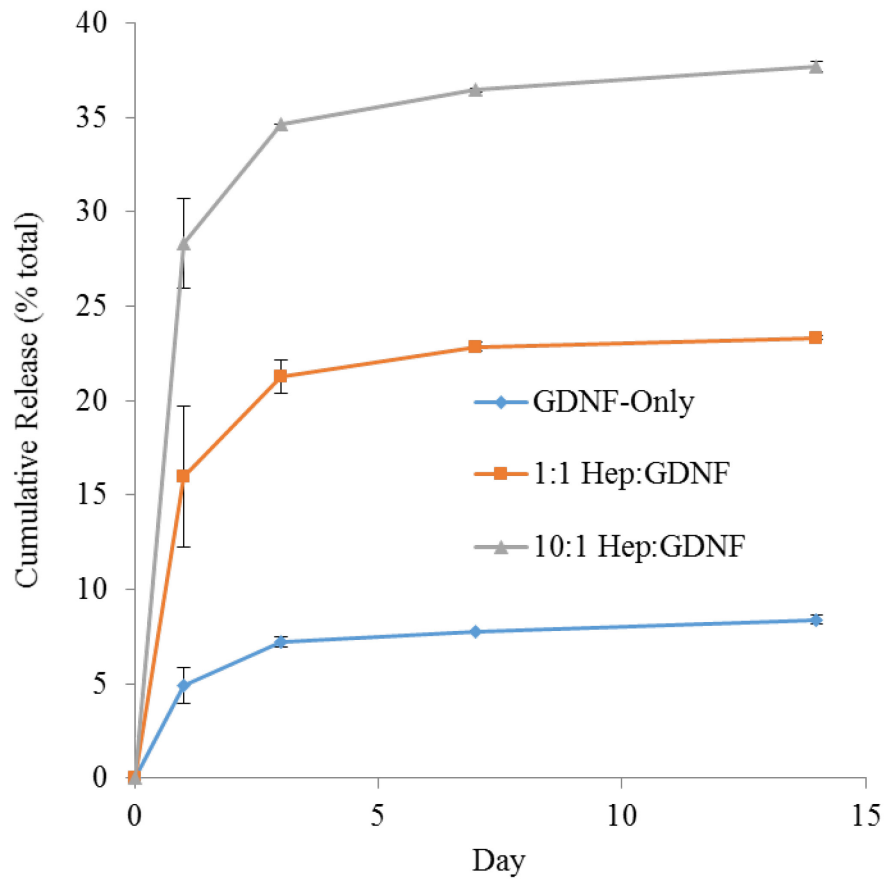


Figure 2.5: Cumulative release of GDNF from methacrylated gelatin with different levels of methacrylated heparin loading (N=3). Release was measured using GDNF ELISA and compared to standards per ELISA instructions. Error bars denote standard error.

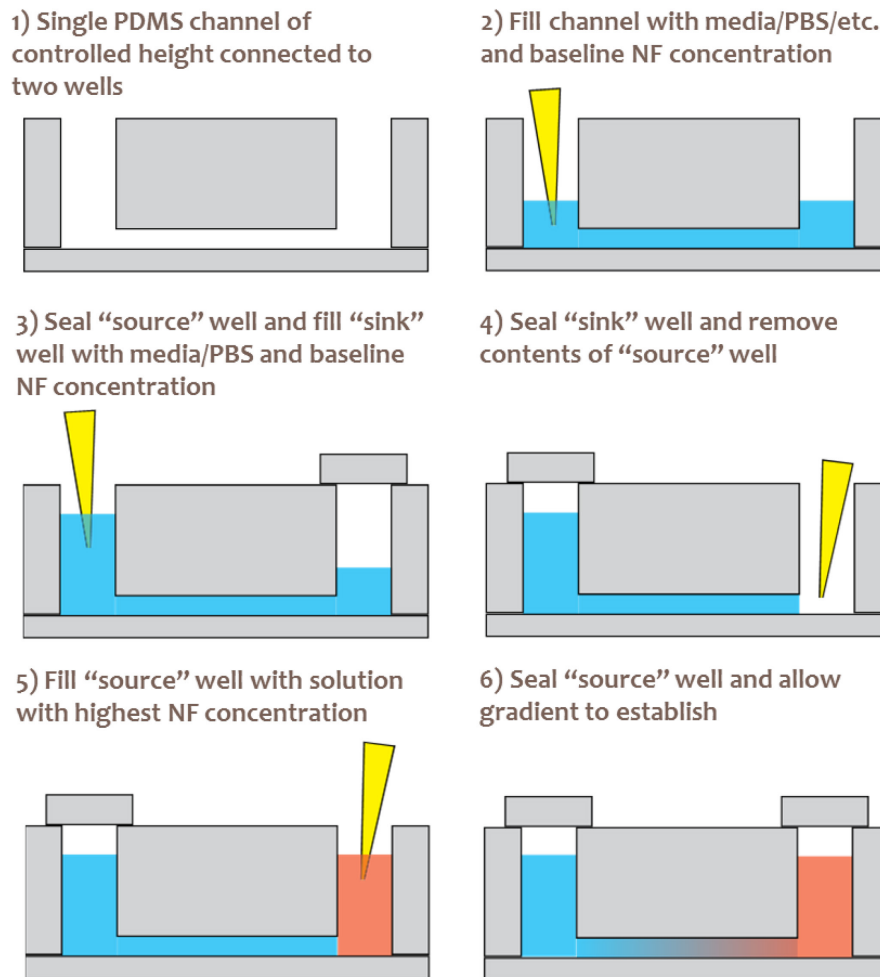


Figure 2.6: Diffusion-based gradient generation platform consisting of a microfluidics channel (10 mm length by 4 mm width by 100 μm height) with a 3 mm diameter "source" well and 3 mm diameter "sink" well. Channel is filled with media or PBS, and "source" and "sink" wells are filled with media/PBS or NF. Diffusion gradient establishes in channel due to differences in concentration between the "source" and "sink" wells.

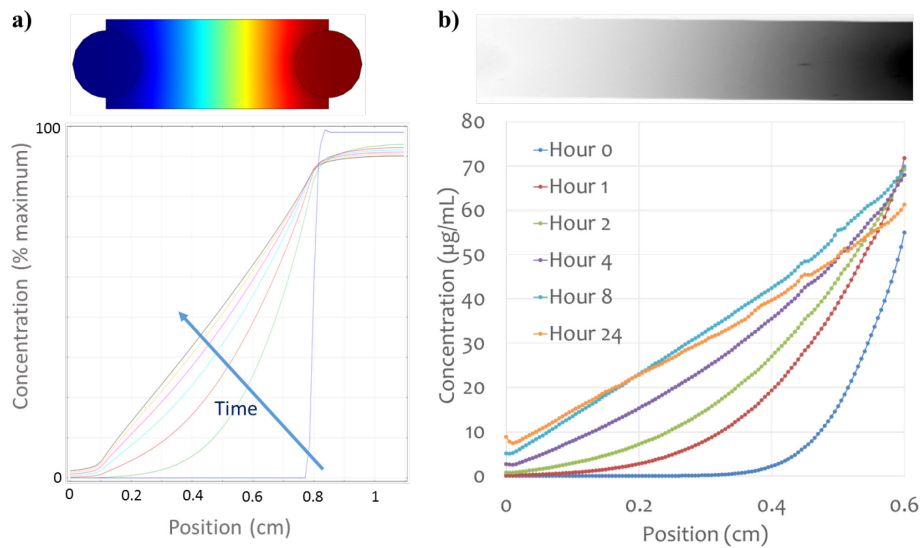


Figure 2.7: Time-progression of diffusion-based gradients. (a) COMSOL modeling of diffusion-based gradient generation platform showing time-course of gradient generation. (b) Experimental generation of FITC-lysozyme gradient in diffusion-based gradient channels. Gradient was measured using a Typhoon Gel Reader and compared against channel standards.

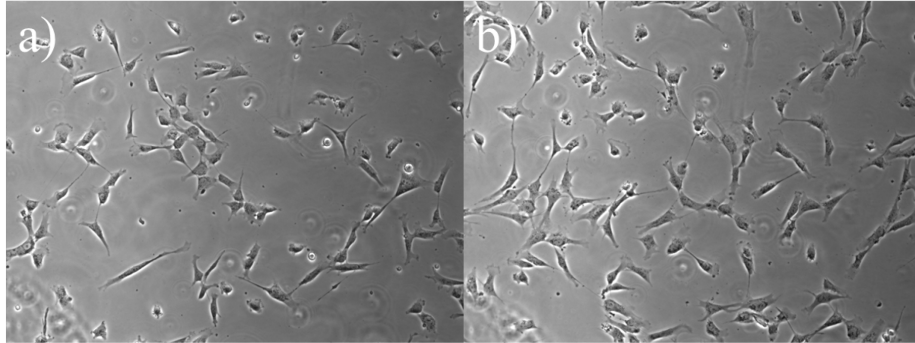


Figure 2.8: Human Schwann cell viability in diffusion-based gradient channel in 0-10 ng/mL NRG1 gradient. (a) Schwann cells were well-adhered 4 hours after beginning gradient generation. (b) Schwann cells remained viable for at least 18 hours after beginning gradient generation.

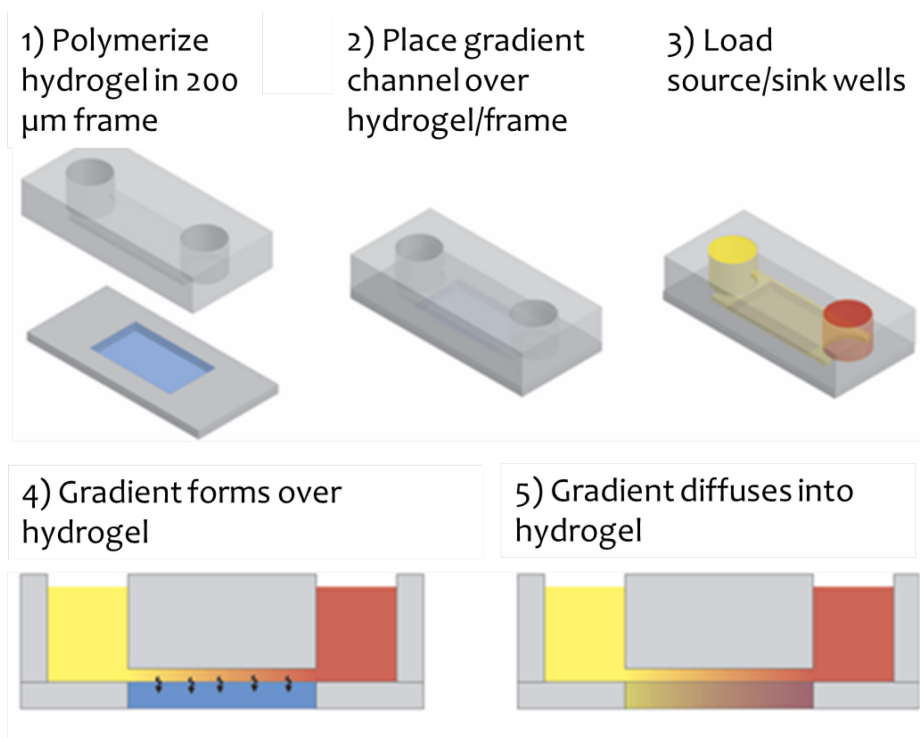


Figure 2.9: Modification of diffusion-based gradient generation platform for functionalization of hydrogel films. Hydrogel films (1 cm by 4 cm by 500 μm) are polymerized in PDMS frames. Gradient channels are placed over the films and gradients are generated in the channel, transferring to the underlying hydrogel film.

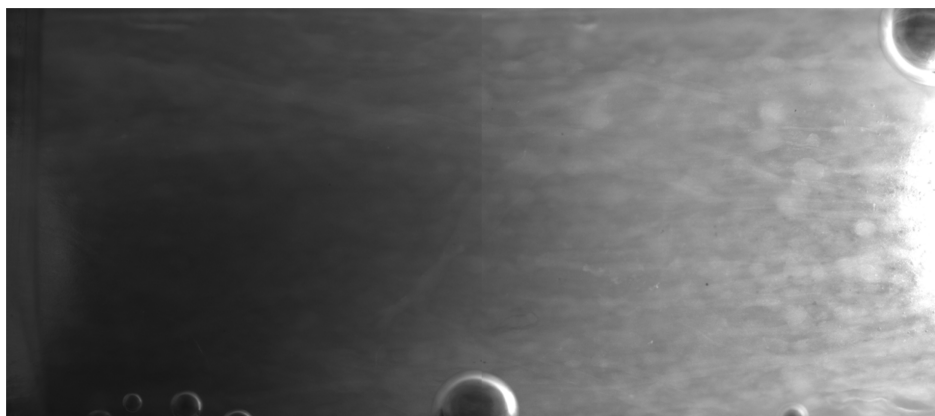


Figure 2.10: FITC-Lysozyme gradient in fibrin hydrogel fiber sheet generated using diffusion-based gradient generation method. High concentration (100 µg/mL) of FITC-Lysozyme located on the right end of the channel. Visualized using 2.5x objective on Nikon Inverted Fluorescence Microscope.

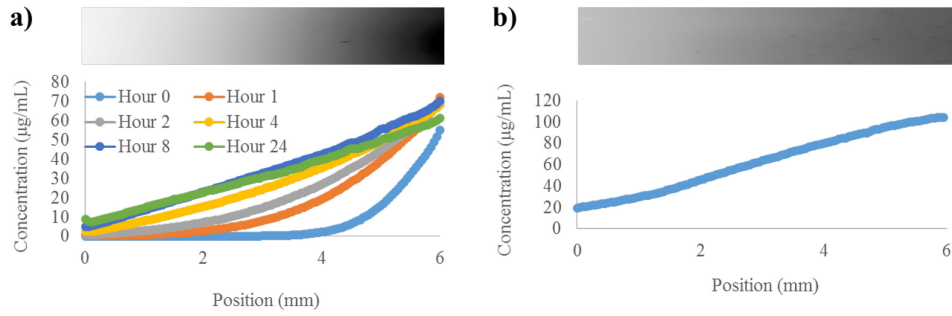


Figure 2.11: FITC-Lysozyme gradient generated in collagen hydrogel using diffusion-based gradient method. (a) Gradient in channel above hydrogel. (b) Gradient in collagen hydrogel after channel has been removed. Gradient was measured using a Typhoon Gel Reader and compared against hydrogel and channel standards.

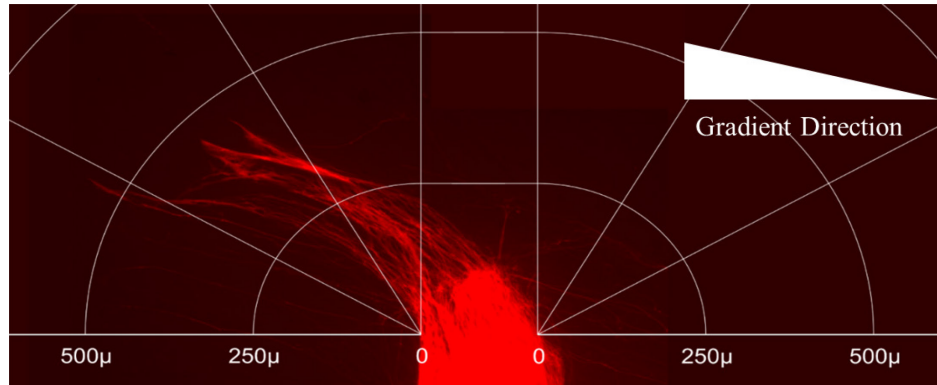


Figure 2.12: Directed motor neuron (red) migration in spinal cord organotypic culture on collagen hydrogel loaded with 0-1 ng/mL GDNF gradient using modified diffusion-based gradient method.

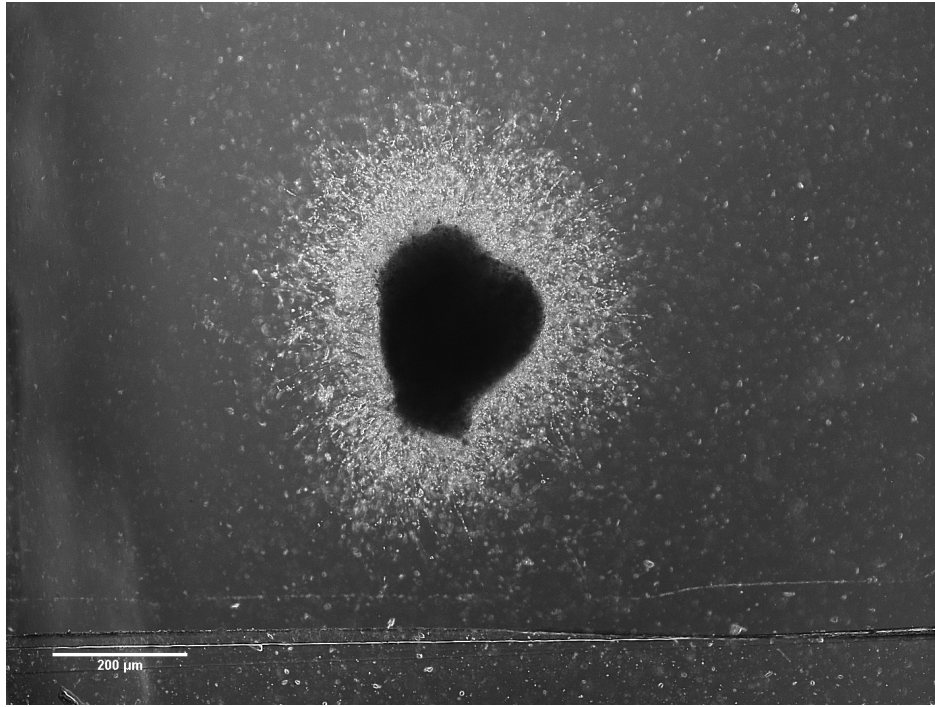


Figure 2.13: Dorsal root ganglion explants cultured on Matrigel, showing neuron survival and growth after 3 days in 0-10 ng/mL NGF gradient culture in modified diffusion gradient channels. Visualized using Nikon Inverted Microscope with 10x objective. Scale bar is 200 μm .

2.6 References

1. Letourneau, P.C., *Chemotactic response of nerve fiber elongation to nerve growth factor*. *Developmental Biology*, 1978. **66**: p. 183-196.
2. Zheng, J.Q., J.-j. Wan, and M.-m. Poo, *Essential role of filopodia in chemotropic turning of nerve growth cone induced by a glutamate gradient*. *Journal of Neuroscience*, 1996. **16**(3): p. 1140-1149.
3. Halfter, W., *The behavior of optic axons on substrate gradients of retinal basal lamina proteins and merosin*. *Journal of Neuroscience*, 1998. **16**(14): p. 4389-4401.
4. Rosentreter, S.M., et al., *Response of retinal ganglion cell axons to striped linear gradients of repellent guidance molecules*. *Journal of Neurobiology*, 1998. **37**(4): p. 541-462.
5. Zheng, M. and D.P. Kuffler, *Guidance of regenerating motor axons in vivo by gradients of diffusible peripheral nerve-derived factors*. *Journal of Neurobiology*, 2000. **42**(2): p. 212-219.
6. Cao, X. and M.S. Shoichet, *Defining the concentration gradient of nerve growth factor for guided neurite outgrowth*. *Journal of Neuroscience*, 2001. **103**(3): p. 831-840.
7. Dertinger, S.K.W., et al., *Gradients of substrate-bound laminin orient axonal specification of neurons*. *PNAS*, 2002. **99**(20): p. 12542-12547.
8. Cao, X. and M.S. Shoichet, *Investigating the synergistic effect of combined neurotrophic factor concentration gradients to guide axonal growth*. *Journal of Neuroscience*, 2003. **122**: p. 381-389.

9. Kapur, T.A. and M.S. Shoichet, *Immobilized concentration gradients of nerve growth factor guide neurite outgrowth*. Journal of Biomedical Materials Research Part A, 2003. **68A**(2): p. 235-243.
10. Rosoff, W.J., et al., *A new chemotaxis assay shows the extreme sensitivity of axons to molecular gradients*. Nature Neuroscience, 2004. **7**(6): p. 678-82.
11. Adams, D.N., et al., *Growth cones turn and migrate up an immobilized gradient of the laminin IKVAV peptide*. Journal of Neurobiology, 2005. **62**(1): p. 134-47.
12. Li, B., et al., *A technique for preparing protein gradients on polymeric surfaces: effects on PC12 pheochromocytoma cells*. Biomaterials, 2005. **26**(13): p. 1487-95.
13. Moore, K., M. Macsween, and M.S. Shoichet, *Immobilized concentration gradients of neurotrophic factors guide neurite outgrowth of primary neurons in macroporous scaffolds*. Tissue Engineering, 2006. **12**(2): p. 267-278.
14. Taylor, L., et al., *Neurotrophin-3 gradients established by lentiviral gene delivery promote short-distance axonal bridging beyond cellular grafts in the injured spinal cord*. Journal of Neuroscience, 2006. **26**(38): p. 9713-21.
15. Kemp, S.W., et al., *A novel method for establishing daily in vivo concentration gradients of soluble nerve growth factor (NGF)*. Journal of Neuroscience Methods, 2007. **165**(1): p. 83-8.
16. Dodla, M.C. and R.V. Bellamkonda, *Differences between the effect of anisotropic and isotropic laminin and nerve growth factor presenting scaffolds on nerve regeneration across long peripheral nerve gaps*. Biomaterials, 2008. **29**(1): p. 33-46.

17. Joanne Wang, C., et al., *A microfluidics-based turning assay reveals complex growth cone responses to integrated gradients of substrate-bound ECM molecules and diffusible guidance cues*. Lab on a Chip, 2008. **8**(2): p. 227-37.
18. Li, G.N., J. Liu, and D. Hoffman-Kim, *Multi-molecular gradients of permissive and inhibitory cues direct neurite outgrowth*. Annals of Biomedical Engineering, 2008. **36**(6): p. 889-904.
19. Mortimer, D., et al., *A Bayesian Model predicts the response of axons to molecular gradients*. PNAS, 2009. **106**(25): p. 10296-10301.
20. Sundararaghavan, H.G., et al., *Neurite growth in 3D collagen gels with gradients of mechanical properties*. Biotechnology and Bioengineering, 2009. **102**(2): p. 632-43.
21. Bonner, J.F., et al., *Promoting directional axon growth from neural progenitors grafted into the injured spinal cord*. Journal of Neuroscience Research, 2010. **88**(6): p. 1182-92.
22. Vetter, I., Z. Pujic, and G.J. Goodhill, *The response of dorsal root ganglion axons to nerve growth factor gradients depends on spinal level*. Journal of Neurotrauma, 2010. **27**(8): p. 1379-86.
23. Eggers, R., et al., *Lentiviral vector-mediated gradients of GDNF in the injured peripheral nerve: effects on nerve coil formation, Schwann cell maturation and myelination*. PLoS One, 2013. **8**(8): p. e71076.
24. Tang, S., et al., *The effects of gradients of nerve growth factor immobilized PCLA scaffolds on neurite outgrowth in vitro and peripheral nerve regeneration in rats*. Biomaterials, 2013. **34**(29): p. 7086-96.

25. Dinis, T.M., et al., *Method to form a fiber/growth factor dual-gradient along electrospun silk for nerve regeneration*. ACS Applied Materials and Interfaces, 2014. **6**(19): p. 16817-26.
26. Alsmadi, N.Z., et al., *Coiled polymeric growth factor gradients for multi-luminal neural chemotaxis*. Brain Research, 2015. **1619**: p. 72-83.
27. Catig, G.C., S. Figueroa, and M.J. Moore, *Experimental and computational models of neurite extension at a choice point in response to controlled diffusive gradients*. Journal of Neural Engineering, 2015. **12**(4): p. 046012.
28. Kim, S.E., et al., *Coextruded, aligned, and gradient-modified poly(epsilon-caprolactone) fibers as platforms for neural growth*. Biomacromolecules, 2015. **16**(3): p. 860-7.
29. Romano, N.H., et al., *Microfluidic gradients reveal enhanced neurite outgrowth but impaired guidance within 3D matrices with high integrin ligand densities*. Small, 2015. **11**(6): p. 722-30.
30. Hypolite, C.L., et al., *Formation of microscale gradients of protein using heterobifunctional photolinkers*. Bioconjugate Chemistry, 1997. **8**: p. 658-663.
31. Venkateswar, R.A., D.W. Branch, and B.C. Wheeler, *An electrophoretic method for microstamping biomolecule gradients*. Biomedical Microdevices, 2000. **2**(4): p. 255-264.
32. Du, Y., et al., *Rapid generation of spatially and temporally controllable long-range concentration gradients in a microfluidic device*. Lab on a Chip, 2009. **9**(6): p. 761-7.

33. Nichol, J.W., et al., *Cell-laden microengineered gelatin methacrylate hydrogels*. Biomaterials, 2010. **31**(21): p. 5536-44.
34. Dodla, M.C. and R.V. Bellamkonda, *Anisotropic scaffolds facilitate enhanced neurite extension in vitro*. Journal of Biomedical Materials Research Part A, 2006. **78A**(2): p. 213-221.
35. Wood, M.D., et al., *Heparin-binding-affinity-based delivery systems releasing nerve growth factor enhance sciatic nerve regeneration*. Journal of Biomaterials Science, 2010. **21**(6-7): p. 771-87.
36. Wood, M.D., et al., *Fibrin gels containing GDNF microspheres increase axonal regeneration after delayed peripheral nerve repair*. Regenerative Medicine, 2013. **8**(1): p. 27-37.
37. Tajdaran, K., et al., *A glial cell line-derived neurotrophic factor delivery system enhances nerve regeneration across acellular nerve allografts*. Acta Biomaterialia, 2016. **29**: p. 62-70.

Chapter 3 : Effect of Neurotrophic Factor Gradient Profile on Schwann Cell Migration in Culture

3.1 Introduction

Neuron guidance by controlled NF delivery, as described in chapter 1 and chapter 2, has been extensively investigated. However, little effort has been made in the guidance of Schwann cells, particularly through the use of topographical and biochemical gradients, to direct endogenous Schwann cell migration into the site of nerve injury to enhance the efficacy of regeneration. The presence and activity of Schwann cells is of great importance in enhancing nerve regeneration due to the numerous roles of Schwann cells in the nerve repair process, during which Schwann cells precede the axons into the lesion site secreting extracellular matrix tracks called bands of Büengner upon which regenerating axons grow [1-4]. It has been shown that Schwann cells, especially in the distal stump of the nerve injury, produce a cocktail of NFs to promote neuron survival and growth of regenerating neurons into the distal stump [1, 2]. Seggio *et. al.* demonstrated the capability for aligned Schwann cell monolayers to guide DRG neuron outgrowth in *in vitro* culture, illustrating the inherent proficiency of Schwann cells in directing axonal extension and regeneration [5]. By harnessing this natural capability of endogenous Schwann cells and increasing the rate of Schwann cell infiltration into a nerve injury gap, regeneration of the injured nerve may be enhanced by utilizing the mechanisms inherent in axon-glial interactions.

One potential method for guiding Schwann cell migration utilizes aligned topographical cues to constrain Schwann cell migration along a single axis. Daud *et. al.* compared the effects of 1, 5, and 8 μm diameter fibers on the migration of Schwann cells, neurons, and neuron-glia co-cultures [6]. It was shown that Schwann cells migrated the

furthest distance on 1 μm diameter fibers, significantly different than result for neurons which extended fastest on 8 μm diameter fibers. In co-cultures, Schwann cells formed a migration front upon with axons trailing behind, migrating preferentially on the Schwann cell basal lamina instead of the underlying fibers. One main limitation of the study was that they did not investigate cell migration on sub-micron diameter fibers to determine if there exists an optimal diameter range for promoting maximal Schwann cell migration rate and migration guidance. However, the study provided substantial evidence that neuronal outgrowth is largely dependent on Schwann cell migration and basal lamina production, and further strengthens the hypothesis that increasing Schwann cell migration into a nerve injury can enhance the regrowth of neurons into the injury site.

Schwann cell migration can also be influenced by the presence of exogenous NF. Paratcha *et al.* have previously shown GDNF to be a potent migratory stimulant for Schwann cells via co-association with GDNF receptor alpha-1 ($\text{GFR}\alpha 1$) and neural cell adhesion molecule (NCAM) [7]. While it has previously been shown that NGF conditioning of Schwann cells increases their motility [8], studies by Cornejo *et al.* using Schwann cell precursor cells showed limited chemotropic activity of NGF compared to GDNF and to a lesser degree, NRG-1 [9]. Certain soluble isoforms of NRG-1 are capable of increasing Schwann cell motility [10], but Cornejo *et al.* demonstrated that NRG-1 exhibits only modest chemotropic activity in Schwann cell precursors compared to GDNF and macrophage inhibitory factor, a known potent chemotropic agent for Schwann cells [9]. Additionally, NRG-1 has been shown to influence Schwann cell proliferation, especially at higher concentrations [11], which may limit its role as a chemoattractant *in*

in vivo NGCs where higher NF concentrations may be necessary to provide prolonged delivery of therapeutic concentrations of NFs.

In Chapter 3, we develop a novel migration chamber which combines topographical and biochemical gradient guidance with a live-cell imaging and analysis program to investigate the migratory response of human Schwann cells to different topographical and biochemical cues. We utilize the migration chamber to track and analyze the migration of thousands of cells simultaneously and compare the influence of fiber diameter, NF type, and NF gradient characteristics on the directed migration of Schwann cells. Here we report Schwann cell migration on a wide range of aligned electrospun fiber diameters ranging from 180 nm to 2 μ m to determine the optimal fiber diameter for use in subsequent *in vitro* cell migration models as well as for incorporation into NGCs which combine aligned nanofibers on the surface of the lumen as well as hydrogel-based NF gradient delivery. The migration platform is used to determine the efficacy of multiple NF and gradient conditions on Schwann cell guidance, eliciting the effects of NF type, gradient concentration range, and gradient steepness in the directional guidance of Schwann cells. Using this method, we gained tremendous insight into which topographical and NF gradient parameters promote optimal guidance of Schwann cells, which can be used to improve the design and function of NGCs capable of enhancing Schwann cell and neuron growth. This work also highlights the potential for utilizing this platform for the study of cell and tissue engineering fields beyond the realm of nerve regeneration.

3.2 Methods

3.2.1 Aligned nanofiber sheet preparation

Nanofiber sheets were generated using an electrospinning setup commonly utilized in our lab (Figure 3.1). In brief, polycaprolactone (PCL)-solvent solution is added to a 1-mL plastic syringe. A blunt-end 27-gauge needle is added to the syringe and the syringe is placed in a syringe pump (KD Scientific, Holliston, MA). The syringe pump is mounted on a linear stage (Newmark Systems, Rancho Santa Margarita, CA) to allow controllable deposition of polymer solution over the area of interest. The needle is connected to a DC power supply (Gamma High Voltage power supply, Ormond Beach FL) to generate a positive charge to the solution at the tip of the of the syringe needle. A rotating collection wheel (40 cm diameter) is placed at a controlled distance from the end of the needle and is attached an electrical ground. Rotation of the collection wheel is controlled by a Dayton DC Speed Control. Aligned fiber sheets are created on the surface of the rotating wheel by extruding PCL solution through the end of the needle and applying a charge to the solution, resulting in deposition of fibers on the rotating wheel surface. After deposition onto the wheel surface, fiber sheets are removed from the wheel and cut to the desired size for *in vitro* migration studies. Fiber diameter can be tailored by controlling the PCL-solvent composition, collection distance, and wheel rotation speed. With this method, fiber sheets can be manufactured with fiber diameters ranging from 180 nm to 8 μm .

3.2.2 Aligned fiber coverslip preparation for fiber diameter screening

Nanofiber coverslips were prepared by modification of the method described in section 3.2.1. Coverslips were taped to the spinning wheel and fibers were deposited on the surface of the coverslips. Fibers were immobilized to the surface of the coverslips by

pipetting Factor 2 silicone surgical glue onto the outer edges of the coverslips. After fiber immobilization, coverslips were sterilized via either 40 min exposure to UV in the biosafety hood or ethylene oxide sterilization. The coverslips were glued to the bottom of the 24-well plates with Factor 2 silicone surgical glue, which was allowed to vent overnight to remove residual solvent. The coverslips were then washed with PBS and coated for cell adhesion by soaking in 1/100 Matrigel solution overnight at 37°C. The coverslips were washed the following day with PBS and were equilibrated for 1 hour at 37°C with the cell media prior to adding the spheroids or single cells for live cell tracking.

3.2.3 Live-cell tracking of human Schwann cells on aligned nanofibers

Fetal-derived primary human Schwann cells were purchased from Sciencell (Carlsbad, CA). The Schwann cells were seeded for two days prior to experiment and exposed to 1 µg/mL Hoechst 33342 (Pierce) for 30 minutes prior to use. Cells were washed to remove unused Hoechst, trypsinized, resuspended in cell solution, and pipetted at a concentration of 1000 cells per well onto each coverslip and allowed to adhere for 6 hours prior to cell tracking. Cell migration was observed every 10 minutes for 12 hours using a live cell imaging microscope with programmable stage (Nikon) and environmental chamber (37°C, 5% CO₂, and 100%RH). Cell migration was analyzed using a custom cell tracking and analysis software package developed by our lab.

3.2.4 Combinatorial biochemical gradient and topographical guidance cell tracking platform

For NF gradient comparison experiments, hydrogels (1 cm in length) containing NF gradients of GDNF (0 to 1 µg/mL and 0 to 10 µg/mL), NGF (0 to 1 µg/mL and 0 to 10 µg/mL), and NRG-1 (0 to 1 µg/mL and 0 to 10 µg/mL) were prepared and placed on 15

mm coverslips. For GDNF steepness comparison experiments, hydrogels (1 cm in length) containing GDNF gradients (0 to 1 $\mu\text{g}/\text{mL}/\text{cm}$, 0 to 10 $\mu\text{g}/\text{mL}/\text{cm}$, or 0 to 20 $\mu\text{g}/\text{mL}/\text{cm}$) were prepared and placed on 15 mm coverslips. Aligned electrospun fibers were placed over the hydrogels and immobilized using factor 2 tissue glue. A custom PDMS migration channel (4 mm by 10 mm by 0.1 mm) was placed over the hydrogel/fiber construct. Primary human Schwann cells (ScienCell) were seeded for two days prior to experiment and exposed to 1 $\mu\text{g}/\text{mL}$ Hoechst 33342 (Pierce) for 30 minutes prior to use, washed with PBS, trypsinized, injected into the channel at 1000 cells per sample and allowed to adhere for 6 hours prior to cell tracking. Cell migration was observed using live cell imaging microscope with programmable stage (Nikon) and migration was analyzed using a custom cell tracking and analysis software package developed by our lab.

3.2.5 Cell tracking and analysis programming

Automated tracking of the cell images was done using the Trackmate plugin within the Fiji image processing program (Trackmate developed by Nick Perry, Jean-Yves Tinevez, Johannes Schindelin). Cells were identified by a Gaussian filter blob detection algorithm, and individual tracks were subsequently stitched together using a Linear Assignment Problem algorithm. Parameters for both detection and stitching algorithms were adjusted to optimize cell path quality on a file-by-file basis. Cell path attributes were calculated with a Matlab and Python-based routine developed in our lab using the spatiotemporal data outputted by Trackmate. Correlations of path attributes to local spatiotemporal areas were made by calculating weighted averages of attributes; the weights being the range of frames across which paths exist. Directionality for each cell is calculated

as follows: $Directionality = \frac{\sum \frac{Cell\ vector \cdot Field\ vector}{norm(Cell\ vector) \times norm(Field\ vector)}}{Number\ of\ frames}$, where “Cell vector” is the

positional vector a cell has moved in one frame and “Field vector” is the vector defined as the direction of the gradient. Error bars show average \pm Standard Error. Migration speeds are represented as average \pm Standard Error.

3.3 Results and Discussion

3.3.1 Effect of aligned fiber diameter on Schwann cell migration

Using a live-cell imaging platform allows us to monitor the migration of large populations of Schwann cells, at a single-cell level, to elucidate the influence of local environmental factors, such as surface topography and the presence of biochemical cues. We first began investigating the effects of aligned fiber diameter on Schwann cell motility, utilizing electrospinning techniques developed in our lab to compare a wide variety of fiber diameters, ranging from 180 nm to 2 μm . In order to image Schwann cells through optically opaque aligned fibers, the Schwann cells first had to be labeled with a nuclear stain, allowing for simple tracking of individual cells by increasing the signal contrast between the cells and the underlying fibers (**Figure 3.2**). By seeding labeled cells on coverslips coated in aligned fibers of different diameters and using our cell tracking and analysis platform to track cell migration over the course of 12 hours, we were able to determine that Schwann cell migration was most optimal on 1.2- μm diameter fibers (Figure 3.3a). Schwann cell migration speed was substantially higher on the 1.2- μm diameter fibers ($37.9 \pm 0.68 \mu\text{m/h}$) compared to smaller ($25.8 \pm 0.80 \mu\text{m/h}$) and larger diameter ($26.9 \pm 0.74 \mu\text{m/h}$) fibers (Figure 3.3b). This result was similar to the finding by Daud *et al.* who found Schwann cell migration was greatest at a diameter of 1 μm [6], but they did not compare fiber diameters below 1 μm . Further analysis of the fiber setup used by Daud *et al.* showed lower density of fibers than those used in our study. Whereas the Schwann

cells were largely restricted to single fibers in the Daud setup, Schwann cells in our migration platform showed preferential migration between multiple fibers regardless of fiber diameter. This disparity results in significant differences in maximum Schwann cell migration rate in our high density 1.2 μm fibers ($37.9 \pm 0.68 \mu\text{m/h}$) compared to that of the low density 1 μm fibers ($11.25 \mu\text{m/h}$) [6] in the setup by Daud *et. al.* Increasing the density of aligned fibers to allow attachment of Schwann cells to multiple adjacent fibers appears to result in increased migration rate compared to Schwann cells restricted to single fibers. This indicates that NGCs designed to increase Schwann cell infiltration should be designed with high aligned fiber densities in order to maximize the motility of Schwann cells migrating on the aligned fiber substrate.

Our results also demonstrate the existence of an optimal fiber diameter range for Schwann cell guidance in high-density fiber substrates. On fibers with an average diameter of below 1 μm , Schwann cell migration was slowed due to the ability for Schwann cells to transmigrate across multiple fibers and was not restricted to the migration axis dictated by the fiber alignment. Fibers with an average diameter of 1 μm and above successfully restricted cell migration along the fiber axis, but Schwann cell migration rate slowed on larger diameter fibers. Schwann cells tended to migrate fastest when migrating between parallel fibers, which was mostly possible for fibers with an average diameter of 1 μm and smaller. For larger diameter fibers, the Schwann cells were restricted to single-fiber migration, potentially resulting in slower migration rate. While we currently lack the mechanistic understanding behind these phenomena, the results gleaned from this experiment were useful in the design of studies incorporating aligned nanofibers into

biochemical gradient models and in the selection of fiber diameter for our aligned fiber NGCs.

3.3.2 Effect of NF type on Schwann cell migration

In order to investigate the influence of different types of NF types and gradient concentrations in Schwann cell guidance, we developed a novel migration chamber, which combined topographical guidance from aligned nanofibers with NF gradients delivered from methacrylated gelatin hydrogels (Figure 3.5). Gradients were generated in 1-cm long methacrylated gelatin hydrogels using the methods described in Chapter 2. The growth factors selected for comparison were glial-derived neurotrophic factor (GDNF), nerve growth factor (NGF), and neuregulin-1 (NRG-1), and 1 cm length gradients were generated for each NF with two concentration ranges, 0 – 1 $\mu\text{g/mL}$ and 0 – 10 $\mu\text{g/mL}$. Human Schwann cells were seeded within the migration chambers and incubated for 6 hours before observing cell migration for an additional 12 hours using a live-cell imaging microscope. The presence of aligned fibers in the migration chamber played an important role in the restriction of cell migration along a single axis, which simplified cell tracking and analysis and to better attribute any directional bias to the specific gradient conditions imposed on the cells.

After cell tracking and analysis, we were able to demonstrate that GDNF was the most potent NF in promoting directional Schwann cell migration (**Figure 3.6**) within the concentration ranges tested, with both the 0 – 1 $\mu\text{g/mL}$ and 0 – 10 $\mu\text{g/mL}$ gradients successfully promoting biased migration of the Schwann cells. The strong migrational bias elicited by GDNF gradients supplements the results from Paratcha *et al.* who have previously shown GDNF to be a potent migratory stimulant for Schwann cells [7]. NGF

and NRG-1 did not elicit a strong directional migratory response in human Schwann cells. Cornejo *et al.* showed limited chemotropism of Schwann cell precursors in response to NGF gradients [9], although there may exist a concentration-dependent effect on Schwann cell motility [8]. The limited directional guidance elicited by NRG-1 was also similar to the results by Cornejo *et al.*, who saw modest chemotropic activity in Schwann cell precursors in NRG-1 gradients with a maximum gradient concentration of 200 ng/mL (2 µg/mL/cm steepness) compared to GDNF gradients with equivalent concentration range [9]. While the chemoattractant effects of these NFs may differ depending on the Schwann cell maturity [9], these data suggest that GDNF is a suitable candidate for the study of gradient-based chemotropic guidance of Schwann cells. With its capability as both a potent Schwann cell chemoattractant and survival cue for motor neurons [12], much of our subsequent *in vitro* and *in vivo* research focused on the delivery of GDNF gradients and the influence of GDNF gradient characteristics on its tropic activity. However, it should be noted that chemotropic efficacy may vary significantly depending on the concentration range of the gradients presented [13-18], and different NFs may have different therapeutic concentration ranges. Future studies will need to consider these differences and investigate larger gradient concentration ranges in order to further optimize gradient migration guidance of Schwann cells.

3.3.3 Effects of GDNF gradient characteristics on chemoattractive activity

Given our findings demonstrating the efficiency of GDNF as a chemoattractant when delivered via gradient-loaded hydrogels, we utilized the combinatorial topographical and biochemical guidance migration chamber platform to investigate the effect of GDNF gradient steepness and concentration range on the guidance of Schwann cells. We

compared three gradient conditions of differing steepness configurations and concentration ranges, and evaluated the effect of different gradient characteristics on the migration guidance of human Schwann cells. One gradient condition ranged from 0 to 1 $\mu\text{g/mL}$ maximum concentration with 1 cm total length (1 $\mu\text{g/mL/cm}$ gradient steepness) while two gradient conditions (10 $\mu\text{g/mL/cm}$ and 20 $\mu\text{g/mL/cm}$) used the same maximum concentration (10 $\mu\text{g/mL}$) of GDNF but differed in gradient length (1 cm for the 10 $\mu\text{g/mL/cm}$ condition, 0.5 cm for the 20 $\mu\text{g/mL/cm}$ condition) allowing us to directly compare both the influence of gradient steepness as well as concentration range. Gradient concentrations were selected based on previous work by Cao *et. al.* who demonstrated dose-dependent PC12 migration in concentration ranges of 0.1 $\mu\text{g/mL}$ to 1 $\mu\text{g/mL}$ NGF [14] and Moore *et. al.* who demonstrated directional guidance in chick DRG neurons in gradients of maximum concentrations up to 50 $\mu\text{g/mL}$ [17], and gradient steepness was based on Cornejo *et. al.* which used 2 $\mu\text{g/mL/cm}$ steepness GDNF gradients for Schwann cell precursor guidance [9]. Taking into account potential differences between the therapeutic window of GDNF and differences between neuronal and Schwann cell guidance, we used intermediate GDNF concentrations between the ranges of those used for NGF and gradient steepness values comparable to those used to guide Schwann cell precursors.

Using our live-cell imaging and analysis platform, we evaluated the migration of thousands of Schwann cells migrating under different gradient conditions and analyzed their migration characteristics in response to the imposed gradients. **Figure 3.7a-c** show positional heat maps of the migration bias of each individual Schwann cell under different gradient conditions. Every dot on the heat map corresponds to the weighted average

directional bias of an individual Schwann cell and is placed at the exact point of origin from which each cell was tracked. In these maps, red corresponds to cells which migrate positively towards the high concentration of the gradient, and blue corresponds to cells which migrate against the concentration gradient. In comparing the three gradient conditions, the shallowest GDNF gradient (1 $\mu\text{g}/\text{mL}/\text{cm}$ steepness) exhibited the greatest level of directional bias of all gradient conditions, promoting a peak directional bias of 63% positive cell migration near the high concentration region of the gradient (**Figure 3.7d**). Peak directional bias decreased as gradient steepness increased, with a peak directional bias of 47% for the 10 $\mu\text{g}/\text{mL}/\text{cm}$ gradient condition and 41% for the 20 $\mu\text{g}/\text{mL}/\text{cm}$ gradient condition. Within the 1 $\mu\text{g}/\text{mL}/\text{cm}$ gradient condition, Schwann cell directional bias increased from 17% positive cell migration in the low concentration region of the gradient to the 63% positive cell migration in the highest concentration region of the gradient (**Figure 3.7d**), indicating a concentration range-dependent chemotactic response. In fact, this phenomenon was conserved within all gradient conditions (**Figure 3.7d-f**) regardless of maximum GDNF concentration or gradient steepness. Additionally, Schwann cell migration exhibited steepness-dependent migration in response to the different GDNF gradient conditions. This was most apparent in gradient regions containing GDNF concentrations near 1 $\mu\text{g}/\text{mL}$ (1 $\mu\text{g}/\text{mL}/\text{cm}$ – Region 6; 10 $\mu\text{g}/\text{mL}/\text{cm}$ – Region 1) (**Table 3.1**), where positive directional bias decreased with increasing steepness with 60% positive Schwann cell migration in the 1 $\mu\text{g}/\text{mL}/\text{cm}$ steepness gradient condition, and 31% positive Schwann cell migration in the 10 $\mu\text{g}/\text{mL}/\text{cm}$ steepness gradient condition. These data suggest Schwann cell guidance is strongly dependent on both the gradient concentration range as well as the gradient steepness. This result is consistent with research conducted

by Mortimer *et al.* demonstrating that concentration range and gradient steepness are both important determinants in the chemotropic effect of a NF gradient [18]. Interestingly, in the gradients with a maximum GDNF gradient concentration of 10 $\mu\text{g/mL}$, similar levels of positive directional guidance (>30% positive migration) were seen in gradient regions 3 – 6 (**Table 3.1**, **Figure 3.7e,f**), but differed substantially in the lowest concentration regions (regions 1&2) where the shallower gradient exhibited greater positive Schwann cell bias. These results indicate that effective GDNF concentration range may differ depending on the steepness of the gradient.

Further analysis of the migration shows that the gradient conditions significantly influence the distribution of Schwann cell migration bias (**Figure 3.8**). The distribution of the shallow GDNF gradient (**Figure 3.8a**) shows a relatively higher proportion of Schwann cells with a positive directional bias compared to cells in the higher concentration gradients (**Figure 3.8b,c**). However, there are also a higher proportion of Schwann cells that migrate against the gradient (**Figures 3.7 and 3.8**). When Schwann cells migrate on aligned fibers, they are able to migrate in two directions along the axis of the fibers. Some cells migrate in a single direction while others frequently switch direction of migration. In an environment where Schwann cells are exposed to a GDNF gradient, some cells oscillate (neutral) instead of migrating up the gradient (positive bias). However, there still exists a population of cells which began migrating against the gradient and maintain their path, thus appearing to migrate towards the low concentration (negative bias) unaffected by the gradient. **Figure 3.8** shows the population distribution of migration directionality in Schwann cells in the three gradient steepness conditions. The distributions demonstrate that the lowest steepness gradient condition provides the strongest positive directional bias

(43% of total cell population), but cannot prevent a subpopulation of cells (15% of total cell population) from continuing to migrate against the gradient. Schwann cells in the highest steepness gradient, while less likely to migrate against the gradient (7% of total cell population), demonstrate a high tendency (62% of total cell population) to remain in a neutral, oscillatory state, and lower tendency to exhibit positive cell migration (30% of total cell population). The steepest concentration gradient thus exhibits the narrowest distribution of Schwann cell migrational bias with a majority of the cells existing in a neutral migratory state (**Figure 3.8d**).

Additionally, both the steepness and concentration range influenced the migration rate of Schwann cells within the different gradient ranges. Cell migration rate was the highest for the 10 $\mu\text{g/mL}$ per cm gradient group ($12.0 \pm 0.11 \mu\text{m/h}$), but decreased as gradient steepness increased ($7.6 \pm 0.24 \mu\text{m/hr}$) (**Figure 3.9**). This result indicates that while Schwann cell migration rate can be increased by increasing GDNF gradient concentration, gradient steepness must be tailored to prevent the “candy store” effect, in which cells are unable to detect the existence of a gradient and the NF conditions are favorable preventing Schwann cell migration out of the gradient region [19].

The existence of optimal effective NF concentration range have been demonstrated in PC12 neurons [13, 15] and DRG neurons [14, 17, 18], but this is the first study, to our knowledge, that elucidates how NF gradient steepness and concentration range effect Schwann cell migration. While we gained tremendous insight into the use of NF gradients as a tool for guiding Schwann cell migration, further studies will be necessary to determine the optimal gradient conditions for maximizing directed Schwann cell migration. Current studies are ongoing which expand the cell tracking and analysis capability to the study of

neuron gradient guidance within our combinatorial platform. Although our migration channel platform is capable of providing significant insight into the influence of NF gradient delivery on single cell populations, it is important to consider how Schwann cells and neurons migrate under gradient conditions when in co-culture, which most closely mimics the conditions in an *in vivo* nerve injury. Further studies will be required to elucidate if axon-glia interactions modulate the response of Schwann cells and neurons to NF gradients by changing NF receptor expression via paracrine or juxtacrine signaling between neurons and glia. However, by creating a powerful gradient generation and migration analysis tool, we will be able to answer some of these questions in the near future and utilize the capabilities of our gradient generation and electrospun fiber platforms to develop the next generation of synthetic NGCs.

3.4 Conclusions

We successfully developed a novel combinatorial migration chamber platform with which we could investigate the effect of topographical and biochemical gradient guidance on the migration kinetics of human Schwann cells. Utilizing live-cell imaging microscopy, we tracked and analyzed the migration of thousands of individual Schwann cells in response to topographical and biochemical cues. We found that Schwann cell migration was the fastest on aligned nanofibers of a diameter of 1.2 μm , a fiber size that was selected for use in future *in vitro* and *in vivo* models. By incorporating gradient delivery into the migration platform, we determined GDNF to be the most potent chemoattractive NF for human Schwann cells, and demonstrated the importance of gradient steepness and concentration on the directional bias and migration rate of Schwann cells. This platform provides insight into important design parameters for creating NGCs containing NF

gradient delivery and nanofiber topographical guidance for improving the efficacy of *in vivo* nerve regeneration. Our platform is a powerful tool for investigating biochemical and topographical guidance, which has potential applications in a wide variety of cell and tissue engineering applications.

3.5 Figures and Tables

Maximum GDNF Concentration ($\mu\text{g/mL}$)			
Gradient Region	Gradient Steepness		
	1 $\mu\text{g/mL/cm}$	10 $\mu\text{g/mL/cm}$	20 $\mu\text{g/mL/cm}$
1	0.17	1.67	1.67
2	0.33	3.33	3.33
3	0.50	5.00	5.00
4	0.67	6.67	6.67
5	0.83	8.33	8.33
6	1.00	10.00	10.00

Table 3.1: Maximum GDNF concentration in different gradient regions based on loading concentration of GDNF in hydrogel.

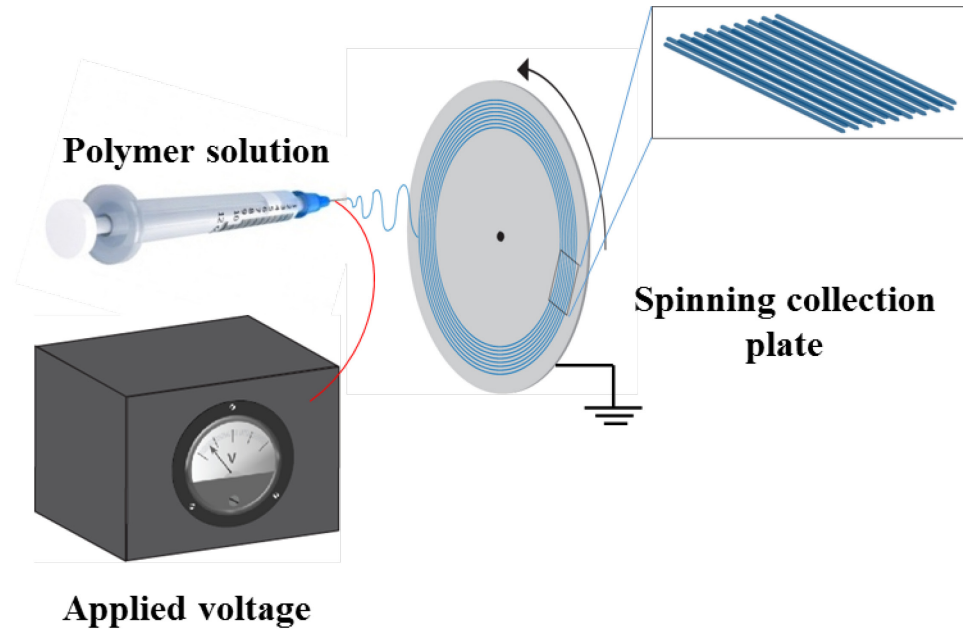


Figure 3.1: Schematic of electrospinning setup used to generate aligned nanofiber substrates. A voltage is applied to an extruded polymer solution, which is deposited onto an electrically-grounded spinning metal wheel, resulting in the formation of aligned, thin-fiber sheets.

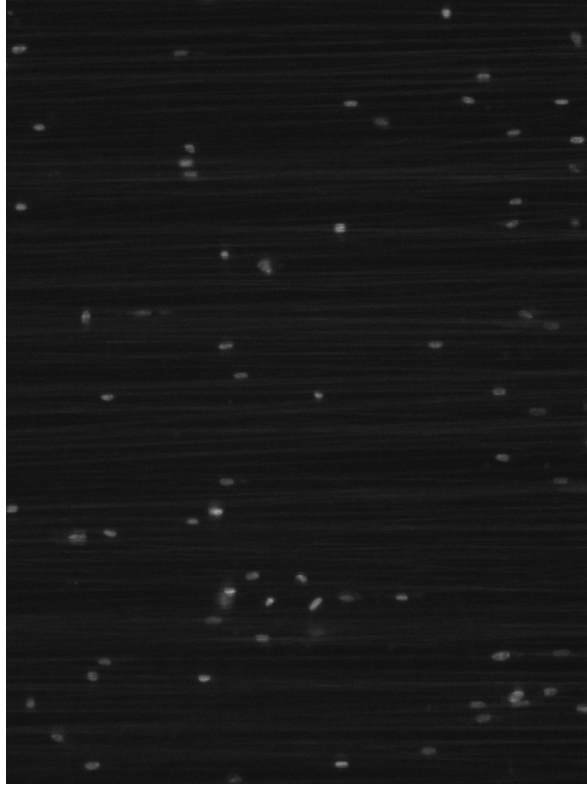


Figure 3.2: Human Schwann cells visualized on aligned nanofibers with fluorescence microscope. Cells are stained with Hoechst stain to increase contrast against underlying fiber substrate.

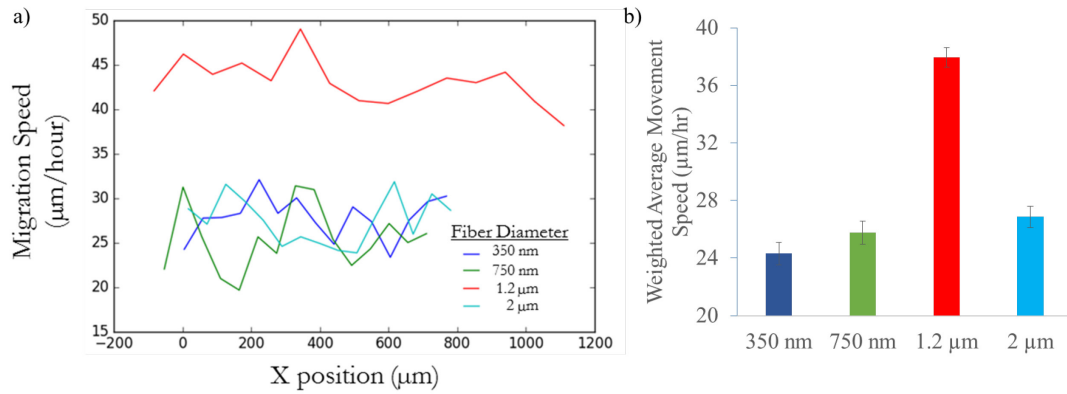


Figure 3.3: Average migration rate of human Schwann cells on aligned fiber sheets with different fiber diameters ($N > 1500$ cells). (a) Migration speed distribution of cells in different regions of fiber sheets. (b) Weighted average migration speed of cells. Error bars signify Standard Error.

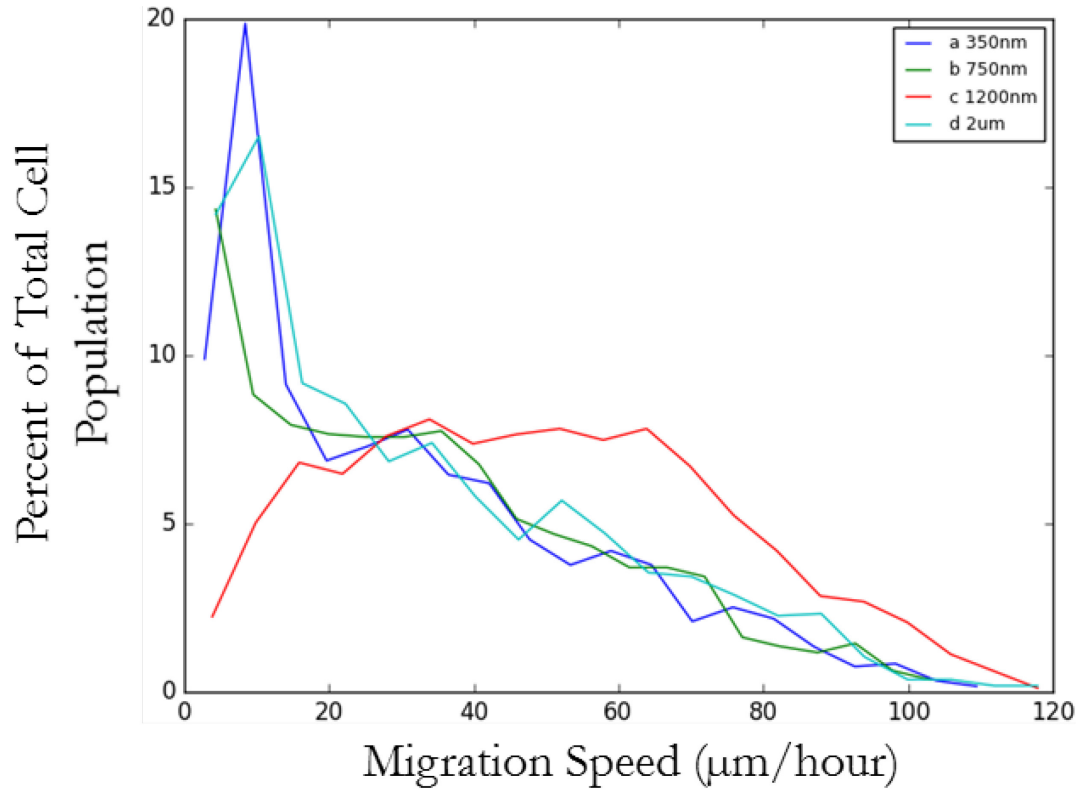
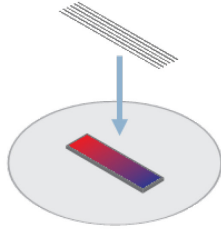
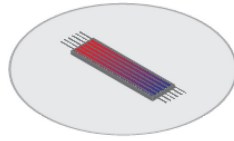


Figure 3.4: Population distribution of human Schwann cell migration speed on aligned fiber sheets with different fiber diameters ($N > 1500$ cells).

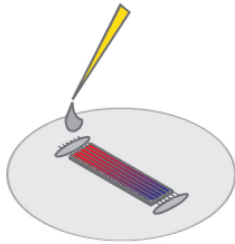
1) Place gradient hydrogel in well plate



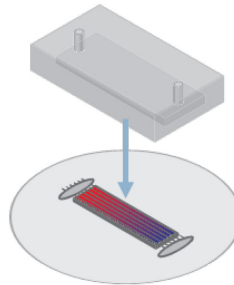
2) Place aligned fiber sheet on hydrogel



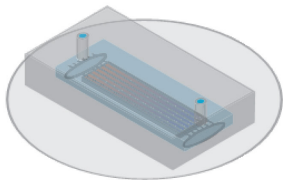
3) Immobilize fibers with tissue glue



4) Place migration channel over hydrogel and fibers



5) Flow cells into chamber



6) Observe cell migration

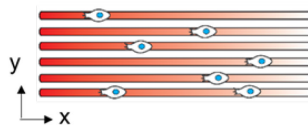


Figure 3.5: Schematic for production of combinatorial migration chambers incorporating aligned fiber topographical guidance and hydrogel-based NF gradient delivery for live-cell imaging and analysis.

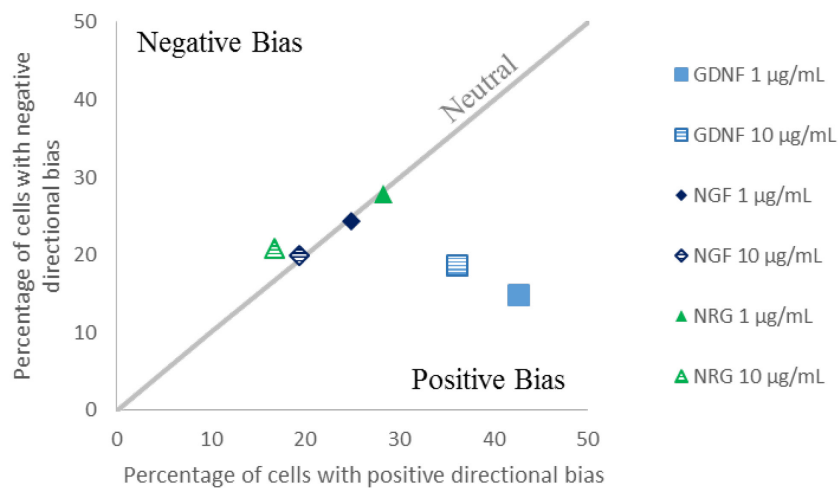


Figure 3.6: Human Schwann cell migration bias in response to gradients of GDNF, NGF, and NRG-1 (N>1000 cells).

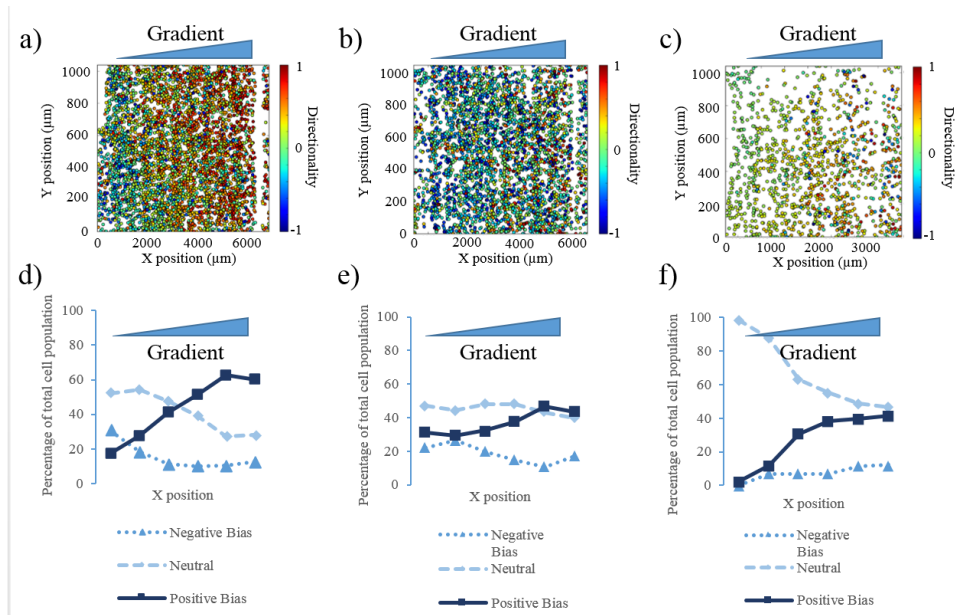


Figure 3.7: Directional guidance of human Schwann cell migration to GDNF gradients ($N > 1000$ cells). (a) Directional bias heat map of Schwann cells in $1 \mu\text{g/mL/cm}$ GDNF gradient. Dots represent position of cells in gradient. Red dots represent cells exhibiting positive directional bias. Blue dots represent cells exhibiting negative directional bias. (b) Directional bias heat map of Schwann cells in $10 \mu\text{g/mL/cm}$ GDNF gradient. (c) Directional bias heat map of Schwann cells in $20 \mu\text{g/mL/cm}$ GDNF gradient. (d) Percent of negative, neutral, or positive migrating cells in different regions of $1 \mu\text{g/mL/cm}$ GDNF gradient. (e) Percent of negative, neutral, or positive migrating cells in different regions of $10 \mu\text{g/mL/cm}$ GDNF gradient. (f) Percent of negative, neutral, or positive migrating cells in different regions of $20 \mu\text{g/mL/cm}$ GDNF gradient.

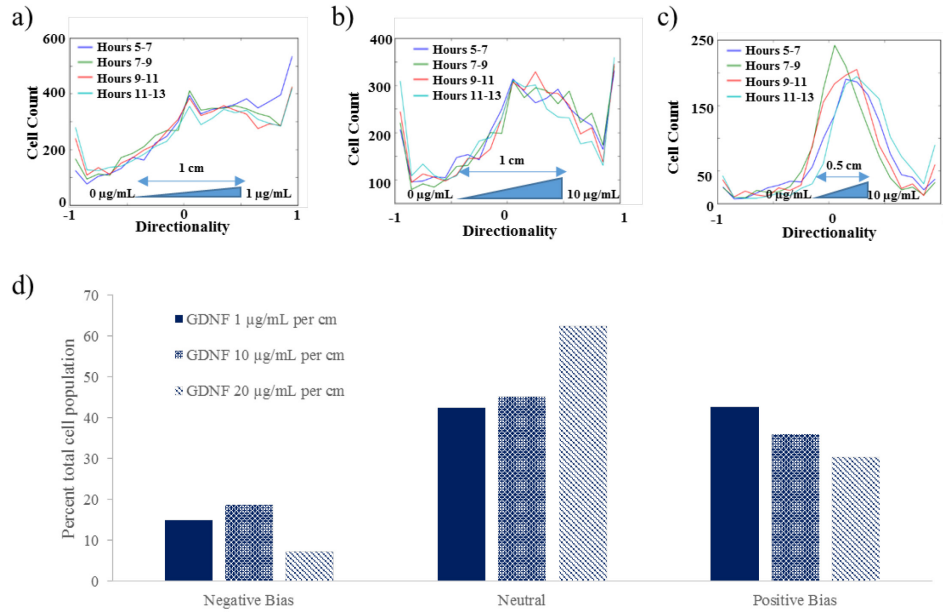


Figure 3.8: Population distribution of directional guidance of human Schwann cell migration to GDNF gradients ($N > 1000$ cells). (a) Directional bias distribution of Schwann cells in 1 $\mu\text{g}/\text{mL}/\text{cm}$ GDNF gradient in different hour ranges. (b) Directional bias distribution of Schwann cells in 10 $\mu\text{g}/\text{mL}/\text{cm}$ GDNF gradient in different hour ranges. (c) Directional bias distribution of Schwann cells in 20 $\mu\text{g}/\text{mL}/\text{cm}$ GDNF gradient in different hour ranges. (d) Percent of negative, neutral, or positive migrating cells in total cell population of cells in different gradient conditions.

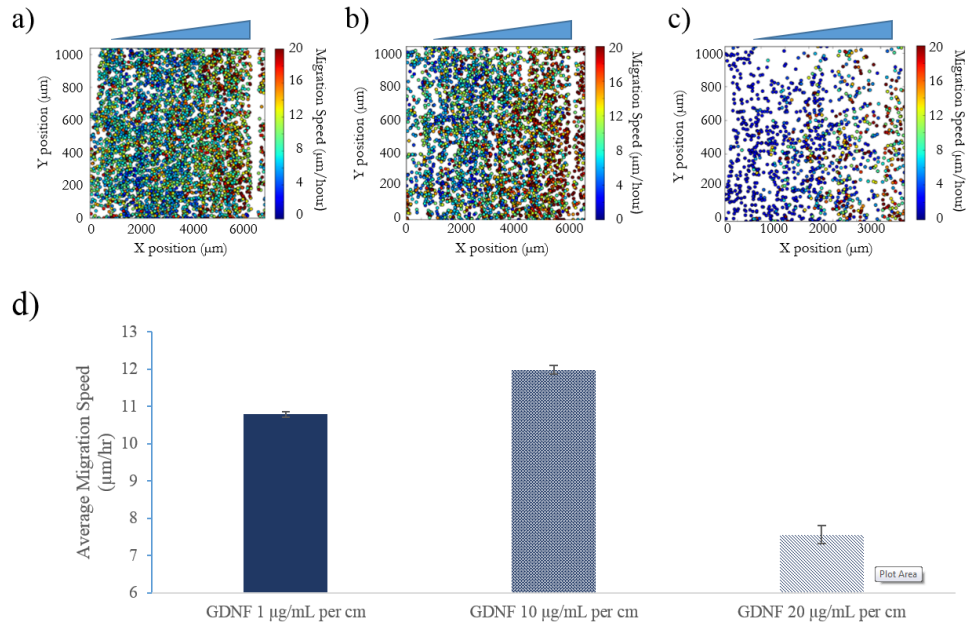


Figure 3.9: Migration rate of human Schwann cells in GDNF gradients (N>1000 cells). (a) Migration rate heat map of Schwann cells in 1 µg/mL/cm GDNF gradient. Dots represent position of cells in gradient. Red dots represent cells migrating at average rate of 20 µm/h. Blue dots represent non-migratory cells. (b) Migration rate heat map of Schwann cells in 10 µg/mL/cm GDNF gradient. (c) Migration rate heat map of Schwann cells in 20 µg/mL/cm GDNF gradient. (d) Average migration rate of total cell populations in different gradient conditions. Error bars represent Standard Error.

3.6 References

1. Bunge, R.P., *Expanding roles for the Schwann cell: ensheathment, myelination, trophism and regeneration*. Current Opinion in Neurobiology, 1993. **3**: p. 805-809.
2. Fu, S.Y. and T. Gordon, *The cellular and molecular basis of peripheral nerve regeneration*. Molecular Neurobiology, 1997. **14**: p. 67-116.
3. Ide, C., et al., *Schwann cell basal lamina and nerve regeneration*. Brain Research, 1983. **288**: p. 61-75.
4. Fawcett, J.W. and R.J. Keynes, *Peripheral nerve regeneration*. Annual Review of Neuroscience, 1990. **13**: p. 43-60.
5. Seggio, A.M., et al., *Self-aligned Schwann cell monolayers demonstrate an inherent ability to direct neurite outgrowth*. Journal of Neural Engineering, 2010. **7**(4): p. 046001.
6. Daud, M.F., et al., *An aligned 3D neuronal-glia co-culture model for peripheral nerve studies*. Biomaterials, 2012. **33**(25): p. 5901-13.
7. Paratcha, G., F. Ledda, and C.F. Ibáñez, *The Neural Cell Adhesion Molecule NCAM Is an Alternative Signaling Receptor for GDNF Family Ligands*. Cell, 2003. **113**(7): p. 867-879.
8. Anton, E.S., et al., *Nerve growth factor and its low-affinity receptor promote Schwann cell migration*. PNAS, 1994. **91**(7): p. 2795-2799.
9. Cornejo, M., et al., *Effect of NRG1, GDNF, EGF and NGF in the migration of a Schwann cell precursor line*. Neurochemical Research, 2010. **35**(10): p. 1643-51.

10. Mahanthappa, N.K., E.S. Anton, and W.D. Matthew, *Glial growth factor 2, a soluble neuregulin, directly increases Schwann cell motility and indirectly promotes neurite outgrowth*. Journal of Neuroscience, 1996. **16**(15): p. 4673-4683.
11. Heermann, S. and M.H. Schwab, *Molecular control of Schwann cell migration along peripheral axons*. Cell Adhesion & Migration, 2013. **7**(1): p. 18-22.
12. Chew, S.Y., et al., *Aligned Protein-Polymer Composite Fibers Enhance Nerve Regeneration: A Potential Tissue-Engineering Platform*. Advanced Functional Materials, 2007. **17**(8): p. 1288-1296.
13. Cao, X. and M.S. Shoichet, *Defining the concentration gradient of nerve growth factor for guided neurite outgrowth*. Journal of Neuroscience, 2001. **103**(3): p. 831-840.
14. Cao, X. and M.S. Shoichet, *Investigating the synergistic effect of combined neurotrophic factor concentration gradients to guide axonal growth*. Journal of Neuroscience, 2003. **122**: p. 381-389.
15. Kapur, T.A. and M.S. Shoichet, *Immobilized concentration gradients of nerve growth factor guide neurite outgrowth*. Journal of Biomedical Materials Research Part A, 2003. **68A**(2): p. 235-243.
16. Belkas, J.S., M.S. Shoichet, and R. Midha, *Peripheral nerve regeneration through guidance tubes*. Journal of Neurological Research, 2004. **26**: p. 151-160.
17. Moore, K., M. Macsween, and M.S. Shoichet, *Immobilized concentration gradients of neurotrophic factors guide neurite outgrowth of primary neurons in macroporous scaffolds*. Tissue Engineering, 2006. **12**(2): p. 267-278.

18. Mortimer, D., et al., *A Bayesian Model predicts the response of axons to molecular gradients*. PNAS, 2009. **106**(25): p. 10296-10301.
19. Eggers, R., et al., *Lentiviral vector-mediated gradients of GDNF in the injured peripheral nerve: effects on nerve coil formation, Schwann cell maturation and myelination*. PLoS One, 2013. **8**(8): p. e71076.

Chapter 4 : Effect of GDNF Gradient Delivery on Peripheral Nerve Regeneration in Rat and Canine Models

4.1 Introduction

Current approaches to nerve regeneration have taken multiple platforms, ranging from biomaterials engineering to cell-based therapies, all attempting to match the current clinical gold standard, the autologous nerve graft. Inherent issues with both the harvest and utilization of the autologous nerve graft have generated momentum to develop effective nerve guidance conduits (NGCs) to repair the damaged nerve. The biomaterials approach to NGC design focuses on providing a microenvironment conducive for nerve regeneration by mimicking the extracellular matrix (ECM) present in regenerating nerves, employing substrate-bound and diffusible signaling cues to promote cell adhesion and survival and to guide axonal re-growth through the lesion site. Neurotrophic factors (NFs) that promote the survival and regenerative activities of nerves, and adhesive cues, such as laminin, are commonly incorporated into NGCs to enhance the regenerative outcomes [1-4]. The cell-based approach to NGC design utilizes Schwann cells, often with potentiated functionality through the over-expression of NFs and the organization of an aligned structure similar to Bands of Büngner, to provide trophic support for axonal regeneration, to secrete relevant ECM and to myelinate regenerating axons. Alternative cell sources such as mesenchymal stem cells (MSCs) [5] and bone-marrow-derived stromal cells (BMSCs) [6-8] transplanted in NGCs have also been shown to be an effective approach to promoting axonal regeneration.

Delivery of extrinsic signaling cues at the repair site has been shown to significantly improve the axonal survival and re-growth and thus the functional recovery. Particularly,

the ‘local’ administration of NFs within NGCs or autographs has demonstrated great nerve regeneration potential, prompting more effort in optimizing systems to regulate the local release of these cues and understanding how to most effectively present these cues to regenerating nerves [1-4, 9, 10]. One of the major challenges in effectively utilizing NFs is how to properly deliver them to the damaged nerve site to provide both *localized* and *sustained* release in order to maximize their efficiency. Sustained NF release can be provided by encapsulating them within crosslinked hydrogels [11, 12], microparticles [13], or micro/nanofibers [4]. The incorporation of NF-binding molecules or direct conjugation of NFs to the NGC substrate using a cleavable chemical linkage can also provide sustained release and enhanced regenerative capabilities [14, 15]. A recent study by Marquardt *et al.*, which injected genetically-modified Schwann cells transfected with a tetracycline-inducible GDNF-overexpressing lentivirus into the distal stump of a 3-cm sciatic nerve defect and showed the greatest regenerative outcome for the groups in which GDNF was overexpressed for 6 weeks, demonstrated the importance of temporal control over NF delivery in promoting successful nerve regeneration [16].

In Chapters 2 and 3, we discussed the importance of Schwann cells in nerve regeneration and the development of gradient generation and cell migration and analysis platforms, which provided significant insight into the topographical and biochemical gradient cues necessary for promoting directional Schwann cell guidance. Human Schwann cells exhibited rapid migration on 1.2 μm diameter, aligned electrospun fibers, and we demonstrated the significant effects of concentration and gradient steepness on the efficacy of GDNF gradients in promoting directional Schwann cell migration. Therefore, we hypothesize that developing an NGC which incorporates both topographical and

biochemical gradient guidance will promote improved axon and Schwann cell migration into nerve injury gaps and increase the regenerative outcomes of peripheral nerve injuries compared to NGCs with uniform spatial NF distribution. Incorporating aligned fibers into the lumen of the conduit would provide a suitable upon which regenerating nerve tissue can grow [4]. Delivery of NFs in a gradient instead of uniformly distributed throughout a conduit will enhance bridging of nerve across the entirety of the nerve gap by increasing Schwann cell infiltration of the nerve gap, encouraging complete extension of regenerating neurons across the nerve gap [3], and preventing the prevalence of the “candy store” effect which occurs in uniform NF delivery [4] or with excessive NF overexpression [16-18]. An NGC such as this would provide great potential for enhancing the regeneration of large gap nerve injuries in which regeneration of nerve tissue across the entirety of the nerve injury gap is generally poor.

In this chapter, we first discussed the development of NGC technologies which are capable of topographical and biochemical guidance (**Table 4.1**). We then demonstrated that delivery of NFs in the form of a gradient substantially improved axonal ingrowth into short-gap nerve injuries within the first month of regeneration. Moreover, we demonstrated a steepness-dependent response in which only the steep gradient condition elicited substantial improvement in nerve regeneration, enhancing axon growth and functional recovery. We also showed that delivery of GDNF gradients in our combinatorial NGCs increases axonal growth into large injury gaps and improves complete regeneration of axons across the nerve gaps compared to NGCs with uniform GDNF delivery. Finally, we demonstrated that functional recovery in NGCs containing GDNF gradients resulted in functional values similar to values measured in a normal nerve before operation, indicating

that GDNF gradient delivery enhanced the maturity of neuron-glia interactions and promoted substantial functional recovery.

4.2 Methods

4.2.1 Electrospinning and preparation of S-Shaped nerve guide

Nerve guides incorporating both topographical and biochemical guidance were produced using modification of an S-shaped conduit design first developed by Andrew Hurtado [19]. Electrospinning was performed as described in chapter 2 and previous work [20]. Briefly, a solution of 8%w/w PCL (molecular weight of 80k, Sigma) in a solvent of 90%w/w DCM and 10%w/w DMF is electrospun at 5 mL/h through a 27-gauge needle at a distance of 11 cm from the face of a 40 cm-diameter wheel rotating at 70 rpm with a 13 kV positive voltage. The apparatus was rastered across the face of the wheel using a programmable linear stage (Newmark Systems), repeatedly moving over a distance of 75 mm at 0.1 mm/sec for 2 h. The nanofiber mat was partially melted to increase strength by heating with a hair dryer for 5 sec to create a mechanically strong film. Aligned PCL nanofibers were then electrospun directly onto the film, by spinning 12%w/w PCL in Chloroform at a flowrate of 0.6mL/hr and +8kV voltage 6cm from the wheel surface, rotating at 750rpm. The aligned fibers were spun for 12 passes at 0.1 mm/sec for travel distance of 70 mm. The conduit outer wall was electrospun with the 8 w/w% PCL in DCM/DMF solution at a flow rate of 0.75 mL/h through a 27-gauge needle 6 cm onto a rotating 1.5 mm steel mandrel. A 7.5 kV positive voltage is applied to the needle tip, while a 2.5 kV negative voltage is applied to the mandrel, spinning over a distance of 23 cm for 70 passes at 5 mm/sec. The tubes were then lyophilized for 48 h to remove residual solvent, then heat-treated to increase strength by soaking in hot water, 20 minutes subsequently at

each of 50°C, 54°C, and 56°C. The tubes were then cut to 10mm segments and sterilized. The aligned nanofiber sheets and nanofiber outer walls were sterilized via ethylene oxide sterilization.

4.2.2 Gradient hydrogels for nerve guidance conduits

Hydrogels containing GDNF gradients were prepared using a 1-cm gradient channel (4.5 μ L channel volume) and cut to 7 mm in length after gradient generation. All groups with GDNF contained 600 ng of GDNF in the final 7 mm hydrogel strip. Uniform GDNF was loaded at 190 μ g/mL. To generate the shallow gradient, 4.5 μ L of 95.2 μ g/mL GDNF was preloaded into channel and 1.5 μ L of 200 μ g/mL GDNF was added at the inlet. Steep gradient hydrogels were generated by adding 1.5 μ L of 400 μ g/mL GDNF solution onto the inlet of a pre-filled channel containing no GDNF. The gradient gels were placed between two layers of aligned nanofibers, which were then wrapped around two 500- μ m steel mandrels to form the S-shape seen in **Figure 3.3**. The wrapped sheets were then inserted into the lumen of the 10mm-long electrospun outer tube, and the mandrels are carefully removed. The sheets were oriented so that fibers were aligned longitudinally along the nerve guide.

4.2.3 Sciatic nerve transection and repair in rats

All animal surgeries and evaluation of the outcome of the nerve repair were carried out according to protocols approved by the Johns Hopkins Institutional Animal Care and Use Committee. The surgeries were performed on adult male Sprague-Dawley rats (200 – 300 g). Following isoflurane anesthetization, the sciatic nerve in the left leg was exposed through a mid-thigh incision. The nerve guidance conduits were pre-wetted by soaking in sterile PBS. Nerve defects were then repaired with no-GDNF NGCs (control, N = 7),

shallow GDNF gradient NGCs (N = 8), steep GDNF gradient NGCs (N = 5) and uniform GDNF NGCs (N = 7). GDNF-loaded NGCs contained 600 ng total GDNF for all conduits. 5mm of the nerve was resected, and each end of the nerve was inserted 1.5 mm into the nerve guidance conduit to leave a gap of 7 mm between the nerve ends. The nerve ends were sutured in place via 10 – 0 nylon sutures (Ethicon). The surgical site was closed with wound clips, and 0.1 mg/kg of buprenorphine was injected for pain management. The animals were allowed free access to food and water and were regularly monitored.

4.2.4 Electrophysiology assessments in rat model

One month post-surgery, the compound motor action potentials were recorded according to standard protocols using LabChart (AD Instruments) [4]. The stimulating needle electrodes were inserted into the sciatic notch, proximal to the nerve guide. The recording electrodes were placed into the ankle, at a distance of 7.2 cm +/- 0.3 mm from the stimulating electrodes.

4.2.5 Harvesting of regenerated nerves in rat model

Following electrophysiology testing (1 month post-surgery), the rats were euthanized. The nerve guide and surrounding nerve was removed and fixed in 4% Paraformaldehyde. After 24 h at 4°C, the middle segment of the nerve guide (2.5-5.5 mm from proximal nerve stump) was resected and fixed for a further 24 h at 4°C in 4% paraformaldehyde and 3% glutaraldehyde. The tissue was mounted in embedding resin, sectioned, and stained with toluidine blue [4].

4.2.6 Canine model protocol overview

All animal studies were performed according to the protocol approved by the Animal Care and Use Committee and in accordance with the Animal Care Policies of Johns

Hopkins University. Twenty three healthy adult beagle canines weighing 9.0–13 kg were included in this study. All surgical procedures were performed in accordance with the “Guide for the Care and Use of Laboratory Animals” published by the National Institutes of Health. The experimental protocol was approved by the Animal Care and Use Committee (ACUC) of Johns Hopkins University, and all efforts were made to minimize animal suffering. Fasting was imposed on all canines for 24 h prior to the operation, but canines were given drinking water *ad libitum*.

4.2.7 Preparation of NGCs for canine model

NGCs were prepared identically to the previous rat S-design NGCs, with variations to the size of the conduit and length of gradients generated to accommodate increased larger diameter of nerve in canine model and increased length of nerve gap (20 mm gap length). The inner diameter of the conduit was increase from 1.5 mm for the rat model to 2.0 mm for the canine model. The conduits were made to be 22 mm in length, so that 1 mm of each nerve end can be inserted into the NGC for suturing, leaving a 20 mm gap for the nerve to regenerate. Aligned fiber sheets were cut into 20 mm long segments to bridge this gap. Hydrogel sheets were generated in 1 cm long gradient channels, with two 1 cm long hydrogels being placed end-to-end in each conduit, such that a total GDNF loading of 600 ng per tube was achieved for the uniform-loading and gradient groups.

4.2.8 Canine peroneal nerve injury surgery preparation

All surgical procedures and physiological measurements were performed under general anesthesia. The animals were premedicated by intramuscular administration of 10mg/kg Ketamin and 0.005-0.01 mg/kg Buprenorphine. They were then anesthetized with isoflurane under mechanical ventilation. Continuous monitoring was performed by

electrocardiography and oxygen saturation by reflectance oximetry using a sensor clipped to the ear. The lateral hind-limb region was shaved and the animals were positioned in the lateral position. The hind-limb region was disinfected with 70% ethanol and iodine tincture, and covered with sterilized drapes.

4.2.9 Canine peroneal nerve injury surgical procedure

The healthy beagles were deeply anesthetized using isoflurane throughout the surgical procedure. Surgery was performed on the canine's hind-limb under aseptic conditions. For nerve conduit implantation, the superficial peroneal nerve was exposed by an incision in lateral leg, overlying muscles were separated by traction and 15 mm of the nerve was resected out to result in a 20-mm defect gap. Nerve defects were then repaired with no-GDNF NGCs (control, N = 10), GDNF gradient NGCs (N = 10), and uniform GDNF NGCs (N = 10). GDNF-loaded NGCs contained 600 ng total GDNF for all conduits. All nerve conduits (length = 20 mm) were filled with 15 μ l of PBS prior to implantation. Next, the proximal and distal stumps were sutured to the conduit using a 10–0 nylon monofilament. For autograft implantation (N = 10), a 20 mm superficial peroneal nerve was transected and reverse transposed into the gap. Both ends were then sutured using 10–0 strings. The incision was then closed using 4-0 absorbable braided suture in a subcuticular pattern, and 3-0 absorbable braided suture in a skin pattern. The canines were monitored and given 2 additional dose of Buprenorphine (0.005-0,01mg/kg, IM) in the evening after surgery and the following morning. For the post-operative care, the canines were monitored daily for three days following surgery, then 2-3 days for the first month, and then weekly until the end of the study. The animals were kept in

temperature (28°C) and humidity (45%) controlled rooms with 12 h light cycles and allowed free access to food and water.

4.2.10 Electrophysiology assessments in canine model

Six months after surgery, compound nerve action potential (CNAP) responses were used to evaluate electrophysiological recovery prior to harvesting the distal nerve and nerve conduits. After anesthetization with isoflurane under mechanical ventilation, superficial peroneal nerve with transplantation of nerve conduits was dissected free from connective tissue and prepared for electrophysiology test. The stimulating electrodes were placed at the proximal end of superficial peroneal nerve, 5 mm from the proximal end of nerve conduits, while the recording electrodes were placed at the distal end of superficial peroneal nerve, 5 mm to the distal end of nerve conduits to record the CNAP values. CNAPs were elicited with a stimulation of 1.00 ms delay, 0.10 ms duration with amplitude voltage ramped from 1 to 5 v. Individual CNAPs were recorded at each step of the ramp.

4.2.11 Harvesting of regenerated nerves in canine model

The superficial peroneal nerve with nerve guide or autograft stump was resected for histologic analyses after electrophysiology test. All other pre-operation, intra-operation and post-operation protocols were the same as described in the nerve guide implantation surgical procedure. After 24 h at 4°C, the middle segment of the nerve guide and segment of nerve 3 mm distal to the nerve guide were resected and fixed for a further 24 h at 4°C in 4% paraformaldehyde and 3% glutaraldehyde. The tissue was mounted in embedding resin, sectioned, and stained with toluidine blue [4].

4.2.12 Histomorphometric analysis

Imaging of the fixed nerve sections was conducted using an inverted microscope (Nikon) at 10× and 63× magnification. Total nerve tissue area was measured at 10×. Nerve count was measured at 63× by averaging the axon count within 5-8 randomized images within each sample nerve area and calculating total nerve count and nerve density using the measured nerve tissue area.

4.2.13 Statistical analysis

Axon counts, axon densities, and nerve area measurements are represented by mean ± Standard Error. Electrophysiology measurements are represented by mean ± Standard Deviation. Statistical comparisons were conducted using ANOVA with Tukey's post-hoc HSD test. Differences were considered statistically significant for $p < 0.05$.

4.3 Results and Discussion

4.3.1 Nerve Guidance Conduit Design

Multiple generations of NGC designs incorporating NF delivery and topographical guidance have been developed by our labs, as seen in Table 4.1. The latest iteration, the S-shaped conduit, was found to be the most effective in promoting nerve ingrowth, providing an optimal combination of aligned fiber surface area and luminal space for tissue ingrowth. This method was first developed by Hurtado *et al.* [19] and was designed as a method for increasing fiber surface area compared to open-lumen designs. We have adopted this conduit design for this study. Modification of the conduit fabrication process allowed for incorporation of gradient-delivery hydrogel sheets between layers of the fiber sheets (**Figure 4.1a**). By placing a gelatin hydrogel sheet loaded with a predetermined GDNF gradient between two adjacent aligned fiber layers (**Figure 4.1b**), the gradient-releasing

feature can be incorporated into the NGC with an S-shaped cross-section insert in the conduit (**Figure 4.1c**). This modular design allows for separate production of the aligned fiber sheets and gradients, providing the ability to independently tailor both the topographical cues and biochemical guidance to the desired length, fiber diameter, NGC diameter, and gradient characteristics.

4.3.2 Non-critical injury gap model for study of acute nerve regeneration

Two nerve injury models were selected for the investigation of the effect of GDNF gradient delivery. The first injury model was a non-critical gap (7-mm injury), acute rat sciatic nerve regeneration model. The primary purpose of this model was to determine if the mode of delivery of GDNF (i.e. gradient vs. uniform) affected the acute regeneration (i.e. regeneration within 1 month) of axons into our combinatorial NGCs to determine which GDNF delivery configuration was most effective in promoting rapid nerve regrowth during the early phase nerve repair. The results of the acute regeneration model were also used to select the most effective gradient condition for use in the large gap (20 mm), long-term regeneration (7 month recovery) model to be conducted in canines. In Chapter 3, we demonstrated that gradient steepness played an important role in the efficacy of GDNF gradient guidance of human Schwann cell migration. We demonstrated that for gradients of equivalent total GDNF loading, the migration rate and directional bias of Schwann cells were dependent on the steepness of the gradient to which they were exposed. Therefore, we elected to compare two gradient conditions for which the total GDNF loading was equivalent, but for which the gradient steepness varied significantly in order to elucidate whether the steepness of a GDNF gradient influenced the efficacy of *in vivo* nerve regeneration.

To investigate acute nerve regeneration, all nerve grafts were harvested 4 weeks after implantation. Histological analysis on the mid-graft sections shows that GDNF delivery, both in uniform and gradient configurations, improves the ingrowth of myelinated axons into the midpoint of the conduit compared to conduits without GDNF (**Figure 4.2a,b**) by significantly increasing the area of functional nerve tissue regenerated into the lesion site (**Figure 4.2b**). Additionally, the delivery of GDNF in the steepest gradient further improves the axonal density and ingrowth and compared to other delivery configurations, providing significantly higher myelinated axon counts (4045.6 ± 1101.8 axons per nerve) compared to that of the shallow GDNF gradient (2084.9 ± 554.6 axons per nerve) or uniform GDNF (1610.3 ± 626.1 axons per nerve) (**Figure 4.3**). This result indicates that the effect of gradient delivery is highly dependent on the concentration range and steepness of the gradient being delivered, but that delivery of selective gradient conditions can be effective in directing nerve growth across lesion gaps.

Although the histomorphometric analysis was conducted at a short 4-week time point, EMG data exhibited impressive, albeit heterogeneous, functional recovery in the steep GDNF gradient group (**Figure 4.4**). Even after only one month of recovery, significant nerve function recovery was found in the steep GDNF gradient group. Additionally, the data revealed that the shallow GDNF gradient, while promoting adequate axonal ingrowth, exhibited markedly poorer nerve function, instead resulting in function comparable to that of the uniform GDNF group. These data indicate the shallow gradient suffered from similar axon trapping seen in NGCs delivering uniform GDNF [4], for which axon regrowth is significant but functional recovery is poor due to regenerating axons becoming entrapped within the NGC and unable to reinnervate the distal nerve stump.

These results emphasize the importance of gradient steepness in the ability for nerves to sense and respond to the presence of NF gradients. In this experiment, although both gradient groups contained the same amount of GDNF, the most pronounced improvement in nerve regrowth was seen in the steepest gradient configuration, which further strengthened the results we found in Chapter 3 demonstrating that gradient steepness plays an important role in the migratory and chemotropic activity of Schwann cells to gradients containing similar levels of NFs. The design of this NGC provides NF delivery localized to the lesion site, but by enhancing nerve growth across the entirety of the nerve gap and maximizing the number of axons successfully reinnervating the distal nerve, NF gradient delivery in NGCs can markedly improve the functional regeneration following peripheral nerve injuries. These results suggest that previous attempts to incorporate NF gradients into NGCs to enhance nerve regeneration may have been limited in their regenerative potential by using non-optimized NF concentration range and gradient steepness conditions, as well as suffering from their use of sensory-specific NFs [3]. While we were limited in the number of gradient groups tested in this experiment, the significant improvement in recovery exhibited by the steep gradient condition demonstrated the potential for NF gradients in enhancing peripheral nerve regeneration and was instrumental in the selection of design of future large animal (canine) experiments.

4.3.3 Large gap injury, long-term nerve regeneration model

In order to elucidate the effects of gradient delivery in long-term regeneration of a critical-gap injury, we developed a large-gap canine peripheral nerve injury model for investigating the efficacy of NGCs delivering NF gradients and topographical guidance in long-term peripheral nerve regeneration. A canine nerve injury model exhibits several

benefits compared to a rat nerve injury model. First, a canine model allows us to repair larger diameter nerves than are available in the rat model that are closer to the nerve diameters of human nerves. Second, because canines are of significantly larger anatomical size compared to rats, the canine model has greater potential for testing longer injury gaps than what is capable for rats [21], and therefore is a more suitable model for large gap injuries where gradient guidance may be necessary to promote complete regeneration across the length of the injury gap. Finally, because of their larger size, canines better potential model animals for peripheral nerve injuries in which the injury occurs significant distances from the target muscle or sensory innervation site, where regenerating nerves must bridge an injury gap and subsequently traverse large distances of distal nerve to reach the reinnervation targets. Long-term, long-distance injury models in rats are limited by their comparatively small anatomical size.

In contrast to the short gap, one-month rat nerve repair model, the canine study was designed to elucidate how NGC-delivered NF gradients influence large gap, long-term nerve recovery. For this study, we reconfigured the S-shaped conduit to bridge a larger injury gap (20 mm), a length which is larger than the critical gap of the more commonly-used rat model [21]. The critical gap of a canine nerve is less known, but using the known critical gap for rats, an animal which exhibits significantly greater regeneration potential than humans and other species [21], provides an adequate estimate for the larger canine model. NGCs were implanted into a canine peroneal nerve injury model, which was selected due to its ease of access for surgical implantation, mixed population of motor and sensory neurons, and ease of electrophysiological testing. Additionally, because canine models require adoption of the animal after all experimental procedures have been

completed, ethical issues can arise if the canines exhibit significant, permanent functional deficits following experimentation. The sacrifice of the peroneal nerve limits the functional loss of the animal, especially compared to models which sacrifice the sciatic nerve, a much larger nerve which innervates a significantly larger portion of the canine hind limb. As such, we are able to obtain a significant amount of information regarding the effect of our NGCs in the regeneration of the canine peroneal nerve without substantially reducing the quality of life of the animal after studies have been completed.

For the canine large gap study, four experimental groups were compared to determine the effect of GDNF gradient delivery on large gap, long-term nerve repair compared to no GDNF, uniform GDNF, and autograft. Initial investigation of the gross histological sections elicited notable differences between the morphology of the nerve sections in the NGCs compared to the normal nerve and autograft (**Figure 4.5**). The canine peroneal nerve consists of four nerve fascicles, as indicated by the morphology of the mid-graft image of the autograft (**Figure 4.5a**) and distal nerve images for all four experimental groups (**Figure 4.5e-h**), contrasted with the two large luminal spaces available in the S-shaped NGCs (**Figure 4.5b-d**). The area of the lumens in the NGCs were, by comparison, significantly larger than the area of the nerve fascicles in the peroneal nerve, and generally had a much higher area of tissue ingrowth in the NGCs compared to that of the fascicles in the autograft and distal nerve. However, upon closer inspection of the nerve areas, much of the tissue in the NGCs consisted of fibrous tissue closely associated with the PCL fibers, which remained intact 7 months post-implantation (**Figure 4.6a,b**). Axonal growth was not present in the fibrous tissue, but rather was localized to small fascicles within the fibrous tissue (**Figure 4.6a**) or in larger regions where fibers were not present (**Figure**

4.6b). The presence of fibrous tissue in the NGC groups reduced the total nerve area in which myelinated neurons were present compared to that of the autograft (**Figure 4.7**), both in the middle of the nerve graft as well as in the tissue distal to the nerve graft. This result indicates that the aligned fibers provide a highly suitable substrate for fibroblasts, which compete with nerve tissue for growth into the NGCs. Future NGC designs should utilize chemical or physical modifications to limit the amount of fibrous tissue production in order to increase potential functional nerve tissue ingrowth.

Although the nerve areas across all three NGC groups were comparable (Figure 4.7), it was evident that delivery of GDNF gradients in the NGCs increased the density of myelinated axons (**Figure 4.8**) growing into the nerve graft and into the distal nerve stump (**Figure 4.9**). GDNF gradient delivery increased the number of myelinated axons growing into the nerve graft, with an average axon count of 1675 ± 325 axons per nerve, compared to that of the no GDNF NGCs (494 ± 127 axons per nerve) and uniform GDNF (1043 ± 286 axons per nerve). Additionally, GDNF gradient delivery improved the number of axons, which successfully bridged the entire 20-mm gap into the distal stump (970 ± 105 axons per nerve), compared to no GDNF (326 ± 86 axons per nerve) and uniform GDNF NGCs (578 ± 128 axons per nerve) (**Figure 4.10**). These results confirmed that over a larger gap, the gradient delivery of GDNF was the most effective method in promoting axonal growth across the entirety of a nerve gap. An optimized gradient GDNF delivery, i.e. with a steeper gradient, improved axonal growth into the conduit and across the gap to reinnervate the distal stump.

The effectiveness of gradient delivery is further indicated by the recovery of nerve function after 7 months. Nerve EMG was recorded prior to nerve harvest and compared to

pre-surgical values. Animals with the GDNF gradient delivery exhibited signal latency values, both onset and peak, similar to that of pre-surgical values (**Figures 4.11 and 4.12**), an indication of the presence of mature, myelinated neurons. Additionally, signal amplitude was improved in both the uniform GDNF and gradient GDNF groups to levels comparable to pre-surgical values (**Figures 4.13 and 4.14**). Interestingly, the GDNF gradient group exhibited better functional recovery than the autograft groups, in spite of having lower nerve area and axon numbers. These data suggest that while the autograft promoted a higher number of axons to bridge the nerve gap, the delivery of GDNF as a gradient may have improved the maturation and function of the neurons, which reinnervated the distal stump, resulting in improved signal transduction and functional recovery. While limitations in the NGC design may have reduced its efficacy in the large animal model, the histomorphometric and functional data provide strong evidence that optimization of NF gradient delivery is an important approach for improving nerve regeneration in both small gap and large gap repairs in peripheral nerve injuries.

4.4 Conclusions

We have successfully developed a NGC, which combines topographical and biochemical gradient guidance for the improvement of peripheral nerve regeneration. In a short gap repair model in rat, we demonstrated the importance of gradient steepness in promoting nerve regeneration, with the steepest gradient group promoting the highest degree of axonal regeneration and functional recovery. This gradient condition was then translated to a large gap repair model in beagles to determine if gradients were capable of improving regeneration across a larger gap. Our results demonstrated that the specific configuration of the GDNF gradient delivered in an NGC significantly influenced the

regeneration of axons across the entirety of a large nerve gap. Although our NGC design exhibited fibrous tissue ingrowth, which competed with growth of nerve tissue, the NGCs delivering gradients of GDNF improved the functional recovery of the large gap injuries and resulted in functional outcomes that were comparable to pre-surgical values. Future studies will aim to further optimize the gradient profiles and NGC designs in order to better improve the functional outcomes of our combinatorial NGCs.

4.5 Figures

	1 st Generation: Open Lumen Conduit	2 nd Generation: Spiral Conduit	3 rd Generation: S-Shaped Conduit
Schematic			
<i>In vivo</i> Histomorphometry			
Pros and Cons	<p><u>Pros</u></p> <ul style="list-style-type: none"> ➤ Large open lumen <p><u>Cons</u></p> <ul style="list-style-type: none"> ➤ Lowest available fiber surface area ➤ No gradient loading ➤ Poor regenerative outcomes 	<p><u>Pros</u></p> <ul style="list-style-type: none"> ➤ Highest theoretical fiber surface area <p><u>Cons</u></p> <ul style="list-style-type: none"> ➤ Smallest theoretical lumen ➤ Fibers/gel swell outwardly, reducing effective fiber surface and growth area 	<p><u>Pros</u></p> <ul style="list-style-type: none"> ➤ Intermediate fiber surface area and lumen space ➤ Simple incorporation of gradient hydrogel <p><u>Cons</u></p> <ul style="list-style-type: none"> ➤ Assembly is more technically challenging

Table 4.1: Generations of conduit designs incorporating aligned fiber topographical guidance and NF delivery. The 3rd generation of conduit was selected for use in our animal models.

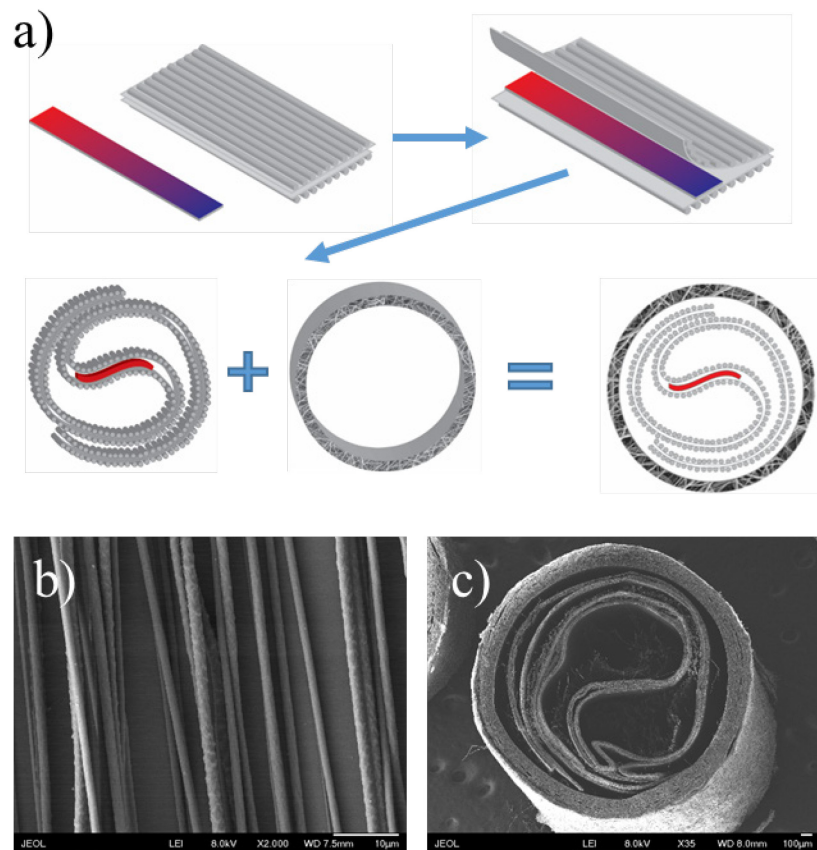


Figure 4.1: Fabrication of S-shaped conduit containing aligned fiber topography and hydrogel-based NF gradient delivery. (a) Gradient-containing hydrogels placed between aligned fiber sheets and rolled into S-shaped conduit. (b) Aligned fibers with average diameter of 1.2 μm . Scale bar is 10 μm . (c) Scanning electron micrograph of S-shaped conduit. Scale bar is 100 μm .

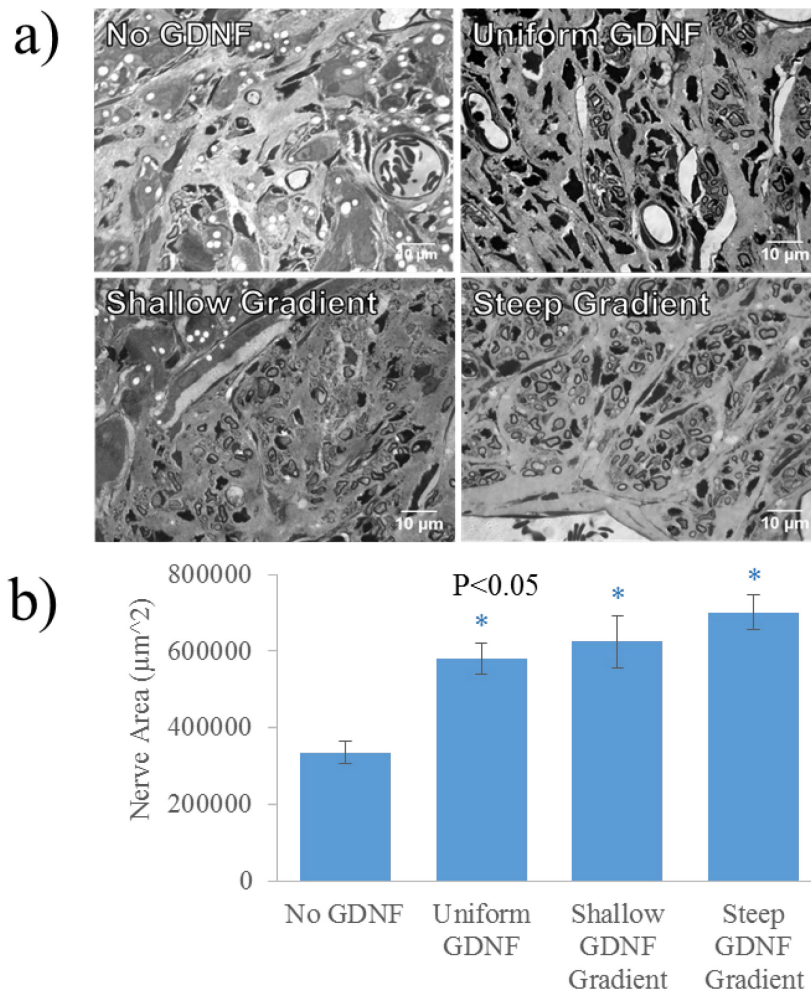


Figure 4.2: Histomorphometry of small gap, acute regeneration rat sciatic nerve injury model ($N > 5$). (a) Representative images of nerve cross sections obtained using 63x objective. Scale bars are 10 μm . (b) Average nerve area of different NGC groups. Error bars represent Standard Deviation. Differences considered statistically significant for $P < 0.05$.

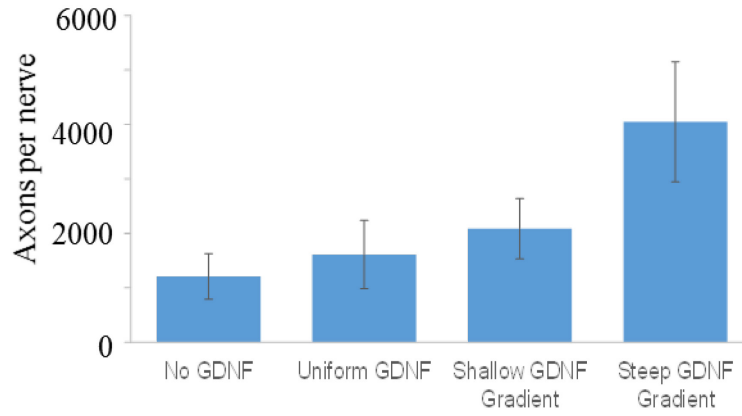


Figure 4.3: Average axon count of different NGC groups in small gap, acute regeneration rat sciatic nerve injury model ($N > 5$). Error bars represent Standard Deviation.

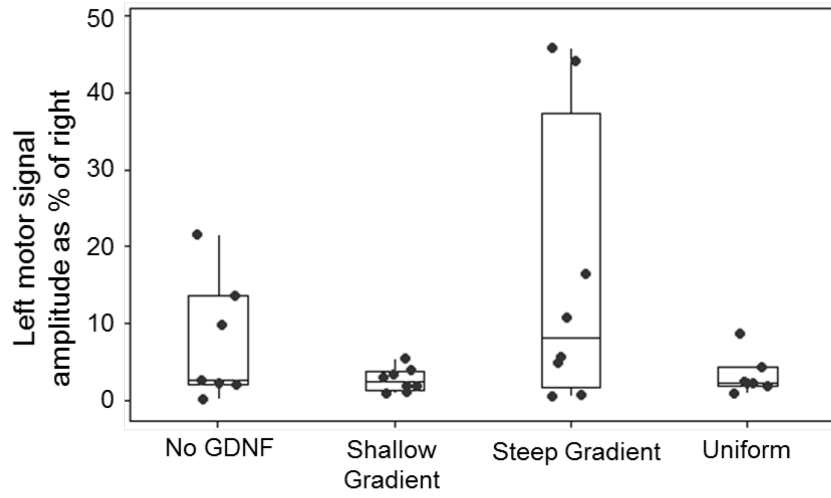


Figure 4.4: Electrophysiological measurement of different NGC groups in small gap, acute regeneration rat sciatic nerve injury model ($N > 5$).

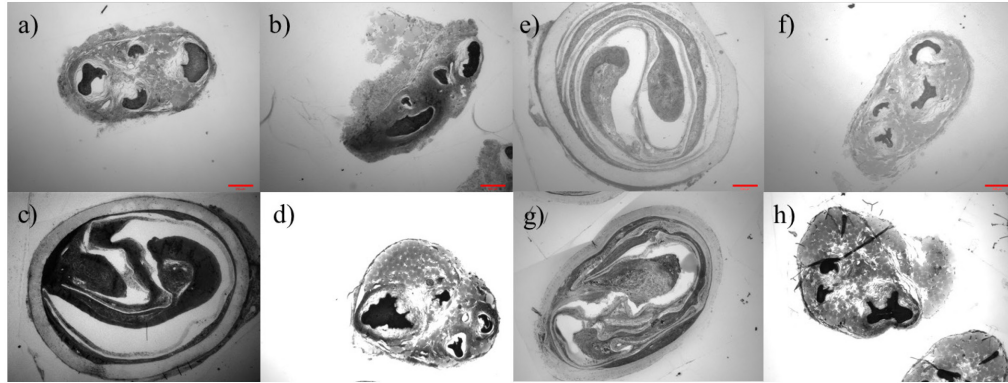


Figure 4.5: Histological cross-sections of nerves of different NGC groups in large gap, long-term regeneration canine peroneal nerve injury model. (a) Mid-graft of autograft control. (b) 3-mm distal to autograft control. (c) Mid-graft of no-GDNF S-shaped NGC. (d) 3-mm distal to no-GDNF S-shaped NGC. (e) Mid-graft of uniform GDNF S-shaped NGC. (f) 3-mm distal to uniform GDNF S-shaped NGC. (g) Mid-graft of gradient GDNF S-shaped NGC. (h) 3-mm distal to gradient GDNF S-shaped NGC. Images obtained with 2.5x objective. Scale bars are 300 μm .

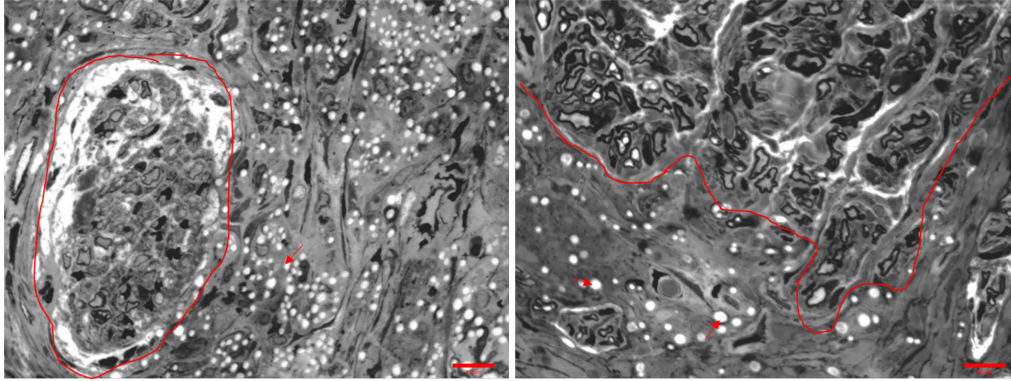


Figure 4.6: Histology of nerve regions showing that PCL fibers remain 7 months after implantation. Fibers (white dots, red arrows) are surrounded by fibrotic tissue, whereas nerve tissue is localized in regions where fibers are not present (tissue border noted by red line). Images obtained with 63x objective. Scale bars are 10 μm .

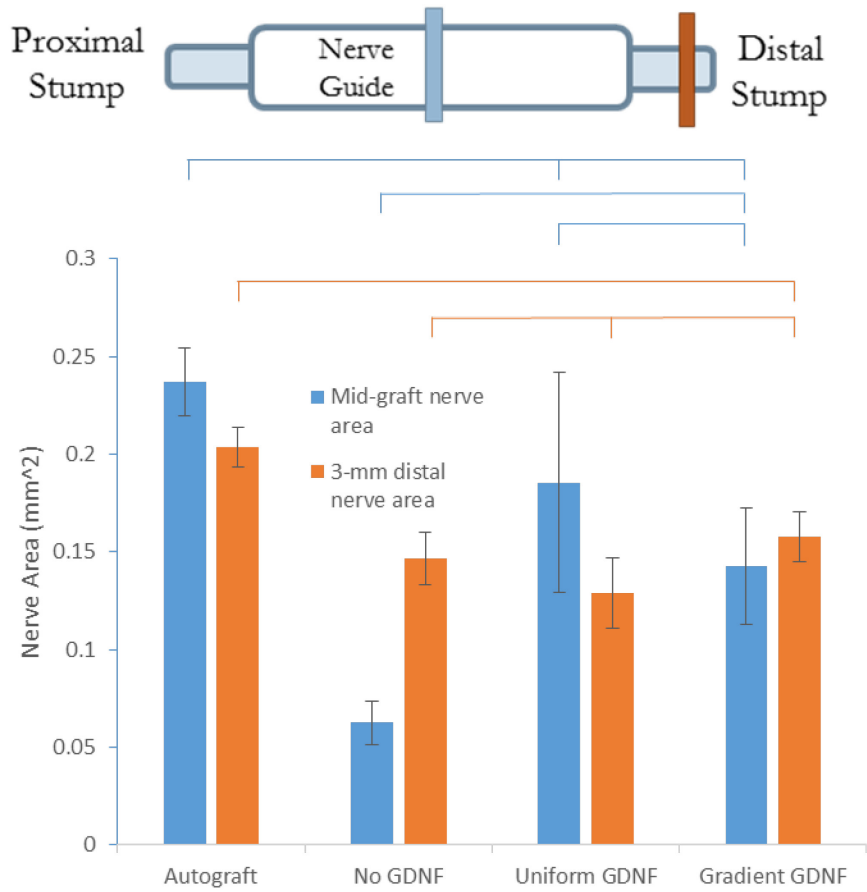


Figure 4.7: Average nerve area of different NGC groups in large gap, long-term regeneration canine peroneal nerve injury model (N >5). Error bars represent Standard Error. Differences considered statistically significant for $P < 0.05$.

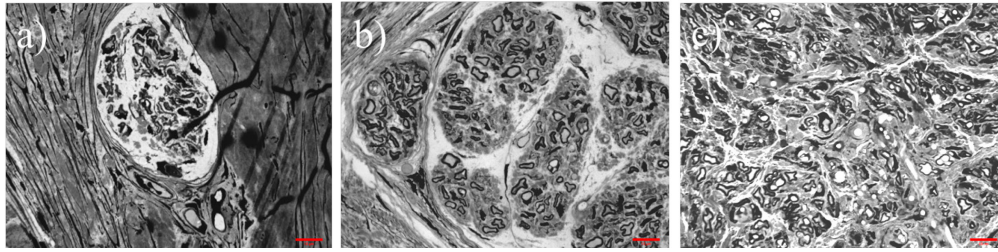


Figure 4.8: Representative histological cross-sections of nerves of different NGC groups in large gap, long-term regeneration canine peroneal nerve injury model. (a) Mid-graft No-GDNF S-shaped NGC. (b) Mid-graft uniform GDNF S-shaped NGC. (c) Mid-graft gradient GDNF S-shaped NGC. Images obtained with 63x objective. Scale bars are 10 μm .

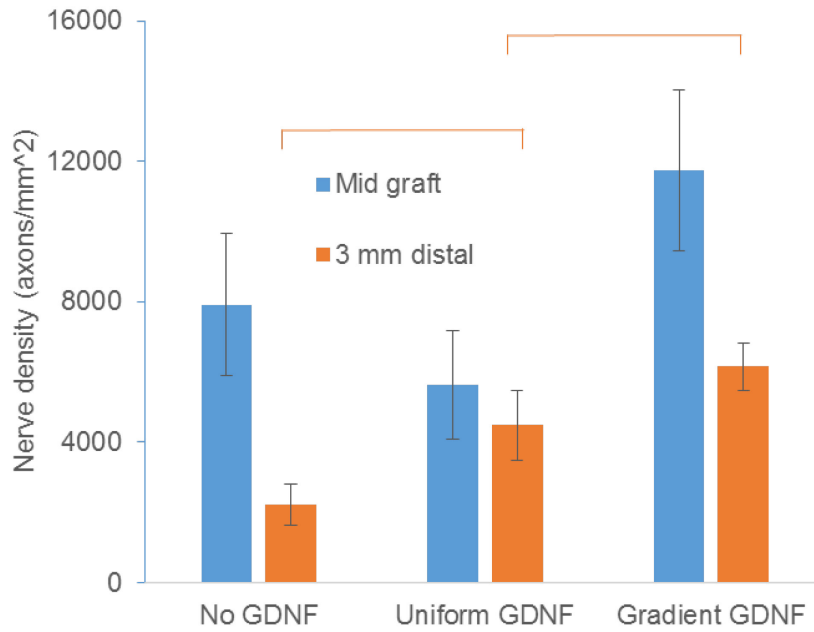


Figure 4.9: Average nerve density of different NGC groups in large gap, long-term regeneration canine peroneal nerve injury model (N > 5). Error bars represent Standard Error. Differences considered statistically significant for $P < 0.05$.

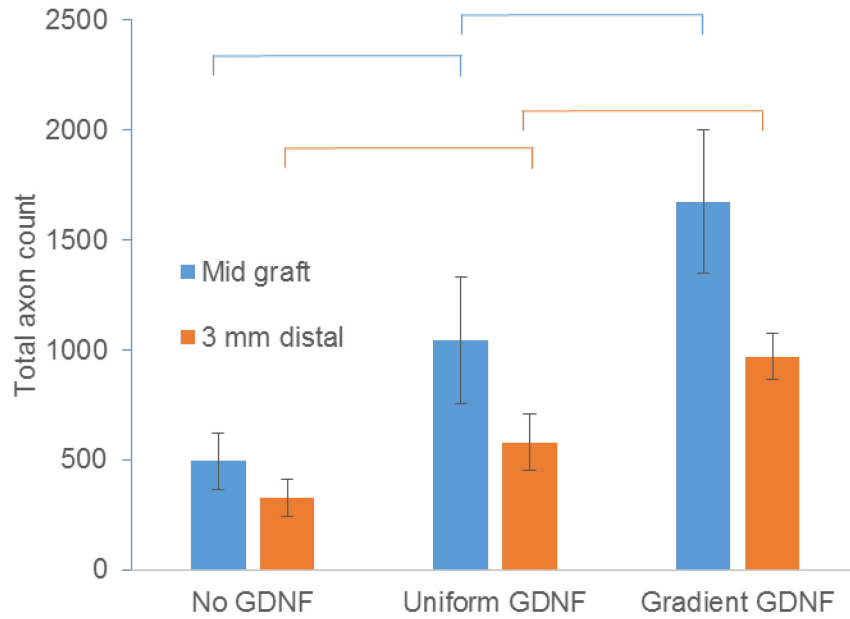


Figure 4.10: Average total axon count of different NGC groups in large gap, long-term regeneration canine peroneal nerve injury model ($N > 5$). Error bars represent Standard Error. Differences considered statistically significant for $P < 0.05$.

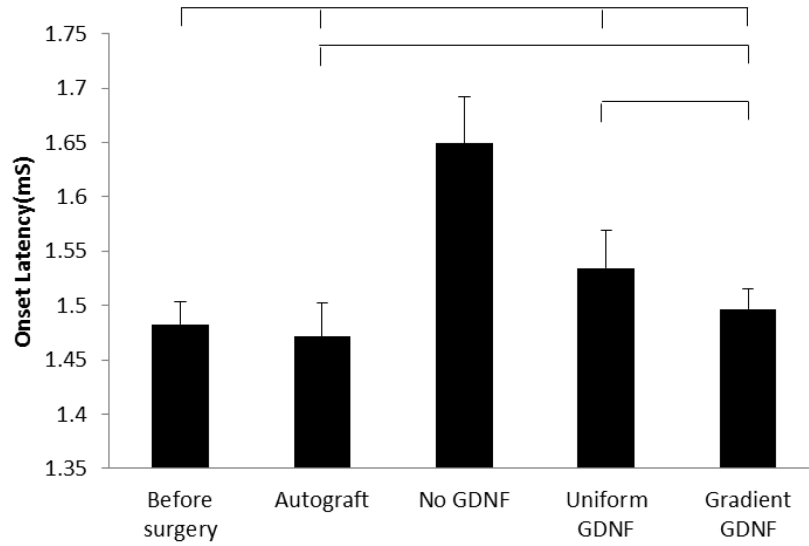


Figure 4.11: Average onset latency of different NGC groups in large gap, long-term regeneration canine peroneal nerve injury model, measured with CNAP (N = 10). Error bars represent Standard Deviation. Differences considered statistically significant for $P < 0.05$.

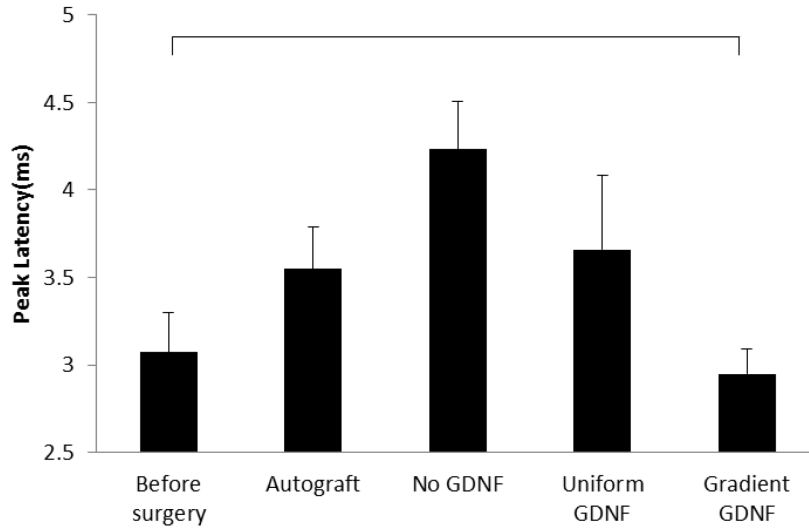


Figure 4.12: Average peak latency of different NGC groups in large gap, long-term regeneration canine peroneal nerve injury model, measured with CNAP (N = 10). Error bars represent Standard Deviation. Differences considered statistically significant for $P < 0.05$.

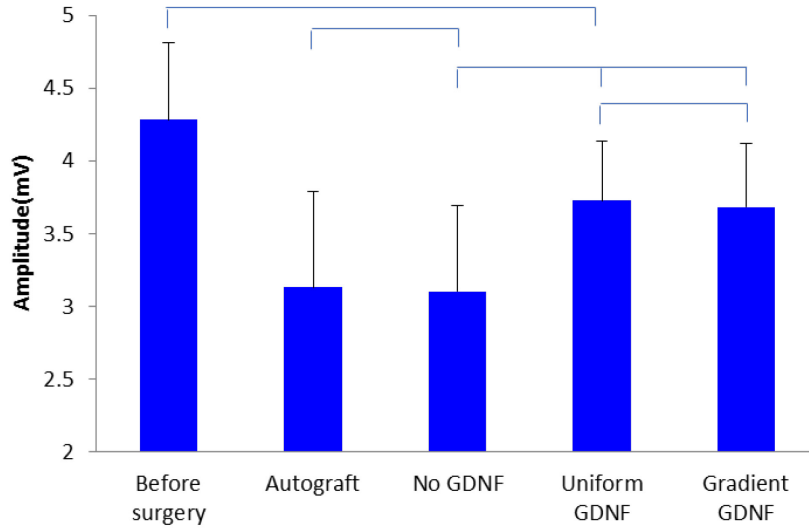


Figure 4.13: Average signal amplitude of different NGC groups in large gap, long-term regeneration canine peroneal nerve injury model, measured with CNAP (N = 10). Error bars represent Standard Deviation. Differences considered statistically significant for $P < 0.05$.

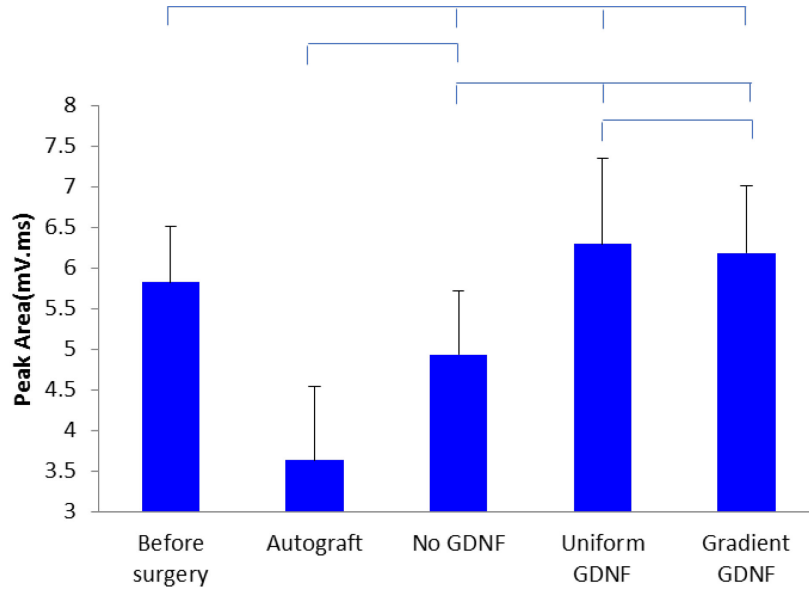


Figure 4.14: Average peak area of different NGC groups in large gap, long-term regeneration canine peroneal nerve injury model, measured with CNAP (N = 10). Error bars represent Standard Deviation. Differences considered statistically significant for $P < 0.05$.

4.6 References

1. Nectow, A.R., K.G. Marra, and D.L. Kaplan, *Biomaterials for the development of peripheral nerve guidance conduits*. Tissue Engineering: Part B, 2012. **18**(1): p. 40-50.
2. Bell, J.H. and J.W. Haycock, *Next generation nerve guides: materials, fabrication, growth factors, and cell delivery*. Tissue Engineering: Part B, 2012. **18**(2): p. 116-28.
3. Dodla, M.C. and R.V. Bellamkonda, *Differences between the effect of anisotropic and isotropic laminin and nerve growth factor presenting scaffolds on nerve regeneration across long peripheral nerve gaps*. Biomaterials, 2008. **29**(1): p. 33-46.
4. Chew, S.Y., et al., *Aligned Protein-Polymer Composite Fibers Enhance Nerve Regeneration: A Potential Tissue-Engineering Platform*. Advanced Functional Materials, 2007. **17**(8): p. 1288-1296.
5. Gros, T., et al., *Regeneration of long-tract axons through sites of spinal cord injury using templated agarose scaffolds*. Biomaterials, 2010. **31**(26): p. 6719-29.
6. Wang, J., et al., *Bone marrow mesenchymal stem cells promote cell proliferation and neurotrophic function of Schwann cells in vitro and in vivo*. Brain Research, 2009. **1262**: p. 7-15.
7. Ishikawa, N., et al., *Peripheral nerve regeneration by transplantation of BMSC-derived Schwann cells as chitosan gel sponge scaffolds*. Journal of Biomedical Materials Research Part A, 2009. **89**(4): p. 1118-24.

8. Pereira Lopes, F.R., et al., *Transplantation of bone-marrow-derived cells into a nerve guide resulted in transdifferentiation into Schwann cells and effective regeneration of transected mouse sciatic nerve*. *Micron*, 2010. **41**(7): p. 783-90.
9. Jiang, X., et al., *Current applications and future perspectives of artificial nerve conduits*. *Experimental Neurology*, 2010. **223**(1): p. 86-101.
10. Guzen, F.P., et al., *Glial cell line-derived neurotrophic factor added to a sciatic nerve fragment grafted in a spinal cord gap ameliorates motor impairments in rats and increases local axonal growth*. *Restorative Neurology and Neuroscience*, 2009. **27**(1): p. 1-16.
11. Kadoya, K., et al., *Combined intrinsic and extrinsic neuronal mechanisms facilitate bridging axonal regeneration one year after spinal cord injury*. *Neuron*, 2009. **64**(2): p. 165-72.
12. Madduri, S., et al., *Effect of controlled co-delivery of synergistic neurotrophic factors on early nerve regeneration in rats*. *Biomaterials*, 2010. **31**(32): p. 8402-9.
13. Kokai, L.E., et al., *Sustained growth factor delivery promotes axonal regeneration in long gap peripheral nerve repair*. *Tissue Engineering: Part A*, 2011. **17**(9-10): p. 1263-75.
14. Moore, A.M., et al., *Controlled delivery of glial cell line-derived neurotrophic factor enhances motor nerve regeneration*. *Journal of Hand Surgery*, 2010. **35**(12): p. 2008-17.
15. Han, Q., et al., *Linear ordered collagen scaffolds loaded with collagen-binding brain-derived neurotrophic factor improve the recovery of spinal cord injury in rats*. *Tissue Engineering: Part A*, 2009. **15**(10): p. 2927-2935.

16. Marquardt, L.M., et al., *Finely Tuned Temporal and Spatial Delivery of GDNF Promotes Enhanced Nerve Regeneration in a Long Nerve Defect Model*. Tissue Engineering: Part A, 2015. **21**(23-24): p. 2852-64.
17. Tannemaat, M.R., et al., *Differential effects of lentiviral vector-mediated overexpression of nerve growth factor and glial cell line-derived neurotrophic factor on regenerating sensory and motor axons in the transected peripheral nerve*. European Journal of Neuroscience, 2008. **28**(8): p. 1467-79.
18. Eggers, R., et al., *Lentiviral vector-mediated gradients of GDNF in the injured peripheral nerve: effects on nerve coil formation, Schwann cell maturation and myelination*. PLoS One, 2013. **8**(8): p. e71076.
19. Hurtado, A., et al., *Robust CNS regeneration after complete spinal cord transection using aligned poly-L-lactic acid microfibers*. Biomaterials, 2011. **32**(26): p. 6068-79.
20. Ren, Y.J., et al., *Enhanced differentiation of human neural crest stem cells towards the Schwann cell lineage by aligned electrospun fiber matrix*. Acta Biomaterialia, 2013. **9**(8): p. 7727-36.
21. Angius, D., et al., *A systematic review of animal models used to study nerve regeneration in tissue-engineered scaffolds*. Biomaterials, 2012. **33**(32): p. 8034-9.

Chapter 5 : Conclusions and future directions for NF gradient-guided nerve regeneration

5.1 Conclusions

In this thesis, we have developed multiple gradient generation and delivery platforms capable of tailorable, controllable gradient generation for *in vitro* and *in vivo* NF gradient delivery. By developing gradient generation techniques capable of establishing well-controlled, centimeter-scale gradients which can be scaled for rapid gradient production, we successfully overcame limitations of prior gradient generation techniques which were restricted to either *in vitro* or *in vivo* gradient delivery. Through use of a rapid, convection-driven gradient technique, hydrogel films could be generated which encapsulated and delivered centimeter-length gradients, and controlled the release rate of NF gradients through the incorporation of methacrylated heparin into the hydrogel film. A diffusion-based gradient generation platform was developed for flow-free gradient generation for in live-cell migration guidance. The technique was also utilized to functionalize a variety of hydrogel materials and was used to begin elucidating the effects of different NF gradients on the guidance of motor and sensory neuron outgrowth. Furthermore, we combined hydrogel-based NF gradient delivery with aligned nanofiber topographical guidance in a novel live-cell imaging and migration analysis platform to examine the effect of nanofiber diameter on human Schwann cell migration, demonstrate the efficacy of GDNF as a chemoattractant for human Schwann cells, and determine the influence of modulating gradient characteristics, particularly gradient concentration range and steepness, in the guidance of Schwann cell migration. Finally, we translated the hydrogel-based NF gradient generation platform into a NGC, which combined

topographical and biochemical gradient guidance, and demonstrated the effectiveness of delivering NF gradients in the enhancement of peripheral nerve regeneration and functional recovery in *in vivo* acute, short-gap injuries and large-gap injury models. The ability to effectively utilize these gradient generation platforms in both *in vitro* and *in vivo* nerve guidance applications provides significant value to the field of nerve regeneration. These methods are promising tools for elucidating the mechanisms underlying directed Schwann cell and neuronal guidance, the knowledge of which can be used to design the next generation of nerve guided capable of enhancing regeneration of severe peripheral nerve injuries.

5.2 Future Directions

While currently available nerve regeneration conduits and techniques have resulted in adequate axonal regeneration, the axonal regeneration does not always result in significant functional recovery [1]. One of the prevailing factors resulting in the discrepancy between promoting axonal growth and enhancing functional outcomes is due to improper reinnervation of motor and sensory targets. Peripheral nerves often consist of a mixture of motor and sensory neurons. In injuries that result in disruption of nerve continuity, axon regeneration is often misdirected resulting in axons innervating improper targets [2, 3]. Without proper axon guidance and repair, motor axons may improperly reach sensory targets or sensory neurons may reach motor targets, causing poor functional recovery resulting from the inability for axons to reach proper reinnervation target organs. Thus, it is important to develop new nerve guidance platforms, which are capable of enhancing the spatial guidance of specific neuronal populations to increase proper reinnervation and maximize functional recovery.

Neurons have been shown to exhibit motor- and sensory-specificity in axonal outgrowth and chemotropism in response to different types of NFs [1]. Höke *et. al.* have demonstrated that following peripheral nerve injury, growth factor expression differs in Schwann cells within motor-associated and sensory-associated nerves [4]. NGF, which is upregulated in sensory-associated Schwann cells following axonal injury, has been shown to act specifically on small primary sensory and sympathetic neurons. While it has been shown to promote chemotaxis of sympathetic [5] and dorsal root ganglion neurons [6-9], the chemotropic activity of motor neurons towards NGF is limited. GDNF is substantially upregulated in motor nerves after injury [4] and has been shown to dramatically improve the survival of motor neurons [10, 11] as well as sensory neurons [11]. PTN, which is also substantially upregulated in motor nerves after injury [4], exhibits mostly motor-specific guidance and regeneration [1, 12]. These inherent differences in motor and sensory neuronal chemotaxis in response to different NFs can potentially be exploited to promote motor-specific or sensory-specific nerve regeneration *in vivo*.

The numerous gradient generation and delivery platforms developed in this thesis may provide significant insight into the utilization of NF delivery as a method for promoting nerve-specific guidance. With our gradient generation platforms, we are capable of examining the migration guidance of a variety of neuronal and glial populations, utilizing the tailorability and controllability of our gradient platforms for investigating the effects of different NFs in guiding migration of separate populations of cells. Our preliminary studies have been investigating the use of our hydrogel-based gradient delivery platforms for motor- versus sensory-specific guidance on collagen hydrogels functionalized with gradients of different NF type and gradient characteristics in motor and

sensory nerve organotypic models. Additionally, we are working to develop divergent gradient systems with which we can examine the use of divergent gradients of neuron-specific NFs in separating mixed populations of motor and sensory neurons into organized, separate motor and sensory paths. These models will potentially uncover new insights into how to promote outgrowth of motor and sensory neuron populations along separate spatial paths. Such insights would be instrumental in the design of new generations of nerve guides capable of improving functional outcomes by better retaining the spatial organization of mixed peripheral nerve populations and improving the selectivity of reinnervation.

5.3 References

1. Allodi, I., E. Udina, and X. Navarro, *Specificity of peripheral nerve regeneration: interactions at the axon level*. Prog Neurobiol, 2012. **98**(1): p. 16-37.
2. Velero-Cabre, A., et al., *Peripheral and spinal motor reorganization after nerve injury and repair*. Journal of Neurotrauma, 2004. **21**(1): p. 95-108.
3. Bodine-Fowler, S.C., et al., *Inaccurate projection of rat soleus motoneurons: a comparison of nerve repair techniques*. Muscle and Nerve, 1997. **20**: p. 29-37.
4. Hoke, A., et al., *Schwann cells express motor and sensory phenotypes that regulate axon regeneration*. J Neurosci, 2006. **26**(38): p. 9646-55.
5. Campenot, R.B., *Local control of neurite development by nerve growth factor*. PNAS, 1977. **74**(10): p. 4516-4519.
6. Letourneau, P.C., *Chemotactic response of nerve fiber elongation to nerve growth factor*. Dev Bio, 1978. **66**: p. 183-196.
7. Gundersen, R.W. and J.N. Barrett, *Neuronal chemotaxis: chick dorsal-root axons turn toward high concentrations of nerve growth factor*. Science, 1979. **206**(4422): p. 1079-1080.
8. Mortimer, D., et al., *A Bayesian Model predicts the response of axons to molecular gradients*. PNAS, 2009. **106**(25): p. 10296-10301.
9. Catig, G.C., S. Figueroa, and M.J. Moore, *Experimental and computational models of neurite extension at a choice point in response to controlled diffusive gradients*. J Neural Eng, 2015. **12**(4): p. 046012.

10. Zhao, Z., et al., *Overexpression of glial cell line-derived neurotrophic factor in the CNS rescues motoneurons from programmed cell death and promotes their long-term survival following axotomy*. *Exp Neurol*, 2004. **190**(2): p. 356-72.
11. Fine, E.G., et al., *GDNF and NGF released by synthetic guidance channels support sciatic nerve regeneration across a long gap*. *European Journal of Neuroscience*, 2002. **15**: p. 589-601.
12. Chu, T.-H., et al., *Implantation of neurotrophic factor-treated sensory nerve graft enhances survival and axonal regeneration of motoneurons after spinal root avulsion*. *Journal of Neuropathology and Experimental Neurology*, 2009. **68**(1): p. 94-101.

Biographical Sketch

Kellin Daniel Krick was born May 24th, 1988, in St. Paul, Minnesota. He began his undergraduate studies at the University of Minnesota, pursuing a degree in Biomedical Engineering. While at Minnesota, he worked under the support and guidance of Chun Wang, Ph. D., developing materials platforms for cardiac tissue regeneration. He graduated *summa cum laude*, with distinction, with a B.S. in Biomedical Engineering from the University of Minnesota in May 2010. In August 2010, Kellin began his doctoral studies in Biomedical Engineering at the Johns Hopkins School of Medicine, under the mentorship of Hai-Quan Mao, Ph. D. His thesis research has focused on the development of biochemical gradient generation platforms for *in vitro* and *in vivo* neurotrophic factor gradient delivery to enhance the regeneration of peripheral nerve injuries.

Kellin Daniel Krick

March 2016

114 N Rose St
 Baltimore, MD 21224
 kkrick1@jhmi.edu

Education:

Ph.D. (expected)	March 2016	Biomedical Engineering Advisor: Hai-Quan Mao	Johns Hopkins School of Medicine
B.S.	May 2010	Biomedical Engineering Summa Cum Laude	University of Minnesota

Other Professional Experience:

Undergraduate Research Assistant	2008-2010	PI: Chun Wang, Univ. of Minnesota
Summer Research Intern	2009	PI: Mehmet Sarikaya, Univ. of Washington

Fellowships:

Neuroengineering Training Initiative Trainee: August 2011-August 2012

- NIH-Funded Neural Engineering Training Center at Johns Hopkins
- Provided stipend support

Awards and Recognition:

August 2011	<i>NIBIB Training Grant Awardee</i>	Johns Hopkins University
May 2010	Summa Cum Laude: Graduation with Latin Honors, with Distinction	University of Minnesota
January 2010	Tau Beta Pi Engineering Honors Society- Accepted Member	University of Minnesota

Peer-Reviewed Publications:

1. **Krick KD***, Han A*, Huang Y-J, Martin R, Searson P, Höke A, Mao H-Q. Live-cell tracking and analysis platform for advanced single-cell migration analysis. In preparation.
2. **Krick KD***, Mi R*, Martin R, Khademhosseini A, Höke A, Mao H-Q. Neurotrophic gradient delivery enhances regeneration of *in vivo* large gap peripheral nerve injuries. In preparation.
3. **Krick KD**, Huang Y-J, Martin R, Han A, Searson P, Khademhosseini A, Höke A, Mao H-Q. Effect of neurotrophic factor gradient presentation and nanofiber topography on Schwann cell migration guidance. In preparation.
4. Johnson BN, Lancaster KZ, Zhen G, He J, Gupta MK, Kong YL, Engel EA, **Krick KD**, Ju A, Meng F, Enquist LW, Jia X, McAlpine MC (2015). 3D Printed Anatomical Nerve Regeneration Pathways. *Adv Funct Mater* 25: 6205-6217.
5. Sluch VM, Chung-ha OD, Ranganathan V, Kerr JM, **Krick KD**, Martin R, Berlinicke CA, Marsh-Armstrong N, Diamond JF, Mao H-Q, Zach DJ (2015). Differentiation of human ESCs to retinal ganglion cells using a CRISPR engineered reporter cell line. *Nat Sci Reports* 5:16595.
6. **Krick KD**, Tammia M, Martin R, Höke A, Mao HQ (2011). Signaling cue presentation and cell delivery to promote nerve regeneration. *Current Opinion in Biotechnology*. 22: 741-746.

Book Chapters

1. Sarhane KA, Cashman C, **Krick KD**, Tuffaha SH, Broyles JM, Khalifian S, Alrakan M, Baltodano P, Ibrahim Z, Brandacher G (2014). Biomarkers of Nerve Regeneration in Peripheral Nerve Injuries: An Emerging Field. *Biomarkers of Brain Injury and Neurological Disorders*: 566-590.

Abstracts, Posters, and Conference Presentations

1. **Krick KD**, Siu I-M, Höke A, Brushart T, Mao HQ. Gradient generation platform for Schwann cell and neuron migration guidance in 2D and 3D cultures (poster). Biomedical Engineering Society Annual Meeting, October 7, 2015.

2. **Krick KD**, Siu I-M, Höke A, Brushart T, Mao HQ. Neurotrophic factor gradient generation within hydrogel sheets for differential guidance growth of a motor and sensory neurons (poster). Tissue Engineering and Regenerative Medicine International Society Annual Meeting, September 8, 2015.
3. Sarhane KA, Tuffaha SH, **Krick KD**, Cashman C, Budihardjo JD, Broyles JM, Martin R, Abraham J, Ibrahim Z, Mi R, Cooney DM, Höke A, Lee WP, Mao H-Q, Brandacher G (2015). A Critical Analysis of Peripheral Nerve Regeneration in a Chronic Denervation Rat Model Using a Sustained Biomaterial-Based Delivery of GDNF, Chondroitinase, and GDNF+ Chondroitinase Growth Factors (abstract). Plastic and reconstructive surgery. 135: 87.
4. **Krick KD**, Huang Y-J, Martin R, Searson P, Khademhosseini A, Höke A, Mao H-Q. Engineering neurotrophic factor gradients to direct human Schwann cell migration on aligned electrospun fiber matrix (poster). Tissue Engineering and Regenerative Medicine International Society Annual Meeting, December 13, 2014.
5. Martin R, Huang Y-J, **Krick KD**, Lim S, Mullen A, Searson P, Höke A, Mao H-Q. The Effect of Fiber Diameter on the Migration Rate of Primary Human Schwann Cells (poster). Biomedical Engineering Society Annual Meeting, October 22, 2014.
6. Sarhane KA, Ibrahim Z, Cashman C, Martin R, **Krick KD**, Tuffaha SM, Broyles JM, Pan B, Prasad N, Tehrani S, Alrakan M, Wallner C, Cooney DS, Mi R, Höke A, Lee WP, Mao H-Q, Brandacher G (2014). Enhanced Nerve Regeneration by Minimizing Intraneural Scarring Using a Semi-Permeable Nanofiber Wrap (abstract). Plastic and reconstructive surgery. 134: 54-55.
7. Sarhane KA, Ibrahim Z, Martin R, **Krick KD**, Cashman C, Tuffaha SH, Mi R, Lee WP, Mao H-Q, Brandacher G (2014). Enhanced nerve regeneration by minimizing intraneural scarring using a semi-permeable nano-construct nerve wrap (abstract). Journal of the American College of Surgeons. 3: S88.
8. Sarhane KA, Ibrahim Z, **Krick KD**, Martin R, Pan B, Tuffaha SH, Broyles JM, Cashman C, Prasad N, Mi R, Alrakan M, Tehrani S, Cooney D, Mao H-Q, Lee WP, Brandacher G (2014). Enhanced Nerve Regeneration After Vascularized Composite Allotransplantation By Minimizing Intraneural Scarring Using a Semi-Permeable Nanoconstruct Nerve Wrap (abstract). Transplantation. 98: 405-406.

9. Sarhane KA, Ibrahim Z, **Krick KD**, Martin R, Pan B, Tuffaha SH, Broyles JM, Cashman C, Mi R, Alrakan M, Tehrani S, Goldberg L, Mao H-Q, Lee WP, Brandacher G (2014). Selectively permeable nanofiber constructs to prevent inflammatory scarring and enhance nerve regeneration in peripheral nerve injury (abstract). *Plastic and reconstructive surgery*. 133: 16-17.
10. **Krick KD**, Huang Y-J, Martin R, Searson P, Khademhosseini A, Höke A, Mao HQ. Directional migration guidance of Schwann cells for enhancement of peripheral nerve regeneration (presentation). *Biomedical Engineering Society Annual Meeting*, September 25, 2013.
11. **Krick KD**, Huang Y-J, Martin R, Searson P, Khademhosseini A, Höke A, Mao HQ. Neurotrophic Factor Gradient Delivery for Migration Guidance of Schwann Cells (poster). *Annual Meeting for the Controlled Release Society*, July 13, 2013.
12. **Krick KD**, Huang Y-J, Searson P, Khademhosseini A, Höke A, Mao HQ. Neurotrophic Factor Gradient Generation for Cellular Guidance (poster). *Annual Meeting for Society for Neuroscience*, October 13, 2012.

Mentoring Experience

Johns Hopkins Undergraduates

Andrew Han	Materials Science and Engineering	Sept. 2015-Mar. 2016
Kalina Martinova	Materials Science and Engineering	Aug. 2015-Mar. 2016
Ashish Aman	Biomedical Engineering	Jun. 2015-Mar. 2016
Clay Andrews	Biomedical Engineering	Sept. 2014-Aug. 2015
Letitia Chim	Materials Science and Engineering	Jun. 2013-May 2015
John DiCapua	Materials Science and Engineering	Mar. 2013-May 2015

Institute for Nanobiotechnology Summer Research Experience for Undergraduates

Cameron Nemeth	University of Washington	Jun. 2013-Aug. 2013
Lauren Lee	Cornell University	Jun. 2012-Aug. 2012
Diane Hwang	Rice University	Jun. 2011-Aug. 2011

Women in Science and Engineering Mentoring Program

High school student Baltimore-area high schools Sept. 2011-Jan. 2012
mentees

Teaching Experience

Cell and Tissue Engineering Lab 580.452 Spring 2013

- Purchased and organized lab materials
- Assisted students during lab sessions
- Compiled and graded final exam
- Managed course website and coordinated with course instructors

Johns Hopkins January Intersessions- Course Instructor January 2013

- “Great Experiments in Science and Medicine” (AS.250.113.13.IN13)
- Designed lectures discussing major discoveries in the field of medicine
- Prepared and presented 6 lectures for bi-weekly, one month course for 14 students.
- Coordinated guest lectures from numerous Hopkins faculty
- Prepared homework and exams based on lecture materials

Johns Hopkins January Intersessions- Course Instructor January 2012

- “The Science and Medicine of the Nobel” (AS.250.113.13.IN12)
- Designed lectures discussing major discoveries of Nobel Prize winners in the fields of medicine, chemistry, and physics
- Prepared and presented 6 lectures for bi-weekly, one month course for 14 students.
- Coordinated guest lectures from numerous Hopkins faculty
- Prepared homework and exams based on lecture materials